Assessment of respiratory mechanics in humans: application to subjects predisposed to apnea

par

Eve Lucienne Bijaoui

Thèse de doctorat effectuée en cotutelle
à l'Institut de Génie Biomédical, Faculté de Médecine
Université de Montréal

et

Laboratoire TIMC IMAG, Faculté de Médecine
Université Joseph Fourier

Thèse présentée à la Faculté des Etudes Supérieures de l'Université de Montréal
en vue de l'obtention du grade de Philosophiæ Doctor (PhD) en Génie Biomédical

et à

l'Université Joseph Fourier en vue de l'obtention du grade de Docteur de l'Ecole Doctorale Ingénierie pour le Vivant, spécialité Modèles et Instruments en Médecine et Biologie

Août 2001

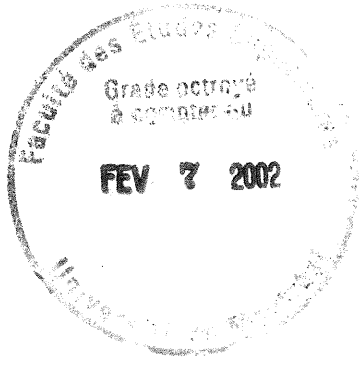

Université de Montréal
Faculté des études supérieures

et

Laboratoire TIMC IMAG, Faculté de médecine
Université Joseph Fourier

Cette thèse intitulée

Assessment of respiratory mechanics in humans : application to subjects predisposed to apnea

présentée et soutenue à l'Université de Montréal par

Eve Lucienne Bijaoui

a été évaluée par un jury composé des personnes suivantes

Président-rapporteur et membre du jury	Pierre Savard
Directeur de recherche	Pierre-A. Mathieu
Co-directeur	Jason Bates, Université McGill
Co-directeur de recherche	Pierre Baconnier, Université Joseph Fourier
Membre du jury	Hélène Perreault, Université McGill
Examinateur externe	Michael C.K. Khoo, University of Southern California, USA
Représentant du doyen de la F.E.S.	Thomas Reader

RÉSUMÉ

La surveillance pulmonaire pendant la ventilation artificielle chez l'adulte et le nouveau-né est généralement obtenue en approximant par une méthode des moindres carrés les signaux de pression et débit mesurés à l'ouverture des voies aériennes à un modèle linéaire simple du système respiratoire. Cependant, l'apparition fréquente d'une fuite d'air entre le tube endotrachéal (ETT) et la trachée des nouveau-nés provoque des erreurs dans la mesure du débit, entrainant une estimation erronée de la résistance et de l'élastance respiratoire et aussi de la pression positive de fin d'expiration (PEEP). Nous avons mis au point une technique permettant corriger le débit pour cette fuite d'air autour du ETT, basée sur l'estimation de la résistance de fuite. La méthode a été testée sur des nouveau-nés prématurés intubés et validée à l'aide d'un poumon mécanique soumis à différents niveaux de fuite. D'autre part, l'impédance mécanique du système respiratoire peut aussi être mesurée pendant la ventilation artificielle. Nous avons développé une nouvelle technique utilisant les déformations mécaniques imposées aux poumons par les battements cardiaques, donnant naissance aux oscillations cardiogéniques (CO), comme source de perturbation naturelle au système respiratoire. A partir d'enregistrements des signaux de pression et débit provenant des CO, ainsi que des sons cardiaques, chez des sujets humains sains pendant des périodes d'apnées volontaires, nous avons montré que les propriétés mécaniques contenues dans les relations pression-débit reflètent celles des voies aériennes centrales. Cette méthode pourrait constituer un outil de surveillance de la résistance des voies aériennes pour des patients anesthésiés et paralysés, par exemple pendant une intervention chirurgicale. Finalement, chez les sujets en respiration

spontanée avec une maladie respiratoire obstructive, l'effondrement des voies aériennes modifie les caractéristiques de leur débit et complique donc l'estimation de la mécanique respiratoire. Nous avons implémenté une méthode des moindres carrés récursifs et développé une version plus robuste de la méthode de Mead-Whittenberger afin d'estimer la mécanique respiratoire en présence d'une limitation inspiratoire du débit pendant le sommeil. Ces deux méthodes ont été testées sur des données expérimentales provenant de cochons obèses pendant le sommeil et validées sur des signaux de débit et pression simulés à partir du modèle viscoélastique du système respiratoire. Nous avons ensuite appliqué ces méthodes à des sujets adultes humains souffrant d'apnées/hypopnées obstructives pendant le sommeil, chez qui nous avons estimé les propriétés mécaniques des voies aériennes supérieures et inférieures (voies aériennes centrales et tissus pulmonaires). Cette étude a démontré que l'élastance pulmonaire augmente de manière importante pendant les épisodes obstructifs. Ces changements pourraient s'expliquer par la diminution du volume pulmonaire induite par l'obstruction, entrainant ainsi le collapsus de certaines unités respiratoires.

ABSTRACT

Pulmonary monitoring during neonatal and adult human artificial ventilation is generally done by fitting accurate measurements of pressure and flow signals at the airway opening to a simple linear model of the respiratory system using multiple linear regression. However, the frequent occurrence of airleaks between the endotracheal tube (ETT) and the trachea of neonates results in errors in flow measurement. These can lead to errors in the estimation of respiratory resistance and elastance, and also in the estimation of positive-end expiratory pressure. We have developed a simple method to correct tracheal flow for a leak around the ETT, based on the measurement of the leak resistance. The method was successfully used on mechanically ventilated preterm infants and on a mechanical test lung. The mechanical impedance of the respiratory system can also be measured during artificial ventilation. We have developed a new technique that uses the mechanical deformations imposed on the lung by the beating heart, resulting in cardiogenic oscillations (CO), as the source of perturbation to the respiratory system. We recorded the pressure and flow signals originating from CO, as well as heart sounds, in healthy human subjects during episodes of voluntary apnea and found that the mechanical information embodied in the pressure-flow relationships reflect the resistance the central airways. This approach provides an easy way to monitor airway resistance during surgery in anesthetized and paralyzed subjects. In spontaneously breathing subjects with a respiratory obstructive disease, the dynamic collapse of the airways alters their flow characteristics and thus complicates the assessment of mechanics. We implemented a recursive least squares algorithm and developed a more robust version of the Mead-

Whittenberger method in order to assess resistance and elastance in the presence of inspiratory flow limitation during sleep. The two methods were used successfully on experimental pressure and flow data from obese sleeping pigs and on simulated data based on the viscoelastic model of the respiratory system. We then applied these methods to adult humans with sleep-disordered breathing, in whom we measured upper airways and lower lung mechanics. We found that lung elastance is markedly increased during sleep-disordered breathing, probably due to airspace closure as lung volume falls during sleep.

TABLE OF CONTENTS

LIST OF FIGURES

LIST OF TABLES

LIST OF SYMBOLS AND ABBREVIATIONS

V	volume of air expressed in litres (l)
$\dot{V}$, D	airflow expressed in litres per second ($l.s^{-1}$)
$\dot{V}_C$	cardiogenic flow ($l.s^{-1}$)
Df	leak flow ($l.s^{-1}$)
Dp	pulmonary airflow, true amount of air going in and out of the lungs ($l.s^{-1}$)
$\ddot{V}$	acceleration of air expressed in $l.s^{-2}$
P	pressure expressed in centimetres of water (cmH_2O)
Ptr	tracheal pressure (cmH_2O)
P_A	alveolar pressure (cmH_2O)
P_C	cardiogenic pressure (cmH_2O)
P_m	Mouth pressure (cmH_2O)
P_{eso}	Esophageal pressure (cmH_2O)
P_{phar}	Pharyngeal pressure (cmH_2O)
P_L	Transpulmonary pressure (cmH_2O)
E	elastance expressed in $cmH_2O.l^{-1}$
E_L	lung elastance expressed in $cmH_2O.l^{-1}$
E_{LL}	lung and lower airway elastance expressed in $cmH_2O.s.l^{-1}$
I	inertance expressed in $cmH_2O.s^2.l^{-1}$
PEEP, P_0	positive end-expiratory pressure expressed in cmH_2O
R	resistance expressed in $cmH_2O.s.l^{-1}$
R_C	cardiogenic resistance expressed in $cmH_2O.s.l^{-1}$
Rf	leak resistance expressed in $cmH_2O.s.l^{-1}$
$Rf,calc$	estimated leak resistance expressed in $cmH_2O.s.l^{-1}$
Rf,mes	measured leak resistance expressed in $cmH_2O.s.l^{-1}$
R_L	lung resistance expressed in $cmH_2O.s.l^{-1}$
R_{UA}	upper airway resistance expressed in $cmH_2O.s.l^{-1}$
R_{LL}	lung and lower airway resistance expressed in $cmH_2O.s.l^{-1}$
X	reactance (imaginary part of the impedance Z) expressed in $cmH_2O.s.l^{-1}$

X_C	cardiogenic reactance expressed in $cmH_2O.s.l^{-1}$
Z	impedance expressed in $cmH_2O.s.l^{-1}$
Z_{in}	input impedance ($cmH_2O.s.l^{-1}$)
Z_C	cardiogenic impedance ($cmH_2O.s.l^{-1}$)
Z_{tr}	transfer impedance ($cmH_2O.s.l^{-1}$)
CO	cardiogenic oscillations
ETT	endotracheal tube
FOT	forced oscillation technique
IFL	inspiratory flow limitation
IWH	information-weighted histogram
LL	lung and lower airway component
MLR	multiple linear regression
MMW	modified Mead-Whittenberger
OSA	obstructive sleep apnea
OSAHS	obstructive sleep apnea/hypopnea syndrome
RLS	recursive least squares
UAW	upper airway

TO MY PARENTS

ACKOWLEDGMENTS

First, I would like to thank my supervisor Pr. Jason H.T. Bates for believing in me from the start, for his constant support and amazing guidance. Thank you for pushing me so hard and making me more confident. I truly admire your ability to resolve any problem instantly but also to decipher my "frenglish" writing.

To my co-supervisor, Pr. Pierre F. Baconnier, who first introduced me to the world of respiratory mechanics and gave me the opportunity to work with an amazing team. I greatly appreciate your guidance and your encouragements throughout the years.

To my other co-supersivor Pr. Pierre Mathieu for his help and good advice throughout the thesis.

I'd like to express my gratitude to Dr. Jim Martin for his enormous help and his constructive advice throughout my thesis. I thank you for your involvement and for always making time to answer my 45-mins "quick" questions.

I would also like to thank Dr John Kimoff as well as Dr Mara Ludwig and Dr. Anne-Marie Lauzon for their precious help, suggestions and encouragements.

To Gila Benchetrit for her amazing energy and her advices. Thank you for welcoming me in your laboratory in France. Many thanks also to the "Groupe de Recherche en Mecanique Ventilatoire" for their kindness and help throughout the years.

To my friends and co-workers at the Meakins-Christie Labs, especially Rute for her good humor and Yasu for keeping me company at the Meakins evenings and week ends. I also want to thank Rosa, Pota and Karim for all the good times we had and their friendship.

To the Meakins staff, Maria, Angie and Liz, for being so helpful and friendly. Thank you for enhancing my daily productivity by keeping the mokas going.

To my family, for your unconditional love, support and patience, for constantly believing in me. I could not have done this without you and this work is dedicated to you. To my sister and best friend Alexandra, thank you for being so supportive, for your little attentions and for increasing your ability to endure time difference. To Michael for being my big brother and a friend, for being so right all the time and for your presence through good and bad times. Many thanks to Sara for her encouragements and understanding.

To my Montreal family, the Assouline, from Albert to Clara, you opened your home and your heart to me. I thank you for your love and encouragements.

I would like to thank Yves, Mme Stephanie, Arnaud, Steph, Jean-Philppe, Lis and Jorge for your friendship and for making my life in Montreal so great.

Finally, I'd like to thank Greg, Eve, Patrick, Anouck and Nicolas for your invaluable friendship throughout these years.

The author acknowledges the financial support of the Délégation Régionale à la Recherche Clinique du CHU de Grenoble.

The author also acklowedges the financial support of the Medical Research Council of Canada, the Canadian Network of Centres of Excellence in Respiratory Health, the Fonds de la Recherche en Santé du Quebec, and the J.T. Costello Memorial Research Fund.

INTRODUCTION

The study of respiratory mechanics, described by the relationships between pressure, flow and volume of gas in the respiratory system, provides a precise characterization of the mechanical behavior of the respiratory system. The detection and quantification of mechanical changes, coupled with a relevant physiological interpretation of the data, are crucial steps for diagnosing pulmonary diseases, assessing the condition of a mechanically ventilated patient or the effect of a treatment. Advances in signal processing and mathematical modelling have provided an ensemble of techniques for assessing respiratory mechanics, the choice of one technique over another depending on the context of measurements. The goal of the research described in this thesis was to develop new tools for assessing pulmonary mechanics in spontaneously breathing subjects and in patients requiring ventilatory assistance. The modelling and signal processing invoked in our methods were applied to the measurement of the mechanical properties of the respiratory system during periods of apnea.

The assessment of respiratory mechanics in the mechanically ventilated patient is important for their management. However, there are a number of key technical issues that must be dealt with if the measurement of respiratory mechanics is to be useful. In particular, the existence of a leak around the endotracheal tube (ETT) in intubated subjects can contribute significantly to systematic errors in the estimation of resistance and elastance and in the estimation of positive end-expiratory pressure (PEEP). Using continuous recordings of pressure and flow signals at the airway opening, we developed a

method that estimates the leak between the ETT and the trachea in neonates and that compensates for errors in airflow measurement. The method, described in Chapter 2, is based on a least squares method for the estimation of PEEP. The method was validated with a mechanical test lung and assessed using data recorded from neonates mechanically ventilated for respiratory distress syndrome.

Once the accuracy of pressure and flow signals is ensured, the next step is to estimate respiratory mechanical parameters using methods that are as noninvasive as possible, that require very little or no active cooperation from the subjects, and which can be used in mechanically ventilated subjects and/or during sleep. One attractive approach for assessing lung function is the forced oscillation technique. The technique is based on the fact that it is possible to characterize a system by applying a known perturbation to the system, measuring the output and computing the transfer function (or more specifically the impedance). However, the equipment required can be cumbersome. We exploit the fact that a natural perturbation to the respiratory system is the periodic mechanical deformation imposed by the beating heart on the lung. This gives rise to so-called cardiogenic oscillations (CO) on pressure and flow recordings. In sleep apnea studies, the presence of CO on flow signal is considered a marker of an apnea of central origin. CO can also be detected during a breath-hold maneuver or during late expiration in artificially ventilated patients. In Chapter 3, we describe a new method that computes the mechanical impedance of the lung based on the frequency analysis of CO. We recorded cardiogenic pressure and flow in spontaneously breathing human subjects and estimated

cardiogenic impedance, which we interpreted as reflecting the resistive properties of central and upper airways.

Another important field of investigation of respiratory mechanics concerns the diagnosis of pulmonary disease. A number of respiratory diseases are characterized by airway narrowing and airflow obstruction. The evaluation of mechanics is complicated in many patients by the presence of airflow limitation even during resting ventilation. The ability to quantify the changes in the mechanical properties of the respiratory system in the presence of flow limitation could help in the evaluation of the degree of obstruction and ultimately of its impact on airway and tissue function.

Inspiratory flow limitation is an important feature of sleep-disordered breathing associated with upper airway obstruction, which ranges from primary snoring to severe obstructive apneas. Obstructive sleep apnea/hypopnea syndrome (OSAHS) is characterized by a decrease in or a cessation of breathing despite increasing respiratory efforts, as a result of partial or total (respectively) collapse of the upper airway. The assessment of lung mechanics during OSAHS is problematic because the usual concept of resistance does not apply in flow limitation. In Chapter 4, we develop numerical methods that provide robust estimates of mechanics, and which reflect the dynamic changes in mechanical properties of the lung caused by the upper airway obstruction. The methods were tested on simulated data and validated with experimental data from obese sleeping pigs. In Chapter 5, we then apply the same methods to humans with sleep-disordered breathing in order to study the effects of sleep stage and arousal on lung

mechanics. This study on humans was also motivated by the fact that there are several anatomic and behavioral differences between the animal and adult human upper airway. For example, pigs regulate ventilation and respiratory cycle timing by expiratory airflow braking involving the glottis. Similar mechanisms apply in human neonates, allowing them to influence ventilation as well as maintain end-expiratory lung volume, but are less prominent in adults. In our human subjects, we found changes not only in lung resistance but also in lung elastance. In the light of these results, we measured both upper airway and lower lung mechanics in some of these human subjects in order to assess whether the changes in parameter estimates were real or just an artefact due to dynamic flow limitation. We confirmed that OSAHS not only affects the upper airway, but also alters the lower lung mechanical properties, most likely due to collapse of some lung regions.

CHAPTER 1

BACKGROUND

1.1. RESPIRATORY PHYSIOLOGY

1.1.1. Overview of the respiratory system

The respiratory system consists of an ensemble of structures interacting with one another in order to maintain adequate gas exchange. It can be viewed as a feedback control system in which information from chemoreceptors (sensitive to P_{aO2}, P_{aCO2} and pH) and from mechanoreceptors (sensitive to respiratory loads and volumes) is integrated in the brainstem and spinal cord, the output of which goes to the effectors, i.e. the respiratory muscles. The response of the system to changes in mechanical load, blood chemistry and metabolic demand allows it to adapt to specific physiologic circumstances (sleep, exercise, altitude) as well as to compensate for pathologic disorders (asthma, chronic obstructive pulmonary diseases, neuromuscular disorder or sleep apnea).

The main components of the respiratory system are presented in Figure 1.1.

- The chest wall consists of the rib cage and the inspiratory and expiratory muscles, which act as a pump to fill and empty the lungs.
- The pleura consist of two sheets: the parietal pleura lining the interior portion of the chest wall and the visceral pleura surrounding the lung. The pleural space lies between these two pleura and normally contains a few ml of lubricating fluid. During breathing, the lungs and chest wall operate in unison and the pleura ensure the smooth mechanical interaction between the lung and chest wall.

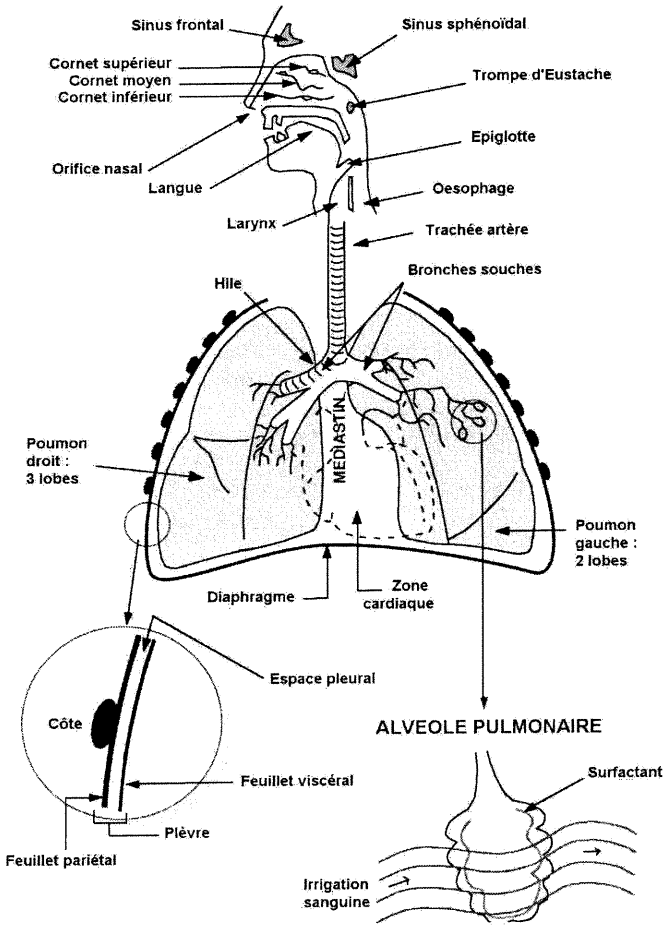

- Upper airways: nose, pharynx, larynx and trachea in its extrathoracic part
- Chest wall: rib cage, external and internal intercostal muscles and diaphragm
- Pleura: mechanical link between the lungs and the chest wall
- Lower airways: 23 generations of branching until air reaches the alveoli, where gas exchange takes place.

Figure 1.1: Anatomy of the respiratory system

- The upper or extrathoracic airways (UAW) constitute a very complicated structure with more than 20 muscles (Aldrich, 1999) that perform several different physiologic functions, including vocalization, swallowing, and respiration. The UAW are essentially a compliant tube extending from the nose and mouth to the trachea, which, along with the bronchial tree, conduct respired gas to and from the lungs. The UAW also moisten, filter, and warm the air to body temperature before it reaches the lungs. Finally, the UAW constitute a defence mechanism by trapping and removing inhaled particles.

- The lower or intrathoracic airways represent a series of bifurcating tubes for the transport of air to the alveoli, where gas transfer takes place between the inspired air and the blood in alveolar capillaries. The asymmetrically branching airway tree can be subdivided into three zones, each with somewhat different but overlapping structural and functional characteristics. The conducting zone represents the airways whose walls do not contain alveoli and are thick enough so that gas cannot diffuse into the adjacent lung parenchyma. These airways do not participate in gas exchange with the blood. They consist of the trachea and both cartilaginous and non-cartilaginous bronchi. These airways, along with pulmonary veins and arteries, nerves, lymphatic vessels, vascular smooth muscle and pleura form the non-parenchymal portion of the lung. The conducting zone is also known as the anatomic dead space and represents a volume of about 150 ml. Alveoli start to appear at the level of the respiratory bronchioles and, together with the alveolar ducts, constitute the transitional zone with both conductive and respiratory functions. Finally, there is the respiratory zone consisting of the alveoli, whose primary function is to exchange gases by a passive diffusion mechanism. This means that air moves from outside the body down to the alveoli where O_2 diffuses to the venous blood and from which CO_2 moves in the opposite direction. The transitional and respiratory zones constitute the so-called lung parenchyma and represent approximately 87% of total lung volume, of which only 6% is tissue and the rest is gas (Stone, 1992).

The intrathoracic airways become narrower and shorter and their structures vary as they progress toward the lung periphery. For example, the shape, thickness and innervation of

bronchial smooth muscle vary according to its location in the tracheobronchial tree (Ebina, 1990). The contraction of smooth muscle decreases the airway diameter and thus increases resistance to airflow. Smooth muscle contraction is involved in the adaptive response of the respiratory system to various conditions (e.g. pollution) but can also compromise ventilation when occurring in a diseased lung (e.g. asthma). The characteristics of cartilage also vary as we go deeper in the lung. The trachea is kept open by rings of cartilage within its walls, which are also present in the large bronchi. Irregular cartilage plates support or partly support bronchi for a number of generations, after which the airways are termed bronchioles. There is no cartilage support in the alveoli which makes them more prone to collapse. They are held open partly because of the attachment of the alveolar septa to their walls, which exert a radial traction. As the size of the cartilage decreases in smaller bronchi, the relative mass of smooth muscle becomes more important and these medium-size bronchi can be the site of significant bronchoconstriction.

The walls of the alveoli constitute the respiratory surface. Blood enters the lungs via the pulmonary arteries and then proceeds through arterioles and into the capillaries surrounding the alveoli. Oxygen and carbon dioxide are exchanged between blood and the alveolar gas. This blood then flows out of the alveolar capillaries, through venules, and back to the heart via the pulmonary veins. Human lungs contain about 300 million alveoli (0.3 mm diameter each), representing a total surface area of about 85 m^2 and a volume close to 4 l. Emphysema, a disease caused by cigarette smoking, can break the walls of the alveoli, which reduces the working area of the respiratory surface. The

alveolar lining layer contains surfactant, which acts to lower the surface tension at the air-liquid interface, thereby enabling alveoli to be stable at low lung volumes and alveolar volume to change at a relatively low energy cost.

Pulmonary diseases are usually classified as obstructive or restrictive. Obstructive diseases are characterized by an increased resistance to airflow and include chronic bronchitis, asthma and emphysema. The differences in the various obstructive diseases come from their different mechanisms of obstruction, that is whether the abnormality originates in the airway lumen, in the walls of the airway or in the peribronchial region. For example, chronic bronchitis is characterized by excessive mucus secretions plugging the airway lumen and small airway obstruction. The anomaly could be from the airway wall, such as in asthma, which is characterized by bronchial smooth muscle contraction, inflammation and hypertrophy of the mucous glands. Finally, the obstruction could be caused by an anomaly in the peribronchial region such as in emphysema, where destruction of alveolar and/or airway walls leads to a loss of elastic recoil and collapse during expiration. In restrictive diseases, lung expansion is restrained either because of alterations of the parenchyma (fibrosis), pleural disease (pneumothorax, pleural effusion), a neuromuscular disease or chest wall restriction (obesity).

1.1.2. Mechanical aspects

Efficient breathing requires appropriately coordinated contractions of upper airway muscles and ventilatory muscles. The timing of inspiratory onset of upper airway muscle

activity differs from that of the diaphragm, varies from breath to breath and is modulated by chemical drive, mechanical afferents from the UAW and state of consciousness. Contraction of pharyngeal muscles, particularly the genioglossus and the tensor palatini, prior to the diaphragm, dilates and stiffens the UAW before the onset of inspiratory airflow and hence produces an early stabilization of the UAW (Hudgel, 1994).

In order to produce a given flow and volume in the lungs, the inspiratory muscles must generate sufficient pressure to overcome the elastic properties of the chest wall and lungs, resistance to flow in the airways, tissue viscosity and inertia. Air moves between the atmosphere and the alveoli following pressure gradients. Therefore, during inspiration, a negative intrathoracic pressure is generated by contraction of inspiratory muscles, mainly the diaphragm. Intercostal muscles generally act to stabilize the chest wall, and neck muscles are used to increase the antero-posterior diameter of the chest wall. During quiet breathing, expiration is passive and results solely from the elastic recoil of the lungs and chest wall. The expiratory muscles are recruited when greater ventilation is required, when airway resistance is increased, during a forced expiration (contraction of abdominal muscles pushing up the diaphragm in order to force air out of the lungs), as well as during loaded inspiration.

The study of respiratory mechanics consists of analyzing the effects of forces on the respiratory system that produce or alter (in case of a respiratory disease) the movement of air in and out of the lungs (Figure 1.2).

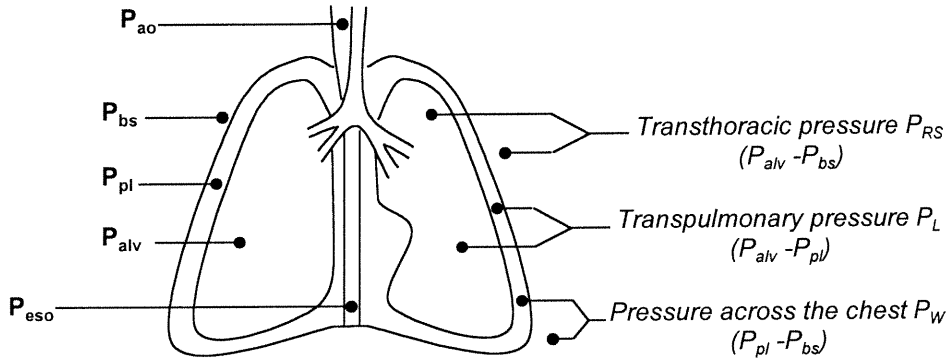

Figure 1.2: Pressures and pressure differences (recoil pressures) generated by the respiratory muscles. P_{ao}: pressure at the airway opening; P_{alv}: alveolar pressure; P_{bs}: pressure at the body surface; P_{pl}: pleural pressure; P_L: transpulmonary pressure; P_W: pressure across the chest

Pulmonary diseases lead to changes in the mechanical properties of the respiratory system, i.e. changes in the relationships between the driving pressure and the flow and volume of air. For example, the pulmonary airways narrow during an asthma attack, increasing the pressure required to transport air. OSAHS is characterized by episodes of partial or complete upper airway obstruction during sleep, leading to a reduction in or complete cessation of airflow despite ongoing respiratory efforts (i.e. bigger driving pressure), until arousal occurs and UAW patency is restored. Conversely, in the case of emphysema, the destruction of lung tissues makes the lungs more compliant so that less effort is required in order to inflate the lungs to a given volume.

1.1.2.1. Elastic properties of the lung

The lungs are elastic structures, containing a meshwork of collagen and elastic fibers. The elastic properties of the lungs are defined in terms of elastance - the change in recoil

pressure of each structure for a given change in lung volume. The elastance of the lung depends on lung volume, increasing as lung volume increases. The relationship between the volume of gas contained in the lungs and the distending pressure necessary to inflate them (in this case, the transpulmonary pressure P_L) gives rise to the pressure-volume curve of the lungs (Figure 1.3).

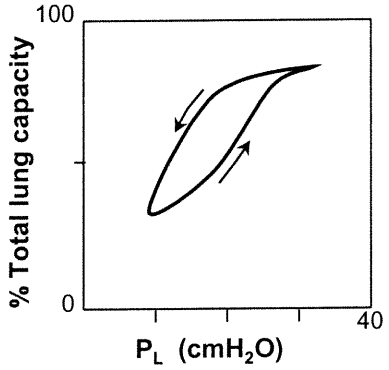

Figure 1.3: Pressure-volume curve of the lungs. P_L: transpulmonar pressure; Inspiration is upward and expiration is downward, i.e. elastic recoil on expiration is less than the distending transmural pressure gradient required to inflate the lung, which reflects a dissipation of energy

The pressure-volume curve displays some hysteresis, which is characteristic of many elastic structures and means that elastic recoil depends not only on the lung volume but also on the volume history of the lungs. Hysteresis results mainly from the elastic forces caused by surface tension at the air-liquid interface over the alveolar surface but also from the elastic forces originating from lung tissues (i.e. the geometrical arrangement of elastin and collagen fibers in the lung parenchyma). The expansion of the alveoli during inspiration is accompanied by an increase in elastic recoil of the airway walls. This recoil is transmitted to the airway-parenchymal attachments, keeping the airways open and stabilizing them.

Surface tension arises at the air-liquid interface because the forces between water molecules are much stronger than the forces between water and gas. As a result, the liquid surface tends to become as small as possible. Pulmonary surfactant reduces the adhesion forces between the water molecules on the alveolar surface, reducing the energy cost of inspiration and stabilizing the alveoli.

It is well established that surfactant plays a critical role in the process of pulmonary airway collapse and reopening (Cassidy, 1999; Ghadiali, 2000). For example, premature babies frequently suffer from a lack of surfactant which causes the collapse of the alveoli at the end of each expiration and an increase in the work of breathing required to produce each breathing cycle. This condition can ultimately lead to respiratory failure. In addition, it has recently been shown that, in the context of OSAHS, the injection of synthetic surfactant helps prevent collapse and facilitates reopening of the UAW (Van der Touw, 1997). Therefore, surface tension and adhesive forces in the upper airway may play a role in the development and/or maintenance of obstruction of the UAW during sleep.

The chest wall tissues also have elastic properties that cause it to recoil either inward or outward, depending on its volume. The elastance of the chest wall is defined as the change in pressure across the chest wall (P_W) for a given change in volume.

1.1.2.2. Resistive properties of the lung

In addition to the pressure generated to overcome lung elasticity, a pressure is required to overcome frictional resistance to airflow in the conducting airways, tissue resistance and inertia of the respiratory apparatus.

Airway resistance

The resistance of the lungs to airflow depends on the flow regimen, which is laminar (dominance of viscous forces) in the small airways and much more turbulent (inertia-dominated) in the large (or central) airways. Fully developed laminar flow is the only flow regimen independent of gas density, so that changes in gas density have little or no effect on small airway resistance. The relationship between the airflow ($\dot{V}$) and the pressure drop (ΔP) between the two extremities of the tube is linear and is described by Poiseuille's law:

$$\Delta P = \frac{8\eta l}{\pi r^4} \cdot \dot{V} = K_1 \cdot \dot{V} \qquad (1)$$

where r is tube radius, l the tube length and η the fluid viscosity. With turbulent flow, which is also observed with changes in diameter, angles and branching tubes, ΔP depends on the square of the flow rate, and thus resistance will vary with $\dot{V}$. In addition, gas density normally affects the resistance of the large airways where the ΔP-$\dot{V}$ relationship is described by

$$\Delta P = K_2 . \; /\dot{V} /. \; \dot{V} \qquad (2)$$

where K_2 reflects the importance of gas density. The tracheobronchial tree experiences both laminar and turbulent flow, so airway resistance is often described by Rohrer's equation (Pedley, 1970a)

$$\Delta P = K_1 . \dot{V} + K_2 . /\dot{V}/.\dot{V} \qquad (3)$$

although the same group of investigators believe that the pressure drop in the human airways are better described by

$$\Delta P = K_3 (\rho\eta)^{1/2} \dot{V}^{3/2}$$

in which K_3 depends on lung geometry and volume, ρ is the coefficient of density.

Since airway resistance is usually measured at the mouth, it describes the resistive properties from the larynx to the respiratory bronchioles. Measurements performed in normal subjects show that the site of resistance is primarily in the large airways (Pedley, 1970b). UAW resistance accounts for 50 % of airway resistance during quiet breathing but this proportion can increase up to 70-80 % when minute ventilation is increased. Although airway radius has a huge influence on resistance during laminar flow (Eq. 1), the small airways of less than 2 mm diameter normally contribute only about 10% of the total airway resistance. This is explained by their large combined cross-sectional area compared to larger airways (Pedley, 1970a,b). Consequently, small airway obstruction has relatively little effect on the overall mechanical properties of the lung, although it affects ventilation distribution significantly.

Contraction of bronchial smooth muscle, flow regimen and gas density are among the factors that modify airway resistance. Airway resistance also depends on lung volume, that is, at higher lung volumes, small airways expand and airway resistance falls. The mechanism by which airway resistance relates to lung volume is believed to be the tethering effect of the parenchyma attachments to the walls of the airways, usually named airway-parenchymal interdependence. The degree of expansion is a function of the compliance of the tissue, which exerts a peribronchial pressure that is equivalent to pleural pressure. Airway closure can occur when the lung reaches very low volumes. For example, pulmonary airways tend to remain closed in premature infants suffering from hyaline membrane disease (respiratory distress syndrome) and in subjects with asthma, emphysema, or cystic fibrosis. These conditions can result in atelectasis and/or local hypoventilation. Pulmonary surfactant deficiency, loss of parenchymal tethering and increased fluid viscosity have been proposed as possible mechanisms of airway closure.

UAW resistance

The Rohrer's equation for fluid flow through rigid tubes has also been used to describe the relationship between airflow and pressure in the nasal airway and the pharynx during wakefulness (Hudgel, 1988). However, this theory assumes that the cross-sectional area of the airway is constant, which does not apply to forced expiration and to the dynamic behaviour of the UAW during sleep (Schwab, 1993). The sleep-induced loss of muscle tone results in variable narrowing of the UAW during inspiration, with consequent flow limitation. The degree of airway narrowing increases as the inspiratory pressure becomes more negative, and hence the pressure-flow relationship becomes curvilinear. Hudgel

(Hudgel, 1988) proposed a mathematical model for the pressure-flow relationship of the UAW incorporating a hyperbolic equation (Eq. 4),

$$\frac{\Delta P}{\dot{V}} = \frac{\beta}{\alpha} + \frac{\Delta P}{\alpha} \tag{4}$$

where α is the asymptote for peak flow (flow at which pressure reaches infinity) and β is the pressure at 50% of peak flow (Figure 1.4).

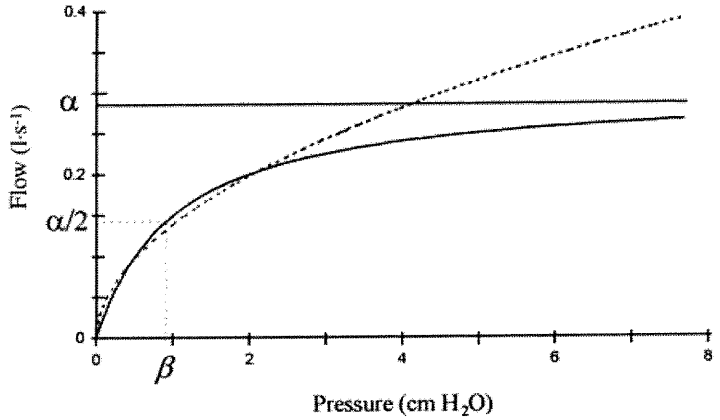

Figure 1.4: Inspiratory pressure-flow relationships in the UAW. Dashed line: Rohrer equation; solid line: Hudgel equation. Reproduced from Tamisier (2000)

This equation better describes the pressure-flow relationship in normal subjects and in patients with various forms of sleep-disordered breathing (Tamisier, 2000). The rigidity of the upper airway depends on static characteristics such as the anatomy and structure of pharyngeal tissues, and dynamic factors such as the pharyngeal muscle activity, highly dependent on the phase in the breathing cycle and the state of consciousness. This leads to differences in the shape of pressure-flow relationships, which can be accounted for by the Hudgel equation.

Tissue resistance

Tissue resistance (R_{ti}) is caused by the internal friction encountered as the lung tissues move during lung expansion. The sum of tissue resistance and airway resistance (R_{aw}) is usually termed pulmonary or lung resistance. The contribution of tissue resistance to the total pulmonary resistance varies amongst species (Table 1.1) but also within species because it depends on frequency, lung volume and lung volume history. R_{ti} can be increased significantly in diseased situations such as during bronchoconstriction and this is helpful in understanding the pathophysiology of some respiratory diseases (Ludwig, 1989; Lutchen, 1994).

Table 1.1: Relative contribution of R_{aw} and R_{ti} to total pulmonary resistance R_L under healthy conditions (adapted from Ludwig (1997) and Kaczka (1997))

	Dog	Rabbit	Rat	Guinea pig	Human
R_L	100 %	100 %	100 %	100 %	100 %
R_{aw}	18.4 %	41.7 %	61.0 %	75.2 %	60 %
R_{ti}	81.6 %	58.3 %	39.0 %	24.8 %	40 %

Unlike airway resistance, tissue resistance increases with lung volume and tidal volume, and decreases as breathing frequency increases (Ludwig, 1997).

Measurements of tissue resistance can be done experimentally using the alveolar capsule technique (Bates, 1988b; Fredberg, 1984; Lauzon, 1995) that will be described later, and clinically using the interrupter technique (D'Angelo, 1991). Recently, information about the tissue mechanical properties in humans was obtained by measuring lung impedance and fitting it to a constant-phase model (Lutchen, 1994). This model, which will be presented in more detail later, represents the lung as a single constant airway resistance

connected to a viscoelastic tissue unit in which the ratio between tissue resistance and tissue elastance (hysteresivity) is frequency-independent.

1.1.2.3. Factors influencing lung and upper airway mechanics

Changes in mechanical properties of the lung occur naturally with age. Indeed, lung elastic recoil decreases with increasing age in adult human subjects (Lai-Fook, 2000) and other species including rats (Nagase, 1994). Alterations in the contribution of elastin to the overall elastic behavior of the lungs might contribute to an increase in tissue forces, which in turn affects the mechanical interdependence between the airways and the surrounding parenchyma. Important changes in lung mechanics also happen during lung development. Both resistive and elastic parameters decrease with age, weight and tidal volume (Barnas, 1991; Galal, 1998; Lanteri, 1993; Pandit, 2000). Lung elastance also decreases with female gender (Pandit, 2000). Gomes et al. (2001) looked at the effect of development on lung mechanics and observed a decrease in lung mechanical parameters of the rat with increasing age, suggesting an increased mechanical coupling between the airways and the parenchyma.

Obesity has been shown to influence forced expiration rates and to increase respiratory resistance (Pankow, 1998; Zerah, 1993). This is because fat deposition in and around the abdomen and rib cage decreases chest wall compliance, and so increases the work of breathing and reduces the functional residual capacity (FRC), especially in the supine position. The low FRC combined with atelectasis may lead to ventilation-perfusion

disturbances that increase hypoxemia. Obesity is associated to a worsening of the condition of a patient with a respiratory disease (Chaouat, 1996; Hakala, 2000).

FRC decrease significantly in healthy nonobese subjects when going from upright to supine, with a further decrease with sleep onset. These posture-related changes in lung volume result in an increase in lung elastance and resistance (Baydur, 1996). Changes in lung volume can affect the mechanical properties of lung tissue and lower airway, and also UAW mechanics. Aronson et al. (1991) and Van de Graaff (1988) previously described the thoracic influence on UAW patency during sleep. The intrathoracic pressure is transmitted to the trachea, thus increasing the transmural pressure, resulting in the dilation of UAW and a decrease in UAW resistance. This mechanism explains the inverse relationship between lung volume and UAW resistance. More specifically, UAW resistance has an inverse curvilinear relationship to lung volume (Aronson, 1991). The fall in lung volume that occurs during sleep, especially in obese subjects, decreases UAW caliber and promotes UAW collapse.

With the onset of sleep, the control of breathing becomes entirely involuntary and metabolism-dependent, responding exclusively to changes in gas exchange and afferent information received from chest wall and lung parenchymal receptors. Human sleep has a cyclic pattern with two major alternating components: non rapid eye movement (NREM) also known as quiet, synchronized sleep, which occupies 75 to 80% of total sleep time, and rapid eye movement (REM), known as paradoxical, desynchronized sleep, occupying the remaining 20 to 25 % of the sleep time of a young adult. NREM sleep is subdivided

into four stages, from stage 1, the transitional state that occurs on going to sleep to stage 4, the deepest stage of sleep. REM sleep is characterized by a high brain activity, depression of muscle tone and important heart and breathing rate variabilities. During NREM sleep, changes include an increase in airway resistance, the loss of the wakefulness stimulus, changes in rate and rhythm of breathing, a change in breathing mechanics that increase the contribution of the rib cage to breathing and a reduction of load compensation. The result is a decrease in ventilation of about 13-15% and a corresponding fall in alveolar ventilation so that arterial P_{CO2} increases and arterial P_{O2} decreases. During REM sleep, changes are even more pronounced because of tonic inhibition of respiratory muscle activity, wide variations in respiratory muscle activity that accompany phasic events of REM sleep, and reduced homeostatic responses. The fall in ventilation at sleep onset is mainly due to (1) a reduced activity of respiratory muscles, either because of a direct reduction in activation of these muscles or because of a reduced response to chemical stimuli (namely P_{CO2} and P_{O2}), and (2) an increase in UAW resistance during sleep, both because of a decrease in UAW reflexes and a reduced activity of the muscles responsible for holding the UAW open during inspiration. The effects of sleep on breathing are summarized in Table 1.2. Ventilation is further impeded in asthmatics and in patients with obstructive sleep apnea/hypopnea syndrome.

Table 1.2: Sleep-induced changes in respiration (compared to wakefulness)

Feature	NREM 1&2	NREM 3&4	REM
Pattern of breathing	Periodic	Stable	Irregular
Apneas	Short, central	Rare	Short, central
PaCO2	Variable	↑ 2-8 mmHg above wakefulness	Variable, similar to NREM 3&4
Rib Cage muscles	Active	Active	Inhibited
Diaphragm	Active	Active	Active
Upper AW muscles	↓	↓ (/ wakefulness)	Inhibited
Ventilatory response to CO_2	↓	↓	↓
Ventilatory response to hypoxemia	↓	↓	↓
Arousability to respiratory stimuli	Low thresholds	Low thresholds	High thresholds

1.1.3. Flow limitation

The dynamic compression of the airways, which leads to flow limitation and airway narrowing, is an important feature of numerous respiratory diseases, including chronic obstructive pulmonary diseases (Mead, 1967) and obstructive sleep apnea syndromes (Clark, 1998). The former category, which has been studied extensively, mainly exhibits expiratory flow limitation (EFL) in the bronchial tree, whereas inspiratory flow limitation (IFL) in the pharynx is an important feature of sleep apnea. In either case, changes in the transmural pressure gradient caused by the inspiratory or expiratory effort result in changes in the cross sectional area of the airway at the site of obstruction.

Flow limitation is a consequence of the collapsibility of the airway. In normal subjects, maximal inspiratory flow is determined by muscle strength, and is thus effort dependent. During forced inspiration, the pressure inside the upper airway decreases below atmospheric pressure, and unless the stability of the UAW is maintained by reflex contraction of pharyngeal muscles or by other structures, the cross-sectional area of the UAW will decrease. In contrast, once a moderate expiratory effort is exerted, expiratory flow reaches a maximal value determined by the intrinsic mechanical properties of the lung and further expiratory effort does not result in greater flow. Airway patency strongly depends on cartilaginous support and/or airway-parenchymal interdependence.

1.1.3.1. Mechanisms of flow limitation caused by upper airway obstruction during sleep

Dynamic collapse was first assessed from isovolume pressure-flow (Fry, 1960) and flow-volume curves (Hyatt, 1979). At the same time, Mead (1967) described EFL in terms of the equal pressure point. Briefly, this approach states that once flow is limited, a site existed along the airways where the pressure inside the airway (intrabronchial pressure) is just equal to the pressure outside the airway (pleural pressure), thus where transmural pressure is equal to zero. The airways upstream cannot be compressed whereas downtream to this point, the only factor that keeps the airways open is their intrinsic elasticity, which will be overcome at high enough pressures, causing airway narrowing.

Many fluid-conveying vessels in the body are elastic and deform substantially in response to the forces that the fluid exerts on them. Since any change to the geometry of the vessel directly affects the fluid flow, the behavior of such systems is often dominated by strong

fluid-structure interactions that can give rise to many phenomena such as flow limitation. The study of fluid flow through collapsible tubes by engineers has resulted in models that have been applied to flow of blood in veins and arteries (Badeer, 1992), airflow dynamics in the bronchial tree (Carry, 1998; Khirani, 2001; Peslin, 1996; Yang, 1996) and the upper airways (Krieger, 1998; Reisch, 1999) and the importance of surface tension on airway closure and reopening (Gaver, 1990; Perun, 1995). Collapse of airways can be modelled in the laboratory by the deformation of a thin-walled elastic tube conveying a viscous flow, mounted on two rigid tubes (Heil, 1999). In its undeformed state, the tube is cylindrical and the ends of the tube are held open. As external pressure increases, the tube deforms markedly. The reduction in tube cross sectional area changes its flow resistance and thereby the pressure distribution in the fluid, which in turn affects the tube's deformation. The Starling resistor or waterfall model is commonly used for flow limitation and is described below in the context of UAW flow mechanics.

UAW patency is maintained by the balance between the negative intrathoracic pressure generated during inspiration and the dilating action of the pharyngeal muscles. The UAW is represented as a collapsible segment (pharynx) located between two rigid bony (nose upstream) or cartilaginous (trachea downstream) segments. The collapsible segment narrows or collapses during processes such as speech or swallowing (Figure 1.5). The rigidity of this segment depends on (i) static characteristics such as the anatomy and structure of pharyngeal tissues and (ii) dynamic factors such as the pharyngeal muscle.

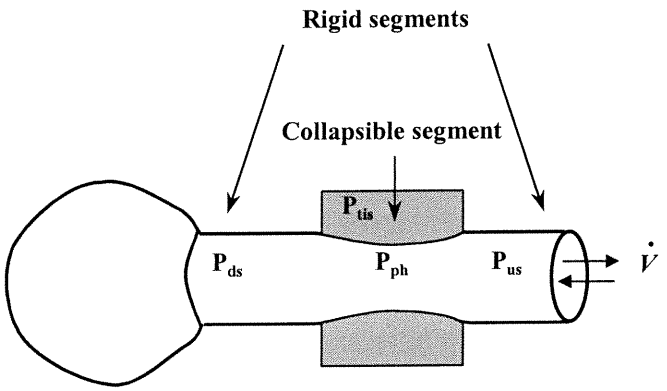

Figure 1.5: Mechanical model of an UAW region with a collapsible segment. The upstream pressure (P_{us}) for the pharyngeal airway is the nasal pressure and the downstream pressure (P_{ds}) is generated from the thoracic pump muscle activity. The closing pressure (P_{crit}) is equal to the pressure exerted on the pharyngeal airway by the surrounding structures (P_{tis}). Adapted from Krieger (1998)

According to the Starling resistor model, flow $\dot{V}$ cannot occur until pressure upstream the collapsible segment (P_{us}) exceeds the surrounding pressure (P_{crit}). The suction pressure applied to the downstream (P_{ds}) of the collapsible segment can increase the flow only to a limited extent beyond which it becomes independent of further increase in the driving pressure. The collapsible segment undergoes dynamic narrowing and the maximal flow becomes a function of the pressure gradient and the resistance in the segment upstream of the collapsible segment. This analog of the upper airways, described in greater detail elsewhere (Krieger, 1998), represents the three different levels of patency of the UAW (Figure 1.6A-C), as follows:

(a) An occluded condition, where $P_{ph} \ll P_{tis}$, so $P_{us}<P_{crit}$. The pharyngeal segment collapses under the pressure exerted by the surrounding structures and no flow is

possible (Figure 1.6A). This condition corresponds to the airway of an individual with obstructive sleep apnea.

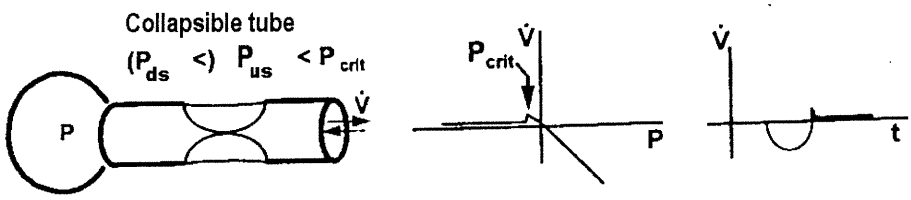

Figure 1.6A: *Left*: Schematic representation of a highly collapsible UAW (e.g. during obstructive apnea). *Middle*: corresponding pressure-flow relationship. *Right*: corresponding time variations of flow (expiration is down).

(b) A patent condition, where $P_{ph} \gg P_{tis}$ throughout the entire breathing cycle, so $P_{us} > P_{crit}$ and $P_{ds} > P_{crit}$ (Figure 1.6B). The tube remains open and the airways can be modeled as a rigid tube. Therefore the flow in the tube, assuming a laminar condition, obeys Poiseuille law (i.e. depends only on the difference between upstream and downstream pressures). This condition corresponds to the airway of an individual during wakefulness.

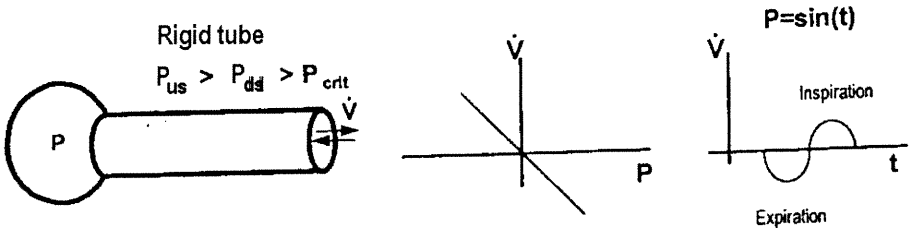

Figure 1.6B: Schematic representation of a rigid UAW (e.g. during normal breathing)

(c) An unstable situation, where P_{ph} fluctuates around P_{tis} and $P_{us} > P_{crit}$ and $P_{ds} < P_{crit}$ (Figure 1.6C). In this case, the airway undergoes partial transient collapse, or flutters, and the maximal inspiratory flow ($\dot{V}_{I,\max}$) is given as follows:

$$\dot{V}_{I,\max} = (P_{us} - P_{crit})/R_{us} \qquad (5)$$

$\dot{V}_{I,\max}$ is independent of respiratory effort and downstream pressure. This condition corresponds to the airway of an individual with obstructive hypopnea (inspiratory flow limitation) or snoring (flutter).

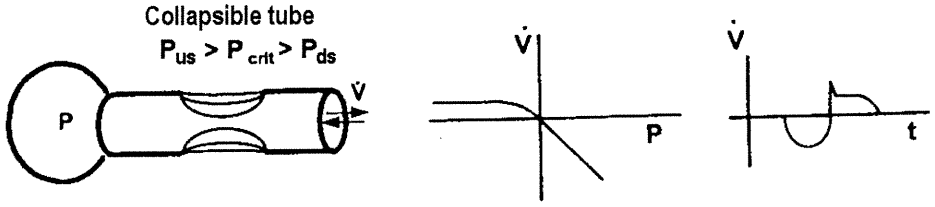

Figure 1.6C: Schematic representation of a collapsible UAW during inspiratory flow limitation.

Although the equal pressure point concept and Starling resistor model provide important insights into the phenomenon of flow limitation, they do not explain its actual mechanics. In particular, they cannot predict the geometry of the flow-limiting site. Advances in the understanding of flow limitation were made possible by the wave speed analysis proposed by Dawson and Elliott (Dawson, 1977). The wave speed theory states that the flow in the airways, like in any other compliant tube, is limited by the velocity of propagation of pressure waves along the walls of the tube. The velocity of propagation varies proportionally with the cross-sectional area of the tube and the elastance of the tube wall (stiffness), which is defined as the slope of the curve of transmural pressure

versus dynamic area. At the site where local fluid velocity first reaches the velocity of propagation of pressure waves, a "choke point" develops, preventing further increases in flow. The location in the choke point is lung volume-dependent and factors such as a neck extension affect the value of the maximum flow. The main limitation of the wave-speed theory is that it assumes that convective acceleration, rather than frictional losses, is the dominant source of the pressure drop along the tube.

OSAHS is characterized by reductions in ventilation resulting from total or partial collapse of the upper airway. Sleep-disordered breathing associated with upper airway obstruction ranges from primary snoring to severe obstructive apneas. The prevalence of the disease depends on the severity of the event. For example, the prevalence of snoring in adults is 40-60% and in general, the index of disturbance increases with age and male gender. On the other hand, the prevalence of OSAHS averages 4 % in middle-aged men and 2% in middle-aged women (Report, 1999). The different levels of IFL encountered during sleep-disordered breathing range from a non flow-limited inspiration, characterized by a linear P-$\dot{V}$ relationship, to a severe IFL where flow decreases despite an increase (magnitude) in driving pressure. The latter is known as negative pressure dependence (Clark, 1998; Isono, 1997). These levels of IFL are strongly determined by the balance between the decrease in cross-sectional area of the collapsible segment and the increase in driving pressure (Isono, 1997; Jones, 1975). Aitokallio et al. (2001) have recently shown that UAW behavior can be different in a group of people having the same breathing pattern abnormality (IFL), and that this is due to the relative importance of the various factors involved in UAW patency. Indeed, along with the phasic activity of the

dilator muscles and the negative driving pressure, the traction exerted by the thorax on the UAW (maximum effect at end-inspiration with high lung volumes) is also important. This explains the effect of lung volume on pharyngeal cross-sectional area, such that UAW patency is best at high lung volume.

1.1.3.2. Models of upper airway collapse during sleep

Animal models of sleep apnea (Hendricks, 1987; Lonergan, 1998; Tuck, 1999) are currently used to investigate the mechanisms of UAW collapse, and have been designed to assist in the development of surgical or pharmalogical treatments. Mathematical models have also been developed, bringing out the importance of the interaction between the neural and anatomic components in order to maintain UAW patency. Recent progress in signal and image processing (Schwab, 1998; Schwab, 1993) has provided robust techniques for evaluating the changes and the treatment associated with the disease.

A better understanding of sleep apnea, its predisposing factors such as obesity and its associated factors such as hypertension has been obtained using animal models of the disease. Ultimately, animal models of sleep apnea hope to mimick human sleep apnea, giving insights into its pathophysiology and possible treatment strategies. Animal models of obstructive sleep apnea (OSA) can be divided into two categories, induced and spontaneous OSA. An example of an animal model in which OSA is induced experimentally is the tracheostomized dog model described by Kimoff et al. (1994). A specialized valve connected to the tracheal opening of the animal is programmed to close when the animal falls asleep and to open when the animal arouses, thus simulating an

obstructive apnea. The main advantage of this model is in the study of mechanisms of apnea termination, as well as the short and long term effects of episodes of sleep-disordered breathing on ventilatory and arousal responses to hypoxia. This model, however, does not provide insights into the mechanisms that initiate apnea and is not suitable for the evaluation of treatment strategies.

Animal models of spontaneous sleep apnea are more difficult to produce. Hendricks et al. (1987) were the first to report a natural animal model of sleep apnea, using the English bulldog because its upper airway configuration contributes to the development of upper airway obstruction. This animal has an anatomically narrowed pharyngeal airway due to a long and thickened soft palate and exhibits disordered breathing episodes with oxygen desaturation, especially during REM sleep. During wakefulness, the animal is hypersomnolent but has normal blood gases. This natural model has proven to be useful in the study of the pharmological treatment of OSA (Panckeri, 1996; Veasey, 1999; Veasey, 1996). The other animal model of spontaneous OSA reported in the literature is the obese miniature pig, described by Lonergan et al. (1998). Obstructive apneas were observed in two of the pigs while another one exhibited central apneas, all associated with oxygen desaturation. Because apneas occurred in only obese pigs and not in nonobese pigs, it seems likely that obesity was the cause. This study also showed that apneas and hypopneas occurred more frequently in REM than in NREM sleep in the pigs with obstructive apnea, which is similar to what has been observed in the English bulldog.

A few mathematical models of sleep apnea have recently been developed. Gavriely et al. (1993) first proposed a model of UAW collapse, in which a single rectangular collapsible segment is supported by a spring characterized by an elastance K. The 2-element compliance model developed by Fodil et al. (1997) is based on the local differences in anatomic and physiological properties of the nasopharynx and oropharynx, where collapse occurs. The model suggests that UAW behavior depends strongly on the relative magnitudes of the compliance values, that is defined for each element as the ratio between the cross-sectional area variation and transmural pressure variation. This model reproduced the IFL associated with segmental narrowing of the UAW, and also the EFL associated with OSA and/or obese patients. Finally, Huang et al. (1999) introduced a model for the dynamic collapse of the UAW, where the neural influence is expressed in terms of a delay between the neural receptors and the dilator muscles in response to the negative pressure generated by the thoracic pump muscles. This model includes the increased latency of muscle response with the progression of sleep and it suggests that there is a "critical" latency, which if exceeded, will lead to airway instability.

1.2. ASSESSMENT OF RESPIRATORY MECHANICS

1.2.1. Measurement of pressures and flows

The accurate measurement of pressure and flow signals is required in order to determine the mechanical properties of the respiratory system. The type of information obtained depends on the sites of measurements. For example, the measurement of P_{eso} in spontaneously breathing subjects gives the pressure variation generated by the respiratory muscles and provides information about the lung mechanical properties. In anesthetized and paralyzed subjects, esophageal and transpulmonary pressure (P_L, Figure 1.2) reflect chest wall and lung properties, respectively. The measurement of mouth or tracheal pressure in these subjects will give the mechanical properties of the entire respiratory system.

P_{eso}, which is an estimate of P_{pl}, is measured for the computation of P_L and lung mechanics. The accurate representation of P_{pl} using P_{eso} requires adequate pressure transmission through the intrapleural to intraesophageal tissue barrier (Hartford, 1997). P_{eso} can be monitored via esophageal balloons (inflated with air) or liquid-filled catheters (filled with water or saline), which are attached to pressure transducers and signal amplifiers. Esophageal balloons are generally preferred to liquid-filled catheters for accurate dynamic pressure measurements because they have better frequency response characteristics and are less sensitive to cardiac artifacts (Hartford, 1997). The balloon is passed transnasally down to the middle third segment of the esophagus (Baydur, 1996),

the distance between the balloon and the entrance at the nares varying typically between 36 and 42 cm. The positioning of the balloon is adjusted by performing an occlusion test in which the subject makes an inspiratory effort against an occluded airway. The plot of P_{ao} versus P_{eso} must be a straight line with a slope close to 1 (0.9-1.1). It is assumed that changes in pleural pressure are uniform over the entire lung surface. The assessment of the frequency response of the balloon-catheter system is a necessity in numerous clinical settings, such as for monitoring during high-frequency ventilation or in newborns who have high respiratory rates (Hartford, 1997). One way to test frequency response is to compute the amplitude ratio and phase angle of esophageal to airway opening pressures while pressure oscillations are applied to the system (Peslin, 1993b).

Technical problems arising from the use of esophageal balloons which may affect the accuracy of the pressure measurements include nasal irritation, inadequate filling of the balloon, movements of the subject and chest wall distortion. Despite some eventual tolerance problems and limitations related to the quality of sleep, the measurement of P_{eso} is considered a gold standard for the identification and quantification of almost all the obstructive sleep disorders (Report, 1999). For example, the measurement of respiratory effort is necessary for the detection of upper airway resistance syndrome, defined by repetitive sequences of increasingly negative inspiratory P_{eso} and decreases in $\dot{V}$, but with no frank apnea/hypopnea or oxygen desaturation (Report, 1999).

Most of our knowledge of respiratory mechanics was acquired through animal experiments, which allow a greater access to key measurement sites than do humans. P_{alv},

and therefore direct information about tissue mechanical properties can be obtained experimentally in open-chest animals using the alveolar capsule technique (Bates, 1988b; Davey, 1993; Fredberg, 1984; Hantos, 1995; Lauzon, 1995). Small piezoresistive transducers are glued onto the surface of the visceral pleura and the sub-pleural alveoli are exposed to the capsule chambers via small holes made in the pleura under each capsule. A miniature pressure transducer is placed in the capsule chamber in order to continuously monitor P_{alv}. Several alveolar sites can be recorded simultaneously. This technique gives precise mechanical information about distal regions of the lung and therefore evidence about the nature of the mechanical heterogeneity throughout the lung. By connecting each capsule to a small oscillating source (e.g. loudspeaker), one can also obtain the impedance of a specific lung region, which in turn will give details about whether the local pressure changes are related to local resistive or elastic properties, or both.

While pressure is directly measured with a piezoresistive pressure transducer, flow is conventionally measured with a pressure transducer placed across the two ports of a pneumotachograph. This flow transducer is based on Poiseuille's law (Eq. 1) and thus assumes a laminar flow through the device. The volume is usually obtained from numerical integration of the flow signal. In order to get the flow in a sleeping patient, the patient must wear a tightly fitting face mask (which covers nose and mouth) with the pneumotachograph attached to it. Although this setup can be cumbersome and may not be tolerated well by the patient, the pneumotachograph is considered a gold standard for

flow measurement (Report, 1999). The pneumotachograph must be tested for linearity in the range of flow rates of interest (calibration at different airflows).

Other devices can be used in a clinical context to measure airflow such as during a polysomnographic exam or during mechanical ventilation in preterm babies. For example, the respiratory inductive plethysmography, which is routinely used during polysomnography, is a useful semi-quantitative tool for detecting inspiratory flow limitation during sleep (Kaplan, 2000) or for characterizing lung function (e.g. increase in airway resistance) in patients with a respiratory disease (Carry, 1997). Thermistors and thermocouples, which provide information about the presence or absence of airflow based on temperature differences when placed in flowing gas, are routinely used during standard nocturnal polysomnography to identify sleep-disordered breathing. The devices incorporate small sensors that can be taped below the patient's nostril and next to the mouth. These sensors cannot be calibrated and therefore provide only qualitative information. In addition, the collection of moisture on a sensor can affect its ability to detect temperature changes and so may adversely affect signal accuracy. The wide spectrum of sleep-disordered breathing goes from simple primary snoring to severe obstructive sleep apnea. Norman et al. (1997) showed that thermistors are unable to detect subtle abnormalities in airflow essential for the identification of upper airway resistance syndrome or mild sleep apnea. This study, along with others (Montserrat, 1997), suggested that thermistors should be replaced by nasal prongs for the identification and classification of respiratory events during a polysomnographic exam. Nasal prongs sense pressure changes associated with airflow turbulence at the nostrils,

and have a quadratic relationship between the signal recorded (pressure) and the flow. Nasal prongs require no calibration. In addition, they have a good dynamic response, much superior to that of the thermistor, which makes them useful in the detection of sleep-disordered breathing of various degrees, such as simple snoring. Like thermistors, the main limitation to the use of nasal prongs is their inability to detect mouth breathing, although it is uncommon during sleep. Also, accumulation of secretions or facial abnormalities such as a deviated septum can result in an increase in nasal resistance and lead to false apnea event detection. Finally, although nasal prongs accurately sense flow variations at the nose (Farre, 2001a), because they are uncalibrated, they cannot replace the pneumotachograph for assessment of lung and/or UAW mechanics.

Tracheal intubation is a frequent procedure in numerous clinical situations. For example, subjects with respiratory insufficiency are intubated and mechanically ventilated. A subject can also be intubated in order to maintain the UAW open in the presence of an obstruction or to protect the UAW in the absence of coughing or swallowing. The measurement of respiratory system resistance in intubated subjects usually includes the resistance of the endotracheal tube (ETT) (Jarreau, 1999; Perez Fontan, 1985). It is important to determine the contribution of the ETT because it can be large. The ETT resistance depends on the geometry of the ETT (diameter, length, shape and cross-sectional area) and on the ventilatory characteristics (flow, gas density and respiratory frequency) (Manczur, 2000). ETTs have highly curvilinear flow resistive properties, the relationship between the pressure drop (ΔP_{ETT}) and the flow ($\dot{V}$) in the ETT is usually being approximated by

$$\Delta P_{ETT} = (\mathbf{K_{1,ETT}} + \mathbf{K_{2,ETT}}\ \dot{V})\ \dot{V} + \mathbf{I_{ETT}}\ \ddot{V} \quad (6)$$

where $K_{1,ETT}$ and $K_{2,ETT}$ are the coefficients of the Rohrer equation for the resistive properties of the tube and I_{ETT} is the tube inertance.

The approaches to mechanical ventilation are very different in neonates and in adults, mainly due to anatomic differences. Uncuffed ETTs are routinely used in the neonatal environment partly because the addition of a cuff would require a smaller tube and therefore increase resistance and work of breathing. Although cuffed tubes are usually used in adults, there are cases, such as in patients with neuromuscular disorders, where uncuffed tubes are used to reduce damage to the trachea caused by the pressure exerted by the cuff against the tracheal wall. The size of the uncuffed ETT is chosen so that it fits snugly within the trachea. However, air leaks between the trachea and the ETT can occur and may induce errors in the measurement of pressure and flow signals. A leak results in overestimation of inspired flow and underestimation of expired flow, as well as overestimation of the mean pressure transmitted to the trachea (Pérez-Fontan, 1985). A leak around the ETT is detected when flow does not reach zero at the end of inspiration while expiration remains essentially normal. This leads to errors in estimates of respiratory mechanics; more precisely, an overestimation of resistance and an underestimation of elastance (Kuo, 1996; Lanteri, 1995). Kondo et al. (1997) showed that, in the presence of a leak, assessing respiratory mechanics during expiration by multiple linear regression provides a good estimation of the true resistance and elastance values. However, their study involved using different leak levels in a physical lung model

and had not been validated in a clinical setting. Also, their method can only be used in the absence of airway obstruction.

1.2.2. Signal processing

The assessment of respiratory mechanics is basically an exercise in inverse modelling, which consists of applying an input (flow or pressure) to the system under investigation and measuring the corresponding output (pressure or flow, respectively), and then interpreting the input-output relationships in terms of a mathematical model. Our understanding of respiratory mechanics relies ultimately on our ability to make accurate measurements of gas pressures and flows as well as on the use of an appropriate mathematical model whose complexity is limited by computational considerations and physiological relevance. The noninvasive assessment of airway and lung tissues mechanical properties in humans has been directly responsible for major advances in understanding, diagnosis and prevention of many of the important respiratory diseases, as well as in ventilator management in intensive care units.

1.2.2.1. Models of the respiratory system

Most parameter estimation methods used in respiratory investigations consist of fitting pressure and flow signals with lumped-parameter inverse models. The main models of the respiratory system will be described below. However, most of them are extensions or variants of a first-order single-compartment linear model, which represents the

respiratory system in terms of only one lumped resistive and one lumped elastic parameter, both constant over the breathing cycle. From a mechanical standpoint, the respiratory system can be modelled as an ensemble of balloons and pipes, in which linear or nonlinear differential equation models relate pressure, flow and volume. These models can be applied in the time domain to track the temporal changes in resistance, elastance and inertance, as well as in the frequency domain to describe the spectral characteristics of the lungs. The models are typically linear in their state variables (e.g. pressures, flows and volumes) but can be nonlinear in their parameters (e.g. resistance, elastance).

In its simplest form, the respiratory system is depicted as a rigid airway of a fixed resistance (R) connected to a single homogeneously ventilated alveolar compartment with a fixed elasticity (E) (Figure 1.7, *left*). This model assumes that the respiratory system behaves linearly so R is independent of $\dot{V}$ and E is independent of V. The pressure P in the alveolar compartment thus increases linearly with V and the pressure difference created between the two extremities of the tube increases linearly with $\dot{V}$. In general, the mechanical properties of the respiratory system are represented by a collection of springs (representing elastances) and dashpots (representing resistances). The mechanical analog of the single-compartment linear model (Figure 1.7, *right*) consists of a spring (E) and a dashpot (R) arranged in parallel, thereby submitted to the same volume deformation.

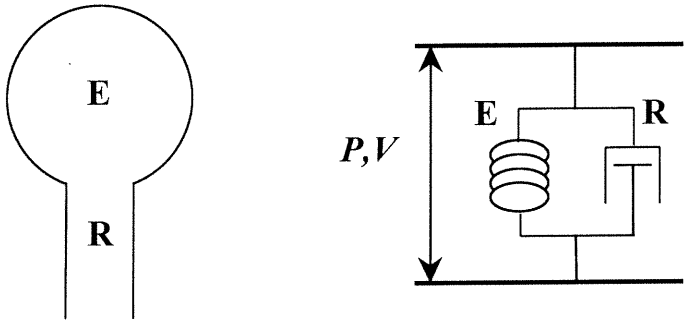

Figure 1.7: ***Left:*** **Anatomic representation of the single-compartment linear model of the respiratory system**, consisting of a rigid bronchial tube, characterized by its resistance to airflow (R), connected to a single uniformly ventilated alveolus, characterized by its elastance (E); ***Right:*** **Mechanical analog**, consisting of a spring (E) and a dashpot (R) in parallel. A pressure P is generated to inflate the lung to a volume V (distance between the two bars); The dashpot represents the energy dissipated during volume cycling and the spring the energy stored.

The equation of motion of the single compartment model of the respiratory system is

$$P(t) = \mathrm{R}\dot{V}(t) + \mathrm{E}V(t) \qquad (7)$$

This model provides a useful description of the behavior of the respiratory system for normal breathing frequencies and tidal volume ranges, where inertial forces can be neglected.

The model parameters are indices of physiological quantities that provide information about the physical structure of interest. Linear and nonlinear mechanisms more complicated than a single resistance and elastance can influence pressure-flow relationships and these mechanisms can be dominant and/or significantly altered in a diseased situation. More complex models are then necessary to more accurately describe the data. One way of extending the simple linear model is to make the parameters of the model nonlinear. The flow dependence of airway resistance (Eq. 3) and the nonlinearity of the static pressure-volume curve as lung volume increases, can be accounted for by

nonlinear expressions for R and E. Nonlinear parameters can also be used to optimize ventilator strategies in artificially ventilated subjects (Kano, 1994) with respiratory distress syndrome (Bates, 1999; Vassiliou, 2000). The other approach to extend the simple linear model is to add more compartments to the model. For example, we know that although airway resistance increases markedly when airways constrict, there is also a frequency-dependent tissue component whose contribution can increase significantly with constriction (Kaczka, 1997; Lauzon, 1992; Ludwig, 1997).

The first order linear model cannot account for the frequency dependence of resistance and elastance, or stress adaptation that occurs in pressure after a sudden volume inflation or deflation. Also, the pressure-volume curve of the lung exhibit hysteresis (Figure 1.3), which means that the inspiratory process is somewhat different from the expiratory process and that some energy is dissipated due to the viscous properties of lung tissues. The single-compartment representation cannot account for these features and therefore more complex models, with at least two compartments, are required. Two categories of linear two-compartment model have been developed - gas redistribution and rheologic models. These models obey the same form of equation of motion.

The gas redistribution models attribute the more complex behavior of the respiratory system to regional differences in ventilation. Otis et al. (1956) first proposed a model of the lungs based on parallel gas redistribution. This model (Figure 1.8A) consists of two single compartment models connected in parallel to a common resistance (central airway resistance R_c). The difference between the time constants τ (expressed as the ratio of R to

E) of each compartment and lung volume history are the two factors deciding the mechanical behavior of this model. Mead (1969) proposed a series model of gas redistribution (Figure 1.8B), consisting of a homogenous lung characterized by an alveolar compartment (E_2) and distal airways (R_2), and connected to a central airway compartment (central resistance R_1 et central airway elastance E_1). Depending on the central and peripheral time constants, a certain amount of inspired gas can remain in the central airways, thus reducing the volume of air available for gas exchange.

The parallel and series models of gas redistribution are mathematically identical since they obey a similar equation of motion. The only difference is in the values of their four respective parameters, which may or may not make physiological sense. Therefore, the choice of one model over another depends on the physiological interpretation to be given to the mechanical parameters. For example, stress relaxation and uneven distribution of ventilation in diseased lungs, such as in emphysema, is best represented by the Otis model. The Mead model can characterize the frequency dependence of resistance and elastance in the context of a respiratory disease such as COPD (Fisler, 1988), but it cannot be applied to normal conditions and breathing frequencies (< 2Hz). Eyles et al. (Eyles, 1981) also chose parallel compartment models to assess respiratory mechanics in spontaneously breathing and mechanically ventilated patients with airway obstruction or stiff lungs. Both models yielded comparable satisfactory results during artificial ventilation but not during spontaneous breathing, during which the parameters obtained with the Mead model were physiologically irrelevant (Eyles, 1982).

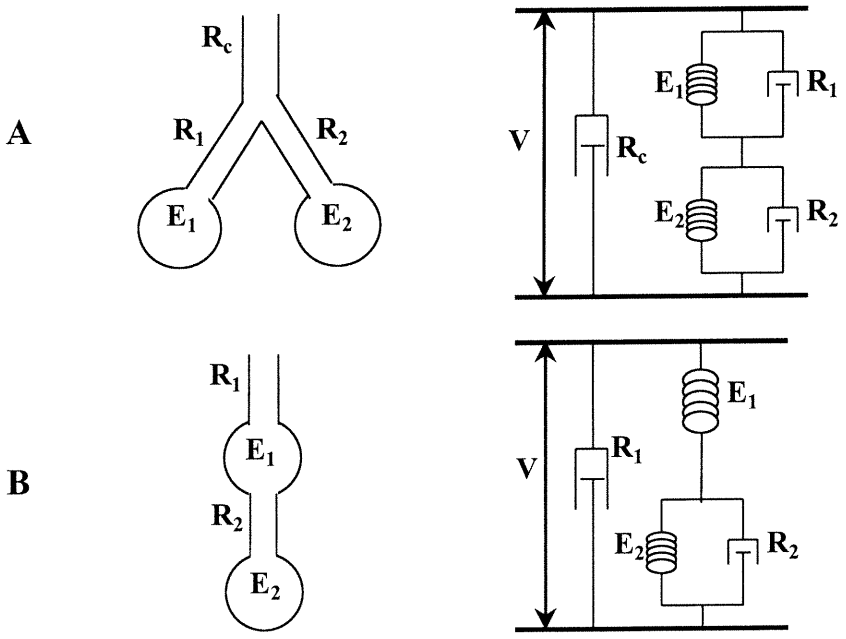

Figure 1.8: Anatomic (left) and mechanical (right) representations of gas redistribution models. *A:* Otis model; *B:* Mead model

The other category of two-compartment model is based on the rheologic properties of the respiratory system tissues. These models usually consist of the elements representing airway resistance and lung elastance in parallel with a viscoelastic or plastoelastic structure. Bates et al. (1989b) developed a model based on the viscoelastic properties of the lung and chest wall tissues. The viscoelasticity of a system embodies characteristics of stress relaxation and hysteresis (Fung, 1981). The mechanical analog for such behavior is the Kelvin body, which consists of two springs and a dashpot (Figure 1.9).

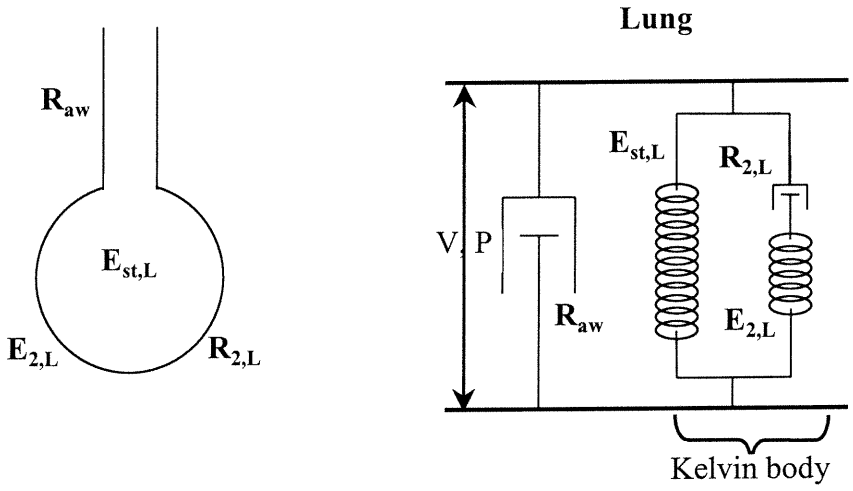

igure 1.9: Anatomic (left) and mechanical (right) analog for the viscoelasticity of the lungs. R_{aw} airway resistance (constant or flow-dependent); $E_{st,L}$ static elastance of the lung; $E_{2,L}$ et $R_{2,L}$ elastic and viscoresitive elements of lung tissues (resp.)

The relative amounts of energy dissipated and stored by the viscoelastic tissues are highly dependent on the frequency at which lung volume is oscillated (Bates, 1989a).

In addition to pressure-volume hysteresis in the lungs, stress adaptation, and frequency dependence of elastic and resistive components, this model describes the double exponential pattern of lung emptying during passive expiration (Bates, 1985a; Chelucci, 1991). Note that Figure 1.9 depicts the behavior of the lungs for spontaneously breathing subjects or mechanically ventilated, but not paralyzed, patients. Chest wall properties can be characterized in anesthetized and paralyzed humans subjects and modelled in the same way by adding in parallel a module comprising a resistance in parallel with a Kelvin body to account for the viscoelastic properties of the chest wall. The equation of motion of the two-compartment viscoelastic model of the lung is

$$E_{2,L}P(t) + R_{2,L}\dot{P}(t) = E_{2,L}E_{st,L}V(t) + R_{2,L}\dot{R}_{aw}\dot{V}(t) + \left[R_L\left(E_{2,L} + E_{st,L}\right) + E_{2,L}R_{aw}\right]\dot{V}(t) + R_{2,L}R_{aw}\ddot{V}(t) \quad (8)$$

This model assumes that the lung is homogeneously ventilated, which is a valid approximation in normal lungs in the physiological range of breathing frequencies. Indeed, homogenous distribution of ventilation has been confirmed experimentally in normal dog lungs with the alveolar capsule technique and therefore, the viscoelastic model best fits the mechanical behavior of the normal respiratory system. However, this assumption is less valid as frequency increases or during severe bronchoconstriction where lungs become inhomogeneous (Sato, 1993) and it is thus necessary to include inertance or add more alveolar compartments each with different time constants.

A plastoelastic element (Stamenovic, 1990) can also be added to the single compartment model to account for pressure-volume hysteresis, but the existence of plasticity has not been confirmed during in vivo experiments and the model parameters have been found difficult to interpret mechanically (Navajas, 1990; Similowski, 1991).

In summary, the choice of a model for the respiratory system is highly dependent on the disease or physiological context under investigation (Similowski, 1991), and the interpretation of model parameters depends on the pressure (transpulmonary, airway opening or alveolar) used in the equation of the model. Since a model is only an approximation to the real situation, the estimated dependent variable (pressure) always includes both a deterministic component and a stochastic component representing noise. If the order of complexity of the model is not sufficient, the residuals between the

computed and the recorded dependent variable will be patterned and not random. To obtain random residuals, one has to increase the model complexity, thus increasing the number of parameters to be estimated and raising problems of physiological interpretation.

1.2.2.2. Parameter estimation in the time domain

Many identification methods have been developed, the quality and amount of information available increasing with advances in the field of signal processing and with the availability of computers. Major insights in the field of respiratory physiology and ventilation strategy have been obtained with the Mead and Whittenberger (Mead, 1953) and the multiple linear regression (Lorino, 1986; Uhl, 1974) methods.

Mead and Whittenberger method

According to the single-compartment linear model, the pressure that needs to be generated in order to produce a given flow and volume in the lungs is the sum of a resistive pressure, an elastic pressure and an inertia-related pressure (Von Neergaard and Wirz in Mead (1953))

$$\boldsymbol{P} = \boldsymbol{P_{res}} + \boldsymbol{P_{el}} + \boldsymbol{P_{in}} = R\dot{V} + EV + I\ddot{V} \qquad (9)$$

in which the lung mechanical parameters R, E and I are linearly related to flow $\dot{V}$, volume V and acceleration $\ddot{V}$ respectively. Mead and Whittenberger (Mead, 1953) proposed that lung mechanics can be assessed during spontaneous breathing by the so called "electrical substraction method". This necessitates the measurements of P_{eso}, $\dot{V}$

and pressure at the mouth (P_m). Transpulmonary pressure (P_L) has both static and dynamic components, represented as the sum of an elastic (P_{el}) and a resistive pressure (P_{res}), assuming that inertial effects are negligible. The idea is to determine P_{el} such that the P_L-$\dot{V}$ relationship becomes a single curve with no looping (Figure 1.10), after which lung elastance (E_L) is estimated by the ratio of P_{el} to V.

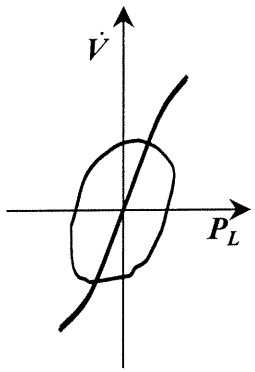

Figure 1.10: Flow vs. transpulmonary pressure curves. *Closed loop*: before substraction of elastic pressure; *Linear curve*: resistive pressure (transpulmonary pressure after substraction of elastic component).

From P_{res}, which is equal to P_L minus P_{el}, we can compute lung resistance (R_L) as the ratio of P_{res} to $\dot{V}$. For many years, the Mead and Whittenberger method was the reference method for the computation of dynamic E_L and R_L in spontaneously breathing subjects and artificially ventilated patients, especially newborns and infants. This approach assumes that the P-V relationship is linear throughout the breath, leading to a constant elastic parameter. Although this is valid in subjects with normal lung function and in the physiological range of breathing, this assumption breaks down in the presence of lung disease (e.g. hyaline membrane disease), with chest wall distortion or during mechanical ventilation when lungs are inflated up to the nonlinear portion of their P-V curve. Also, the method uses measurements of P and V at only two points within the

breathing cycle in order to estimate E_L, which makes it sensitive to noise (e.g. cardiogenic oscillations on P_{eso} signal) and less robust compared to regression techniques in the presence of a leak around the ETT (Kuo, 1996).

Multiple linear regression

Currently, the conventional way to assess respiratory mechanics is to fit P, $\dot{V}$ and V data to the first-order single-compartment linear model by linear regression techniques (Baconnier, 1995; Lanteri, 1995; Peslin, 1992; Rousselot, 1992; Seear, 1991). Unlike the Mead and Whittenberger approach, this method computes R and E using all the data points within the breath. The equation of motion of the single compartment model is

$$\boldsymbol{P} = R\dot{\boldsymbol{V}} + E\boldsymbol{V} + P_0 \qquad (10)$$

where P_0 is the residual pressure at end-expiration (when $\dot{V}$ and V are equal to zero). Some studies omit the parameter P_0 in the equation since it is substracted in advance from P (equivalent to Eq. 7). This equation can be written in a matrix notation for n measurements of the variables

$$\boldsymbol{Y} = \boldsymbol{X}.\boldsymbol{A}$$

where $\boldsymbol{Y}$ is the vector of dependent variables,

$$\boldsymbol{Y} = \begin{bmatrix} \boldsymbol{P}_1 \\ \boldsymbol{P}_2 \\ \vdots \\ \boldsymbol{P}_n \end{bmatrix}$$

$\boldsymbol{X}$ is the matrix of independent variables,

$$\boldsymbol{X} = \begin{bmatrix} \dot{\boldsymbol{V}}_1 & \boldsymbol{V}_1 & 1 \\ \dot{\boldsymbol{V}}_2 & \boldsymbol{V}_2 & 1 \\ \vdots & \vdots & \vdots \\ \dot{\boldsymbol{V}}_n & \boldsymbol{V}_n & 1 \end{bmatrix}$$

and $\boldsymbol{A}$ is the vector of parameters to be estimated

$$\boldsymbol{A} = \begin{bmatrix} R \\ E \\ P_0 \end{bmatrix}$$

The multiple linear regression (MLR) technique estimates the parameters of a model that minimize the sum of the squared deviations between the measured pressure and the pressure reconstructed from the model. The least-squares estimate $\hat{\boldsymbol{A}}$ of the parameter vector is

$$\hat{\boldsymbol{A}} = \left[\boldsymbol{X}^{\boldsymbol{T}}\boldsymbol{X}\right]^{-1} \cdot \boldsymbol{X}^{\boldsymbol{T}} \cdot \boldsymbol{Y} \tag{11}$$

R and E may be estimated for one or a series of breaths, or for inspiration and expiration separately. However, the parameter values are assumed constant over the analyzed data segment.

Nonlinearities in respiratory mechanics can be introduced into the single compartment model by making R and E nonlinear. For example, volume-dependent

$$\boldsymbol{P} = R\,\dot{\boldsymbol{V}} + \left(E_1 + E_2\boldsymbol{V}\right)\boldsymbol{V} + P_0$$

or flow-dependent (Kano, 1994)

$$\boldsymbol{P} = \left(K_1 + K_2\left|\dot{\boldsymbol{V}}\right|\right)\dot{\boldsymbol{V}} + E\,\boldsymbol{V} + P_0$$

single compartment models are used to account for overdistension of the lung during mechanical ventilation or mixed flow regimen in the airways, respectively. Although these equations are nonlinear in their dependent variables (V, V^2, $\dot{V}$, $\dot{V}|\dot{V}|$), they are linear in their new parameters (E_1, E_2, K_1, K_2), which can therefore be estimated using MLR.

Recursive techniques

Continuous monitoring of mechanical parameters is important as a tool for assessing respiratory mechanical status, optimizing ventilator settings in mechanically ventilated subjects, and tracking the timing and effects of a drug. The recursive implementation of the multiple linear regression, called recursive least squares (RLS) technique, provides the time course of mechanical parameters by updating the parameter values each time a new P and $\dot{V}$ data point arrives. A finite memory may be incorporated into the algorithm, such that past data have an exponentially decreasing influence on the current parameter estimate. The time-constant of the memory represents a trade-off between noise sensitivity and the ability of the algorithm to track rapid parameter changes. For example, a large time-constant value is used to describe relatively slow changes in mechanical parameters such as the ones occurring from a healthy to a critical state. Conversely, a smaller value gives access to more rapid variations of the parameters, and would therefore be useful to study the effect of bronchoconstriction on R and E.

Avanzolini et al. (1985) were the first to adapt recursive algorithms to a cardiorespiratory setting. They developed a real-time algorithm that expresses the impedance of a two-

compartment system in discrete-time form. With the same method, Chapman et al. (1989) found that both the one- and two-compartment models applied separately to inspiration and expiration provide relevant information about the diseased lung. They found that recursive estimation of the four mechanical parameters of the parallel model together with the ratio between the time constants of the two compartments, was useful in following the development of edema. Their primary concern was the progress of a pathology so they focused on slow changes in the parameters and used a large memory time-constant. Barbini et al. (1988) measured mechanics in mechanically ventilated dogs before and after oleic acid-induced respiratory distress syndrome. This study showed that RLS successfully detected slow changes in mechanics due to the pathology, without being too sensitive to noise. Recently, Nucci et al. (2000) looked at the RLS estimates of intrinsic end-expiratory pressure (PEEPi) in mechanically ventilated subjetcs as a tool for assessing dynamic hyperflation caused by decline in the patient's status or by inadequate ventilator settings.

In general, real-time recursive algorithms have the advantage of providing parameter values that follow slow changes of a system due to its inherent nonlinearity and non-stationarity. However, they are less efficient than conventional MLR because the parameter estimates they provide have a higher variance (Avanzolini, 1985).

The physiological meaning of the parameters of a multiple compartment model can be difficult to determine. Eyles et al. (Eyles, 1981; Eyles, 1982) showed that the confidence intervals of the parameters estimated with both parallel and serial two-compartment

models were highly dependent on the context, such as during quiet breathing, artificial vs. spontaneous breathing or respiratory disease. Also, when airways become obstructed, such as following a bronchoprovocation test or an asthma attack, it is important to detect rapid parameter changes. Therefore, the most recent studies dealing with recursively estimated parameters have focused on the fast-tracking ability of the technique applied to the single compartment linear model of the respiratory system. Lauzon and Bates (Lauzon, 1991) developed a RLS method that utilizes a variable memory time-constant, which is inversely related to the sum of squared residuals between the measured and the predicted pressures. In other words, the time-constant increases when data are stable and residuals are small, and decreases when parameters change rapidly and residuals are large. Avanzolini et al. (1992) used a similar approach to monitor the mechanics of arterial circulation, in which the memory time-constant was adjusted in order to keep the sum of squared residuals below an arbitrary threshold.

Bates and Lauzon (Bates, 1992) developed a method that represents respiratory mechanics parameters as time-varying quantities whose values vary in a deterministic manner throughout a breath. Fitting a model to data classically assumes the residuals between the measured and estimated dependent variable (i.e. P) describe only random noise. This is never precisely the case when dealing with respiratory data. In the method proposed by Bates and Lauzon, the memory time-constant is chosen in order to obtain sufficiently small residuals so as to represent only noise. Subsequent studies (Avanzolini, 1997; Nucci, 2000) involving rapidly changing mechanical parameters have used this specific strategy for the determination of the time-constant. This approach gives rise to

recursive estimates of R and E that vary throughout the breath. R and E over the data segment of interest are then expressed as histograms where each R and E data point is weighted by the corresponding estimate of uncertainty (also provided by the RLS algorithm). This study showed that even during normal breathing, the information-weighted histograms for each breath have a certain width, which means that the parameters are not constant throughout the breath due to higher order and nonlinear behavior of the respiratory system.

Interrupter technique

The interrupter technique was developed for the determination of passive respiratory mechanics (Von Neergaard and Wirz in Similowski (1989)). It allows the computation of resistance as the ratio of the sudden pressure change subsequent to a rapid occlusion of the airways at the end of a passive inflation, to the flow immediately prior to occlusion (Figure 1.11).

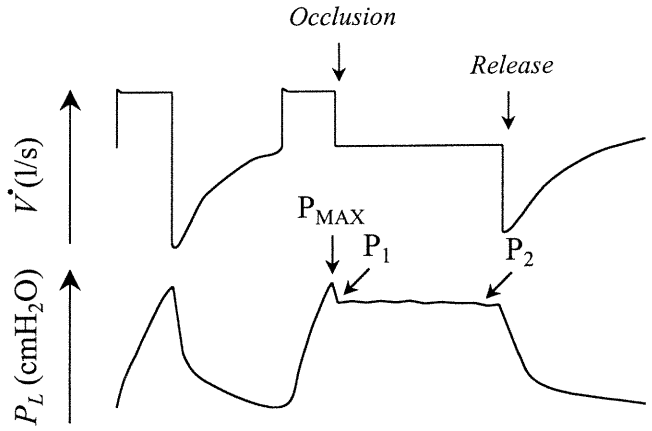

Figure 1.11: Schematic of the changes in airflow (top) and in transpulmonary pressure (bottom) after flow interruption. P_{MAX}: peak pressure before occlusion; P_{MAX}-P_1: sudden fall in pressure immediately after flow interruption; P_2: plateau pressure representing quasi-static recoil pressure of the lungs

The sudden pressure drop that occurs with airway occlusion represents the pressure dissipation within the central airways. Therefore, airway resistance can be approximated by the ratio of this pressure difference to the airflow prior to the occlusion. The slow pressure decay (P_1-P_2) accounts for the viscoelastic properties of the lung tissues as well as for any time-constant inequalities (Bates, 1985b). Dividing this pressure change by the airflow preceding the occlusion gives the corresponding tissue resistance (ΔR). In normal lungs, the contribution of pulmonary tissues to the total lung resistance is small (originating from stress relaxation) (D'Angelo, 2000). In subjects with an obstructive pulmonary disease (Guerin, 1993), the degree of frequency-dependence of the parameters increases, as a result of an increase in the contributions of both viscoelastic properties and time constant inequality. From ΔR values, it is then possible to compute the viscoelastic parameters depicted in Figure 1.9. The properties of the chest wall and respiratory system can be determined in the same way when using P_{eso}.

Assessment of flow limitation from P, $\dot{V}$ and V measurements

The principles of flow limitation are similar whether it occurs during inspiration and/or expiration. The various ways to characterize its presence are therefore applicable to both situations. A widely used but qualitative method consists of plotting flow-volume curves ($\dot{V}$ - V). While a convexity of the expiratory segment is the criterion for expiratory flow limitation, the flattening and/or saw-tooth shape during inspiration can reflect IFL and/or UAW wall fluttering (Figure 1.12).

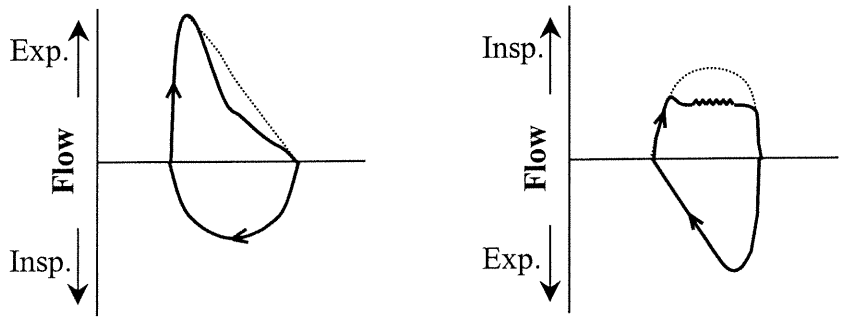

Figure 1.12: Schematic representation of the $\dot{V}$-V loops obtained during flow limitation in expiration (left) and in inspiration (right); *dashed line*: normal tidal breath.

The $\dot{V}$ - V tracings, which are primarily used in the context of expiratory flow limitation, are useful in the detection of an abnormality in the breathing pattern but lack specificity. Series et al. (1995) noted that FIF50 (inspiratory flow at 50% of forced vital capacity) is decreased in snoring patients with and without OSA, suggesting that these patients have increased upper airway resistance. The presence of a saw-tooth pattern on the flow-volume curves, as well as a FEF50 /FIF50 (ratio of expiratory flow to inspiratory flow at 50% of forced vital capacity) greater than 1.0 were thought to be characteristic of IFL during sleep (Series, 1995). However, this approach failed to detect the obstructed breath when the expiratory limb of that same breath was also limited (Sanders, 1983; Stanescu, 1996). In addition, many investigations (Hoffstein, 1989; Katz, 1990; Rauscher, 1990; Vincken, 1985) reported a low specificity for the combination of these tests, and no correlation was found between the severity of the disease (respiratory disturbance and desaturation indexes), and the information from the $\dot{V}$ - V curves.

A quantitative assessment of respiratory mechanics in the context of flow limitation would provide information on airway caliber and stiffness of lung tissue, both of which are hallmarks of various respiratory obstructive diseases. Nonetheless, the presence of flow limitation (Figure 1.6) is likely to complicate the estimation of respiratory mechanics since the usual concept of resistance ceases to apply and the linear models cannot be fit over the entire breathing cycle. In addition, in subjects with sleep-disordered breathing, inspiratory flow patterns can be very different (Aittokallio, 2001) and mechanics parameters may be misleading depending on the method of detection (Clark, 1998; Lorino, 1998).

Even though the Mead-Whittenberger method has been surpassed by MLR for many clinical applications, the latter approach is only valid when the system is mechanically stable over the time during which the measurements are made (Peslin, 1992). Indeed, in many studies dealing with UAW obstruction and flow limitation during sleep, the Mead-Whittenberger method is still preferred to MLR (Lofaso, 1998; Tuck, 1999) for the computation of dynamic elastance and P_{res}. Resistance is then obtained either by taking the value of P_{res} at peak flow or at some fixed intermediate flow (Lofaso, 1998), by taking the mean values for inspiration and expiration, or by least square analysis separately of inspiratory and expiratory phases.

An alternative to these methods is to identify mechanical parameters in the Fourier domain, which will be developed in the next section. We will describe how both expiratory flow limitation caused by an obstructive pulmonary disease (Kaczka, 1999;

Peslin, 1996) as well as inspiratory flow limitation caused by upper airway obstruction during sleep (Farre, 1997a,b) can be quantified by analysis of P and $\dot{V}$ signals in the frequency domain.

1.2.2.3. Parameter estimation in the frequency domain

As mentioned earlier (Section 1.2.2.1), respiratory mechanics are frequency dependent, in relation to the viscoelasticity of the respiratory (lung + chest wall) tissue and ventilation inhomogeneity. This frequency dependence of respiratory mechanics can be evidenced by the measurement of the mechanical impedance Z of the respiratory system. The measurement of Z by analysis of P-$\dot{V}$ relationships in the frequency domain is based on the assumption of linearity of the respiratory system. Z is a complex function of frequency that takes into accounts both energy dissipation (resistive behavior) and storage (through elastic or inertial mechanisms) characteristics of the system (Figure 1.13)

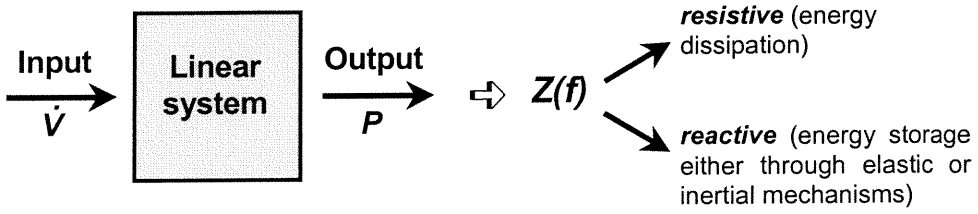

Figure 1.13: Principles for measuring mechanical impedance. *Z(f)*: ratio in the Fourier domain of pressure P to flow $\dot{V}$

The forced oscillation technique (FOT) is a simple and noninvasive approach to measure the mechanical impedance of the respiratory system, defined as the complex ratio of

pressure to flow (Daroczy, 1982; DuBois, 1956). To obtain input impedance (Z_{in}), a flow (or pressure) perturbation is applied externally (usually at the mouth/airway opening) by means of an external generator (loudspeaker, computer-controlled piston oscillator) and the resulting pressure (or flow, respectively) is measured simultaneously at the same site (Figure 1.14).

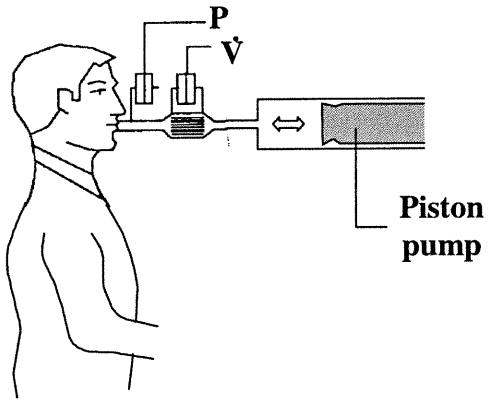

Figure 1.14: System for measurement of input impedance Z_{in}.
Pressure P and flow $\dot{V}$ are recorded at the same site.

This approach requires no active cooperation from the subject and is therefore very easy to perform in a clinical environment. It has been used successfully in adults as well as infants for the assessement of lung function (in the presence of an airway obstruction) (Badia, 1998; Farre, 1999; Lebecque, 1997; Van Noord, 1991), during spontaneous breathing and during invasive and noninvasive ventilation (Navajas, 1990; Peslin, 1993a) and recently during sleep studies to characterize the degree of UAW obstruction (Farre, 2001b; Farre, 1997a; Lorino, 1998). The measurement of Z_{in} is influenced by all the respiratory structures, especially the UAW and cheeks (Cauberghs, 1989; Hantos, 1986; Peslin, 1986a). Physiological and clinical interpretation depends on the choice of the model and the frequency range of interest (Lutchen, 1993a).

To obtain transfer impedance (Z_{tr}), pressure oscillations are imposed around the chest wall, usually by having a subject sitting in a modified plethysmographic chamber, while flow is measured at the airway opening. Z_{tr}, although more cumbersome to obtain than the Z_{in}, can provide information about tissues and airways properties (Lutchen, 1993a; Lutchen, 1992) and is less influenced by UAW shunting than is Z_{in} (Lutchen, 1998). The major technical problem arises from the difficulty of maintaining a uniform pressure field over the body surface, especially at high frequencies (Peslin, 1986b). Transfer impedance has advantages over input impedance in the context of severe bronchoconstriction, which is characterized by a significant increase in both resistance and reactance and often accompanied by ventilation inhomogeneity. In such a situation, central airways tend to act as a shunt to flow oscillations applied at the mouth, which can limit the information obtained concerning the more distal airways (Lutchen, 1998).

Forced oscillatory signal

The use of FOT is based on linear system theory, which implies that the respiratory system behaves linearly and that the linearity condition is not altered by the perturbation applied. Respiratory mechanics are flow and lung volume dependent and have airway and tissue properties that vary substantially over the entire physiological range of frequencies and amplitudes. One way to proceed is to apply a broadband pseudo-random oscillating flow signal at the airway opening by means of a loud-speaker or a computer-controlled piston oscillator, estimate the impedance of the system and interprete it using the appropriate mathematical model. The oscillations can be applied to apneic subjects (Hantos, 1986; Sly, 1996) or superimposed on spontaneous breathing (Lutchen, 1993b;

Peslin, 1986a). In the latter case, the spectral content of the perturbation should not overlap that of respiration.

A composite flow perturbation $\dot{V}(t)$ is defined as follows

$$\dot{V}(t) = \sum_{i=1}^{n} A_i \sin(2\pi f_i t + \phi_i) \qquad (12)$$

where f_i are the frequencies of the sinusoids, A_i their amplitudes and ϕ_i their phases. A useful design strategy is to make f_i mutually prime in order to avoid harmonic distortion and to that extent, some studies (Lutchen, 1993b; Suki, 1992) used sets of frequencies for which none of the sums or differences of the f_i are equal to any of the f_i. The A_i are chosen to optimize signal-to-noise ratio at each f_i. The ϕ_i may be chosen in order to minimize peak-to-peak excursions of the resulting signal (Lutchen, 1993b; Suki, 1992). The peak-to-peak amplitude of the perturbation should not typically exceed 10% of the individual's tidal volume if one wants to be sure that respiratory system behaves linearly.

The individual frequencies in the flow and resulting pressure signals are separated by fast Fourier transform (FFT), after which the amplitude and phase relationships between the pressure-flow pair at each frequency are determined. Alternatively, the impedance can be expressed in terms of its real and imaginary part, or its resistance (R) and reactance (X), respectively.

Choice of the model

The impedance of the single compartment linear model (Figure 1.7) is

$$Z(f) = R - iE/(2\pi f) \tag{13}$$

The real part is thus considered frequency-independent whereas the imaginary part (reactance) is negative and hyperbolic with frequency.

The impedance of the two-compartment linear viscoelastic model (Figure 1.9) is:

$$Z(f) = R_{aw} + \frac{E_{2,L}^2 R_{2,L}}{E_{2,L}^2 + 4\pi^2 f^2 R_{2,L}^2} + i\frac{E_{st,L} + 4\pi^2 f^2 E_{2,L} R_{2,L}^2}{\left(E_{2,L}^2 + 4\pi^2 f^2 R_{2,L}^2\right) 2\pi f} \tag{14}$$

The resistive and reactive parts are frequency-dependent. The parallel and series two-compartment linear models (Figure 1.8) have an impedance of similar form.

The real part of Z (Figure 1.15) represents the resistive component (R) and its imaginary part represents the reactive component (X). An inverse frequency dependence of respiratory tissue impedance can be seen at low frequencies (typically below 2 Hz) in both R and X. The plateau at higher frequencies in R represents the frequency-independent airway resistance. Studies have shown that tissue resistance decays hyperbolically over the range of physiological breathing frequencies whereas airway resistance remains fairly constant (Bates, 1989b; Lutchen, 1994).

If we add an inertive component (I_{aw}) to the single-compartment linear model, its reactance becomes

$$X = i \cdot \left(I_{aw} - \frac{E}{2\pi f} \right) \tag{15}$$

The frequency at which this quantity equals zero is called the resonant frequency, with the inertive properties of the airways dominating at frequencies above this point (Figure 1.15, dashed line).

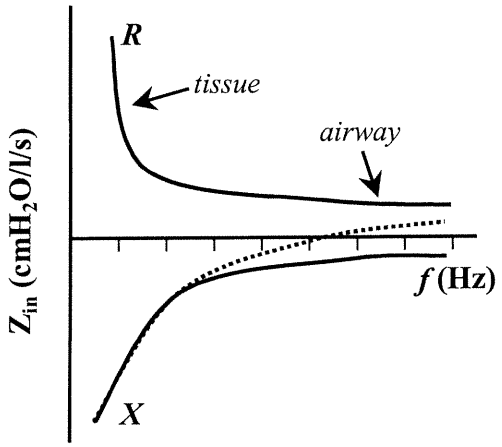

Figure 1.15: Schematic of the partitioning of the respiratory system input impedance into its resistive (R) and reactive (X) components based on the viscoelastic model. *Dashed line*: X when inertia (dashed line) is considered

The low frequency behavior of the respiratory system under normal conditions and during modest levels of lung constriction can be characterized by measuring then fitting input impedance data to the so-called constant-phase model (Farre, 1994; Hall, 2000; Lutchen, 1996a; Lutchen, 1994; Sly, 1996) (Figure 1.16). This model contains a homogeneous airway compartment, characterized by a frequency-independent resistance (R_{aw}) and inertance (I_{aw}), leading to a viscoelastic "constant-phase" tissue compartment in which the phase angle between pressure and flow across the tissues is independent of frequency. This model implies that there is a coupling of dissipative (expressed as tissue damping G) and elastic (expressed as tissue elastance H) processes in the lung tissues, and their ratio, termed hysteresivity η, is constant with frequency. This model is believed

to describe the low-frequency behavior of the lung better than other lumped viscoelastic models.

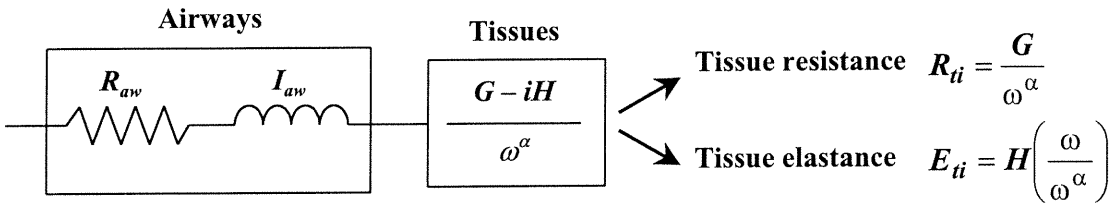

Figure 1.16: Constant-phase model representing airway and tissue contributions to total lung resistance. R_{aw}, I_{aw}: airway resistance and inertance (resp.); G, H: tissue damping and tissue elastance; ω: angular frequency; α: degree of frequenc dependence, function of η equal to G/H

Fitting Z_{in} to the constant-phase model (Eq. 16) showed (Hantos, 1992; Lutchen, 1994) that a major response to bronchoconstriction occurs in lung tissues, resulting in a large increase in R_{ti} and E_{ti}.

$$Z(f) = R_{aw} + i2\pi f I_{aw} + \frac{G - iH}{(2\pi f)^{\alpha}} \qquad (16)$$

With severe constriction, significant increases in R_{aw} and airway inhomogeneities occur as well (Bates, 1988a; Lutchen, 1996b; Suki, 1992). H thus seems to be a reliable indicator of tissue changes during severe constriction. The partitioning of airway and tissue properties using Z_{in} estimated from a composite $\dot{V}$ perturbation avoids the use of alveolar capsules and thus represents an effective noninvasive tool for the assessment of airway and tissues mechanical characteristics in humans as well as in animals (Hantos, 1992; Lutchen, 1994).

Frequency range and applications

The interpretation of the impedance depends on whether Z_{tr} or Z_{in} is being used, on the choice of the model, on the species under study (humans/animals), and also on the frequency range used to collect the data (Lutchen, 1996c) (Table 1.3). The mechanical characteristics of healthy subjects can be easily obtained in the 2-32 Hz frequency range by fitting input impedance data to the single compartment linear model described above (Michaelson, 1975; Oostveen, 1989; Peslin, 1985; Rotger, 1991).

Table 1.3: Summary of the information available from impedance data as a function of the frequency range. Adapted from Lutchen and Suki (1996c)

f < 2 Hz	2 Hz < f < 64 Hz	100 Hz < f < few kHz
Tissue structure/function	Lumped total respiratory properties	Airway geometry/structure
Airway tissue coupling	Lumped airway vs. tissue properties	Airway walls
Nonlinear vs. linear mechanisms		Airway wall - airway geometry interactions
Airway inhomogeneties		
Mechanical efficiency		

Noninvasive separation between airway and tissue properties can be obtained in humans with transfer impedance Z_{tr} in the 2-64 Hz frequency range (Lutchen, 1992). More specifically, the use of Z_{tr} over the 32-64 Hz range gives reliable estimates of tissue properties (Lutchen, 1993a). Although Z_{in} is very useful in humans for the characterization and understanding of lumped airway properties in respiratory diseases, it cannot isolate the tissue properties over this frequency range (Lutchen, 1990).

The mechanisms that influence breathing in subjects with healthy or diseased lungs, such as the viscoelastic properties of the tissues, the mechanical coupling between the airways and tissues, lung inhomogeneties (Lauzon, 1995; Lutchen, 1996a; Lutchen, 1994) and nonlinearities (Suki, 1997; Suki, 1995), are characterized by measuring impedance at frequencies below 2 Hz.

Impedance data at very high frequencies (up to several kHz), obtained using the acoustic reflection technique, provides information about airway geometry and airway wall properties. An acoustic impulse travels down a wave tube into the airways and the input waveform and its reflection from the airway walls are recorded. The area profile of the airway is reconstructed from the analysis of the reflected sound waves, and displayed as a function of the distance along the airways. This technique represents the airways as a series of discrete cylinders, and so assumes rigid airway walls as well as a symmetrical airway tree. These assumptions are the main limitations of the acoustic reflection technique (Brooks, 1984; Marshall, 1991). Applications of this technique include the determination of changes in lung density (hence lung morphology) caused by changes in lung volume (Pohlman, 2001) and the detection of changes in tracheal (Brooks, 1984; Fredberg, 1980), bronchial (Julia-Serda, 1996) and pharyngeal (Bradley, 1986; Martin, 1995; Schwab, 1998) cross-sectional areas along the airway, allowing continuous assessment of the patency/geometry of the airway of interest. Although the use of acoustic reflection equipment may be impractical in some clinical situations, this technique have recently provided promising results for the detection of the site of UAW collapse during sleep in subjects with sleep-disordered breathing (Huang, 2000) and the

detection of an obstruction in the endotracheal tube in mechanically ventilated babies (Jarreau, 2000).

FOT and sleep-disordered breathing

There are numerous applications of FOT in the context of sleep-disordered breathing, including the determination of the site of pharyngeal collapse, the evaluation of the efficacy of various therapeutic methods for sleep apnea, and the measurement of UAW collapsibility during sleep. The assessment of UAW obstruction during CPAP titration (Farre, 2001b; Navajas, 2000; Yen, 1997) can be done by applying an oscillatory pressure signal to the respiratory system through the nasal mask and estimating respiratory impedance from the complex ratio of nasal pressure to airflow signals. The forced oscillatory signal consists of a single frequency, typically above 4Hz, where the resistive component mainly accounts for airway resistance and the reactive component is close to zero (near resonant frequency in humans).

Farre et al. (1997a) submitted an airway analog to increasing levels of CPAP. They showed that the amplitude of the impedance ($|Z|$) positively correlates with the degree of UAW obstruction. Several experimental studies (Badia, 1998; Badia, 1999; Farre, 2001b; Yen, 1997) confirm the ability of FOT to provide real-time estimates of the level of obstruction and therefore determine the appropriate level of pressure that can restore UAW patency. The estimate of airway impedance can thus be used as a feedback signal to adjust CPAP pressure in order to eliminate sleep apnea. Reisch et al. (2000) applied FOT to simulated situations of UAW collapse in a respiratory system analog and showed

that changes in the temporal pattern of the phase angle between P and $\dot{V}$ correlated with changes in the stiffness of the UAW walls. This showed that FOT is a sensitive tool for early detection of UAW collapse. Although there are still some limitations due to the presence of leaks around the nasal mask and the occurrence of mouth breathing, the FOT may be suitable for assessing UAW obstruction in sleep apnea, for diagnosing the type of apnea (obstructive /central), and for optimal CPAP titration.

CHAPTER 2

CORRECTION OF AIRFLOW MEASUREMENT IN THE PRESENCE OF A LEAK BETWEEN THE TRACHEA AND ENDOTRACHEAL TUBE

Authors :

Bijaoui Eve, Carry Pierre-Yves, Eberhard André, Andrini Pierre, Perdrix Jean-Pierre and Baconnier Pierre

Published in :

Canadian Journal of Anesthesia (1997); 44(2): 216-224

RÉSUMÉ

Objectifs: Présenter une méthode d'estimation de la fuite entre trachée et sonde endotrachéale chez le nouveau-né afin de compenser l'erreur sur la mesure du débit et de surveiller les caractéristiques mécaniques respiratoires par l'analyse des signaux de débit et de pression mesurés à l'origine de la sonde.

Méthodes: On suppose la résistance de fuite (*Rf*) constante sur un cycle et on mesure les caractéristiques résistives du tube endotrachéal.

La méthode a été validée avec un modèle mécanique de poumon et appliquée aux enregistrements de trois nouveau-nés prématurés admis en réanimation néonatale pour des détresses respiratoires. Une méthode des moindres carrés a permis d'estimer, avant et après correction du débit, la pression positive de fin d'expiration (PEEP).

Résultats: Pour les simulations, l'estimation de *Rf* concorde avec la mesure directe. En clinique, l'efficacité de la correction est démontrée: le débit corrigé revient à zéro pendant la pause de fin d'inspiration.

En simulation, avant correction du débit, la PEEP est sous-estimée de 10 à 20 cmH_2O, alors qu'après correction l'erreur est inférieure à 2 cmH_2O. En clinique, la PEEP estimée passe de valeurs négatives (-0.3 ± 1.3 cmH_2O avant correction) à des valeurs positives (3.6 ± 0.7 cmH_2O après correction) supérieures à la PEEP imposée (2 cmH_2O).

Conclusions: Cette méthode est simple et son efficacité a été démontrée. Elle pourrait être utilisée avec profit sur des patients adultes, la correction sur le débit n'étant pas effectuée en l'absence de fuite.

ABSTRACT

Purposes: Estimate leak between the endotracheal tube and the trachea in newborns in order to compensate error to airflow measurement and to monitor the mechanical parameters from pressure and flow signals.

Methods: The leak resistance (*Rf*) is supposed to be constant over a respiratory cycle and the resistive properties of the endotracheal tube are evaluated.

This method was validated with the help of a mechanical test lung and assessed on records of three newborns from the intensive care unit, mechanically ventilated for respiratory distress. We used a least squares method for the estimation of positive end expiratory pressure (PEEP) in both newborns and simulated data.

Results: Direct measurements of simulated leak resistances in the mechanical lung were in good agreement with our estimation of leak resistances. In newborns, the success of the flow correction was evidenced on end inspiratory pauses: corrected flow was zero while raw data showed a constant nonzero flow.

In the simulated lung, the PEEP with non corrected flow was underestimated from 10 to 20 cmH_2O while the corresponding underestimation with corrected flow was less than 2 cmH_2O. In newborns, flow correction changed the estimated PEEP from negative values (-0.3 ± 1.3 cmH_2O before correction) to positive values (3.6 ± 0.7 cmH_2O after correction) that were higher than the imposed PEEP (2 cmH_2O).

Conclusions: The efficiency of this simple method has been demonstrated. It could be used successfully on adult patients, knowing that there will not be flow correction in absence of leak.

2.1. INTRODUCTION

Les nouveau-nés ventilés en réanimation néonatale sont intubés avec des sondes endotrachéales sans ballonnet, d'une part, pour éviter des traumatismes de la trachée que le ballonnet peut induire et d'autre part, car les sondes sans ballonnet maximisent le diamètre interne disponible. Ces sondes ne peuvent assurer l'étanchéité de la liaison sonde-trachée et on observe une fuite entre la sonde et la trachée dans la plupart des cas (Perez Fontan, 1985). Cette fuite présente deux inconvénients: d'une part il est difficile d'assurer une ventilation pulmonaire correcte en présence d'une fuite, et, d'autre part, il n'est plus possible d'utiliser les signaux de débit et de pression mesurés à l'entrée de la sonde endotrachéale pour estimer les caractéristiques mécaniques du système respiratoire (Perez Fontan, 1985). Nous présentons une méthode de correction de ce débit basée sur l'hypothèse que la résistance de fuite (*Rf*) est constante. Une fois la fuite connue, il est possible 1) si la fuite est trop importante, de remplacer la sonde endotrachéale par une sonde de diamètre supérieur, 2) sinon, d'estimer le débit pulmonaire vrai et donc d'appliquer des méthodes maintenant classiques d'analyse des signaux débit et pression (Peslin, 1992) qui permettent de surveiller les caractéristiques mécaniques du système respiratoire. Cette méthode de calcul de *Rf* a été validée à l'aide d'un modèle mécanique de poumon et appliquée sur des enregistrements de nouveau-nés. Nous avons en particulier recherché quel était l'effet d'une telle correction sur l'estimation de la pression élastique de fin d'expiration obtenue à l'aide de la méthode des moindres carrés appliquée aux signaux débit et pression (Peslin, 1992; Uhl, 1974).

2.2. MÉTHODOLOGIE

2.2.1. Théorie

Calcul de Rf à partie des signaux de débit et pression

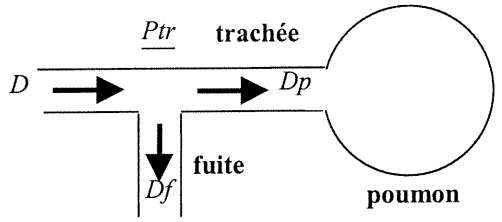

Figure 2.1: Représentation schématique du circuit respiratoire avec une fuite. *Ptr: pression* trachéale à la sortie de la sonde; *D* : débit dans la sonde trachéale (gaz provenant du respirateur); *Dp* : débit pulmonaire; *Df* : débit de fuite.

On suppose que la résistance de fuite (*Rf*) est constante sur un cycle respiratoire, c'est à dire qu'elle ne dépend pas du débit ou de la pression.

En caractérisant les différents écoulements dans le circuit respiratoire par des relations pression-débit classiques, et en admettant qu'en état stationnaire, l'intégrale sur un cycle du débit des voies aériennes (débit pulmonaire) est nulle, la résistance de fuite peut être estimée cycle à cycle. Les calculs développés en annexe montrent que cette résistance s'exprime par:

$$Rf = \frac{\int_{cycle} Ptr.dt}{\int_{cycle} D.dt} \qquad (6)$$

où *Ptr* est la pression trachéale, assimilée à la pression à l'extrémité de la sonde endotrachéale et *D* est le débit de gaz provenant du respirateur.

Il suffit donc de déterminer la pression trachéale *Ptr*(*t*), le débit *D*(*t*) et la pression *P*(*t*) à l'entrée de la sonde étant connus. Le tableau 2.1 regroupe les unités et les abréviations des grandeurs utilisées.

Tableau 2.1 : récapitulatif des différentes abréviations

Pressions (en cmH_2O)	
Ptr	pression trachéale à la sortie de la sonde
P	pression dans les voies aériennes
PEEP	pression posive de fin d'expiration
PEEPmes	valeur de la pression dans le soufflet à la fin de l'expiration
PEEPnc	PEEP estimée avant la correction du débit
PEEPc	PEEP estimée après la correction du débit
Débits (en $l.s^{-1}$)	
D	débit de gaz (provenant du respirateur) dans la sonde trachéale
Df	débit de fuite
Dp	débit pulmonaire
Résistances (en $cmH_2O.l^{-1}.s$)	
Rf	résistance de fuite
Rf,mes	Rf mesurée directement
Rf,calc	Rf calculée
Rtt	résistance du tube trachéal utilisé, caractérisé par K_1 et K_2
Constantes	
K_1 $cmH_2O.l^{-1}.s$	Ces deux constantes sont telles que $Rtt = K_1 + K_2.\|D\|$
K_2 $cmH_2O.l^{-2}.s^2$	

Estimation de la pression à l'extrémité de la sonde

L'objectif du présent travail est de fournir une méthode de correction du débit permettant l'analyse des signaux pression et débit pour la surveillance des caractéristiques mécaniques du système respiratoire. La seule pression mesurée couramment par les respirateurs est la pression des voies aériennes ($P(t)$), à la sortie du ventilateur ou à l'entrée de la sonde trachéale au niveau de la pièce en Y. Il faut donc, pour mettre en œuvre notre méthode, estimer la pression trachéale à l'extrémité de la sonde. Pour cela, il suffit de connaître les propriétés résistives du circuit entre le point de mesure et l'extrémité de la sonde, en général caractérisées par l'équation de Rohrer (Peslin, 1992):

$$P(t) - Ptr(t) = K_1.D + K_2.D.|D| \qquad (8)$$

Une fois K_1 et K_2 connus, il est facile d'obtenir $Ptr(t)$ à partir de $P(t)$ et $D(t)$.

2.2.2. Protocoles expérimentaux

Simulations

Afin de valider notre méthode, nous avons effectué des simulations à l'aide d'un modèle physique de poumon (Model 2600i Dual Adult TTL, Michigan Instruments) relié à un respirateur (César, TAEMA) par une sonde trachéale à ballonnet (diamètre interne 5.5 mm) insérée dans le tube reliant le soufflet à l'extérieur (Figure 2.2). Ce montage permet, en gonflant plus ou moins le ballonnet, de simuler une fuite variable entre sonde et trachée. Nous avons enregistré simultanément les pressions et débit (respectivement *P(t)*

et $D(t)$) délivrés par le respirateur et la pression dans le soufflet du modèle physique de poumon ($P_A(t)$), assimilée à la pression à l'extrémité de la sonde trachéale.

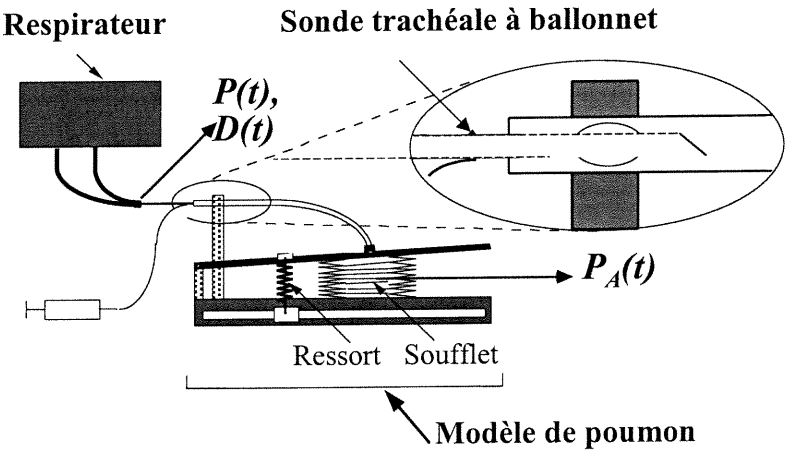

Figure 2.2: Montage expérimental des simulations de fuite. Le respirateur fournit les signaux $P(t)$ et $D(t)$ à l'entrée de la sonde trachéale. La seringue permet de gonfler plus ou moins le ballonnet et de faire varier ainsi la fuite entre la sonde trachéale et le tube de connexion du soufflet simulant la trachée. La résistance du tube reliant le soufflet à l'extérieur est considérée comme négligeable ce qui permet d'assimiler la pression dans le soufflet ($P_A(t)$) à la pression à l'extrémité de la sonde. Le ressort permet de régler l'élastance du modèle de poumon.

Les composantes de la résistance du tube trachéal à ballonnet (K_{1TB}, K_{2TB}) ont été obtenues par l'étude de la relation entre la pression résistive $P(t)$-$P_A(t)$ et le débit ($D(t)$) lorsque le ballonnet était assez gonflé pour assurer une étanchéité parfaite. Nous n'avons pas trouvé de différence significative entre les valeurs mesurées à l'inspiration et celles mesurées à l'expiration (Chang, 1981). Les valeurs que nous avons utilisées sont donc des moyennes entre ces deux conditions: $K_{1TB} = 2.1 \pm 0.1$ $cmH_2O.l^{-1}.s$ et $K_{2TB} = 27.4 \pm 0.8$ $cmH_2O.l^{-2}.s^2$.

L'élastance du modèle de poumon a été fixée à 100 $cmH_2O.l^{-1}$ afin de simuler au mieux les caractéristiques du poumon d'un nouveau-né. Le ventilateur était en mode *Ventilation Contrôlée* à pression constante pendant l'inspiration avec une pression positive de fin d'expiration (PEEP) imposée de 4 cmH_2O et un rapport des durées inspiratoire/expiratoire égal à 2/1 (5 cycles) ou 3/1 (7 cycles) pour obtenir des hyperinflations dynamiques significatives. La résistance de fuite a été réglée à 5 niveaux différents.

Enregistrements de nouveau-nés

Les parents des enfants étaient prévenus de l'utilisation des données recueillies à des fins de recherche. Cette étude a obtenu l'accord du comité d'éthique local.

Tableau 2.2: Caractéristiques des nouveau-nés étudiés

Pat. n°	Age (jours)	Poids (g)	Pathologie	Mode ventilatoire	FiO_2 (%)	PMax (cmH_2O)	FR (/mn)	I/E	Cycles retenus
1	5	1670	MMH	VAC	30	22	50	1/1.5	8
2	11	1600	MMH st 4	VACI	35	20	40	2/1	14
	18	1740	MMH DBP	VACI	25	18	40	1/1	7
3	7	1610	MMH sévère	VC	21	24	50	1/1	3

VAC: ventilation assistée contrôlée ; VACI: ventilation assistée contrôlée intermittente ; VC: ventilation contrôlée; MMH: maladie des membranes hyalines ; DPB: dysplasie broncho-pulmonaire; FiO_2: pourcentage d'oxygène insufflé; PMax: pression maximale en cmH_2O; FR: fréquence respiratoire en nombre de coups par minute; I/E: rapport des durées inspiratoire/expiratoire; Cycles retenus: nombre de cycles passifs analysés.

Nous avons enregistré les signaux pression et débit ($P(t)$ et $D(t)$) fournis par le respirateur chez des nouveau-nés prématurés admis dans le service de Réanimation néonatale, intubés et ventilés artificiellement (Babylog 8000, Draeger) pour des détresses respiratoires. Parmi ces patients, nous en avons sélectionné trois pour lesquels une fuite

importante pouvait être mise en évidence par la différence entre les volumes courants inspiré et expiré.

Le Tableau 2.2 résume les caractéristiques de ces trois nouveau-nés prématurés (âge gestationnel compris entre 26 et 33 semaines, l'enfant n°2 a été enregistré à deux dates différentes).

Le respirateur fonctionne comme un générateur de pression: il a pour consigne, pendant la phase inspiratoire, d'augmenter progressivement la pression des voies aériennes puis de se stabiliser à une pression maximale donnée et, pendant la phase expiratoire, d'imposer une pression basse. On règle la pente de montée en pression, la pression maximale, la pression expiratoire, la durée de l'inspiration et la durée totale du cycle. Les sondes d'intubation sont des sondes trachéales pédiatriques de diamètre interne 3 mm.

Les valeurs de K_1 et K_2 correspondantes (K_{1NN}, K_{2NN}) ont été obtenues en étudiant la relation pression-débit d'un tel tube trachéal isolé: $K_{1NN} = 21.9 \pm 1.0$ $cmH_2O.l^{-1}.s$ et $K_{2NN} = 327.3 \pm 8.1$ $cmH_2O.l^{-2}.s^2$.

Aucune modification du processus de soins n'a été induite par les enregistrements. Afin de pouvoir analyser les cycles en termes de mécanique ventilatoire, seuls ceux où le nouveau-né était totalement passif ont été retenus (Tableau 2.2). Parmi ces cycles, on a pu en sélectionner 11 pour lesquels la phase de plateau à pression maximale était suffisamment longue (cf. Figure 2.3) pour que le débit se stabilise en fin d'inspiration.

Lorsqu'il n'y a pas de fuite au niveau de la sonde, et quand le poumon a atteint un état d'équilibre élastique avec la pression imposée par le respirateur avant la fin de cette phase

de plateau, le débit retombe à une valeur nulle. Lorsqu'il y a une fuite autour de la sonde, le débit ne revient pas à zéro mais se stabilise à une valeur qui est celle du débit de fuite, comme l'illustrent les courbes de la figure 2.3.

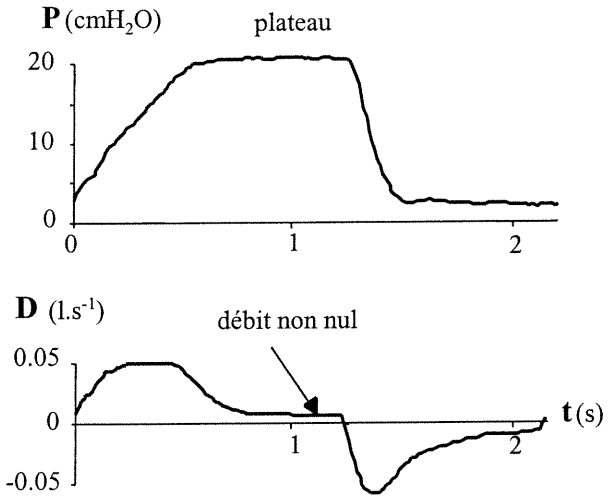

Figure 2.3: Caractérisation graphique de la fuite. Pour ce cycle, l'inspiration occupe les 2/3 du temps total du cycle. La courbe de pression (*P*) imposée par le respirateur montre un plateau pendant près de la moitié de l'inspiration. Pendant ce plateau, le débit (*D*) ne revient pas à zéro mais se stabilise à une valeur qui est le débit de fuite.

2.2.3. Traitement des données

Saisie informatisée des courbes et calcul de Rf

Les signaux *P(t)* et *D(t)* sont fournis par les respirateurs (César/TAEMA et Babylog 8000/Draeger) sous forme de tensions électriques variables disponibles sur deux connecteurs situés à l'arrière de l'appareil. Pour les enregistrements, les connecteurs ont été reliés par des câbles à une carte d'acquisition analogique/numérique équipant un micro-ordinateur PC compatible. Un programme (Baconnier, 1995), permet de 1) piloter

la carte pour acquérir les signaux à une fréquence d'échantillonnage donnée (200 Hz pour les nouveau-nés et 100 Hz pour les simulations), 2) sauvegarder les données numérisées sous une forme exploitable par un tableur.

Pour chaque cycle retenu (11 chez les nouveau-nés et 12 avec le modèle de poumon), nous avons calculé la résistance de fuite (*Rf,calc*) selon l'équation (6) (donnée en annexe) après correction de la pression selon l'équation (8) avec les coefficients K_1 et K_2 correspondants.

Mesure de Rf pendant la pause

Afin d'obtenir une valeur de référence pour la résistance de fuite (*Rf,mes*), nous avons réalisé une mesure directe du débit et de la pression de fuite dans les deux situations expérimentales.

Chez le nouveau-né, nous avons mesuré le débit de fuite pendant la pause sur les cycles présentant un plateau de pression suffisamment long pour que le débit se stabilise. La résistance de fuite mesurée (*Rf,mes*) est obtenue en divisant, pour chacun des 11 cycles retenus, la moyenne de la pression trachéale (pression mesurée pendant la pause, corrigée de la résistance du tube trachéal) par le débit moyen.

Pour les simulations sur modèle de poumon, nous avons d'abord estimé le débit pulmonaire (*Dp(t)*): il est égal à la vitesse de variation du volume du modèle de poumon (*dV(t)/dt*) qui peut être estimée à partir de la pression dans le soufflet ($P_A(t)$) et de l'élastance du soufflet (*E*):

$$Dp(t) = \frac{dV}{dt} = \frac{d(P_A(t)/E)}{dt} = \frac{1}{E}\frac{dP_A(t)}{dt} \qquad (9)$$

Nous avons vérifié que l'élastance du modèle de poumon est bien linéaire ce qui permet d'estimer le volume alvéolaire et sa vitesse de variation à partir de $P_A(t)$. Le débit de fuite est calculé (Eq. 1) comme la différence entre le débit mesuré à l'entrée des voies aériennes ($D(t)$) et le débit pulmonaire ($Dp(t)$). Rf,mes est alors obtenue pour chaque cycle en calculant la pente de la relation $P_A(t) = Rf,mes \ . \ Dp(t)$ par régression linéaire. Seules les phases de quasi-stabilité de $P_A(t)$ ont été retenues car, en dehors de ces phases comme le montre la figure 2.4, le débit de fuite calculé était trop variable.

Estimation de la PEEP par la méthode des moindres carrés

Afin d'évaluer l'apport de la correction du débit dans l'estimation des paramètres de la mécanique ventilatoire, nous avons estimé l'élastance (E), la résistance (R) et la PEEP totale (imposée + intrinsèque), à partir des signaux débit et pression obtenus chez les nouveau-nés et sur le modèle de poumon, par la méthode des moindres carrés (Modèle 1 de la référence (Peslin, 1992)) avant et après correction du débit.

Pour les simulations sur modèle de poumon, l'élastance était constante (100 $cmH_2O.l^{-1}$) et la résistance négligeable. Nous avons comparé les estimations de l'élastance et de la PEEP avant et après correction du débit avec les mesures obtenues à partir des courbes de la P_A pour l'élastance (E = pente de la relation P_A =f(V)) et la PEEP (PEEPmes = P_A de fin d'expiration).

Chez les nouveau-nés, nous avons comparé la PEEP estimée par moindres carrés à la PEEP imposée, seul paramètre accessible sur les 32 cycles enregistrés.

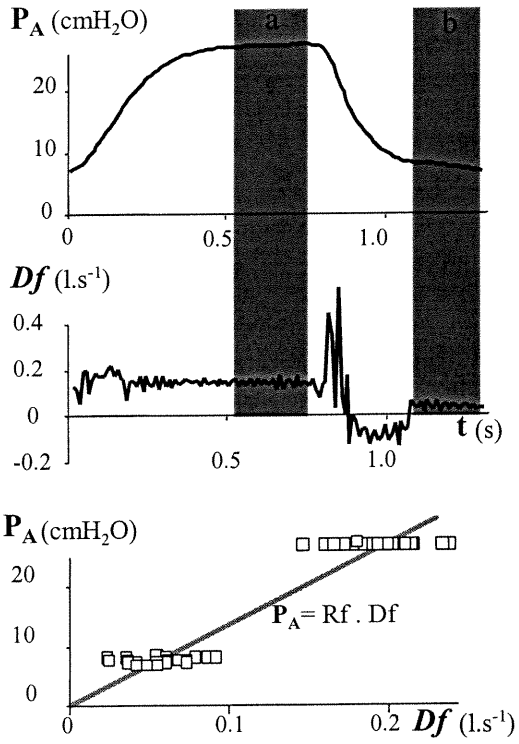

Figure 2.4: Mesure de *Rf* à partir de $P_A(t)$ et *Df(t)*. La pression dans le soufflet ($P_A(t)$) est assimilée à la pression à l'extrémité de la sonde trachéale et le débit de fuite (*Df(t)*) est obtenu par la formule *Df(t) = D(t) - Dp(t)* (*Dp(t)* est calculé selon l'équation (9)). Les zones a et b retenues correspondent aux deux phases à débit de fuite à peu près constant (il y a une PEEP imposée, ce qui explique que le débit de fuite en fin d'expiration n'est pas nul). La résistance de fuite *Rf* est obtenue comme la pente de la droite de régression du nuage de points, passant par l'origine.

Statistiques

Pour évaluer le niveau de concordance entre les valeurs obtenues par notre méthode et les valeurs mesurées, nous avons utilisé la régression linéaire et nous avons calculé les limites de confiance de la différence (test t pairé, $p<0.05$). Les résultats sont exprimés comme la moyenne ± 2 écarts types. Nous avons aussi tracé le graphique de la différence

entre les méthodes en fonction de leur moyenne, comme proposé par Bland et Altman (Bland, 1986).

Nous estimons qu'une variabilité de la différence (entre les deux méthodes) de 10% de la valeur moyenne des *Rf* est acceptable pour que les deux méthodes soient interchangeables, sans qu'il y ait un risque de mauvaise interprétation clinique.

Les limites d'accord entre les deux méthodes seront déterminées en utilisant les limites de précision et le biais (différence moyenne non nulle). Selon la largeur des intervalles obtenus et la variation des différences, nous pourrons juger du degré d'accord (Bland, 1986).

2.3. RÉSULTATS

2.3.1 Simulations

L'estimation de l'élastance par la méthode des moindres carrés a été améliorée de 10% (87 ± 0.5 $cmH_2O.l^{-1}$ avant correction du débit, 96 ± 0.5 $cmH_2O.l^{-1}$ après correction pour une valeur mesurée de 98 ± 0.5 cm $H_2O.l^{-1}$)

Les résultats de la comparaison entre *Rf,calc* et *Rf,mes* obtenus pendant les simulations sont présentés sur les figures 2.5 et 2.6. La différence moyenne entre *Rf,calc* et *Rf,mes* n'est pas statistiquement différente de 0 (-0.8 ± 13.8 $cmH_2O.l^{-1}.s$). Les écarts entre *Rf,calc* et *Rf,mes* se situent, à l'exception d'un point, dans un zone d'amplitude inférieure à 20% de la valeur moyenne de *Rf*. L'intervalle de confiance à 95% pour le biais va de -9.7 à 8.0 $cmH_2O.l^{-1}.s$, pour la limite inférieure d'accord de -43.8 à -13.0 $cmH_2O.l^{-1}.s$ et pour la limite supérieure d'accord de 11.4 à 42.1 $cmH_2O.l^{-1}.s$. Ces intervalles sont relativement étroits par rapport à la valeur moyenne de *Rf* (267.4 $cmH_2O.l^{-1}.s$), reflétant la faible variation des différences et donc la possibilité d'interchanger les deux méthodes.

La PEEP estimée par la méthode des moindres carrés passe en moyenne de -9.9 ± 3.1 cmH_2O, avant correction, à 6.7 ± 1.3 cmH_2O, après correction. Cependant cette valeur est significativement supérieure ($p<0.05$) à la PEEP mesurée moyenne (7.8 ± 0.8 cmH_2O). L'écart moyen entre PEEP estimée par les moindres carrés après correction du débit et PEEP mesurée est faible (1.2 ± 0.6 cmH_2O). On voit sur la figure

2.7 que, comme pour les nouveau-nés, l'erreur sur l'estimation de la PEEP avant correction augmente lorsque *Rf* diminue, c'est à dire lorsque le débit de fuite augmente.

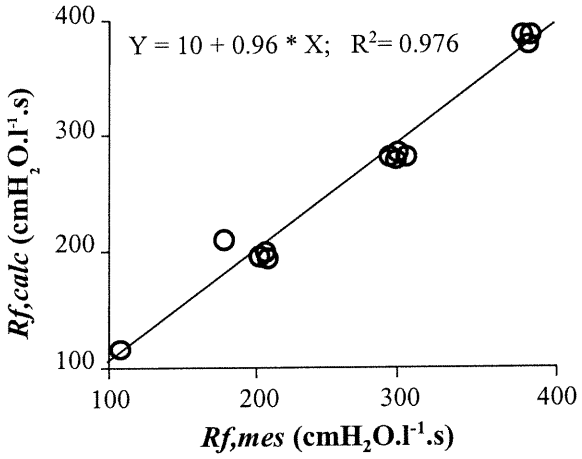

Figure 2.5: Comparaison de *Rf* estimée (*Rf,calc*) avec *Rf* mesurée directement (*Rf,mes*) au cours des simulations. La ligne continue représente la droite de régression. La pente n'est pas statistiquement différente de 1 et l'ordonnée à l'origine n'est pas statistiquement différente de 0 ($p<0.05$ dans les 2 cas).

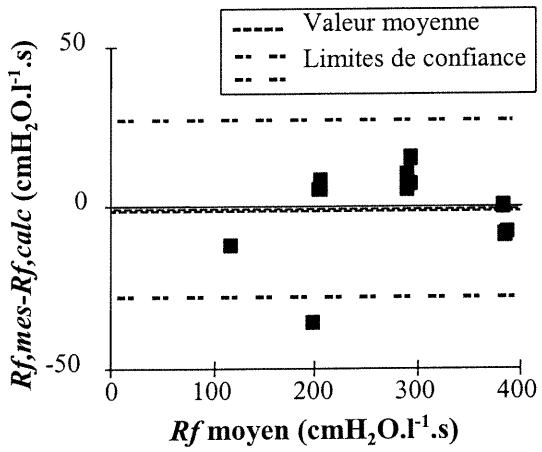

Figure 2.6: Niveau de concordance entre *Rf,calc* et *Rf,mes* pour les simulations. L'amplitude de la zone de confiance à 95% est inférieure à 20% de la valeur moyenne de *Rf*.

Avant correction la PEEP estimée était négative alors qu'après correction elle se rapproche notablement (erreur inférieure à 3 cmH_2O) de la valeur mesurée directement.

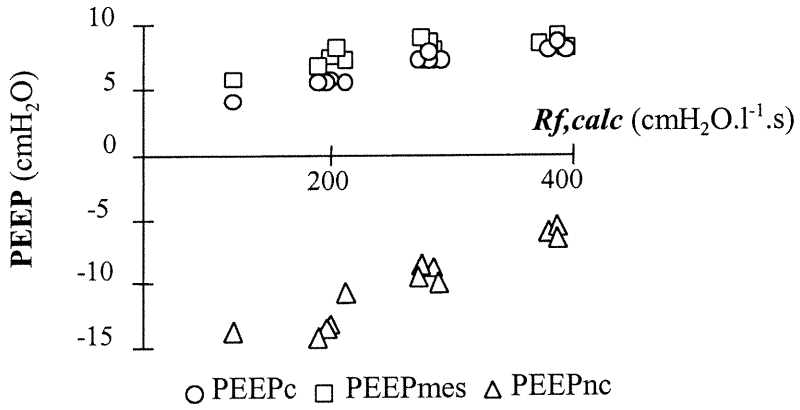

Figure 2.7: Effet de la correction du débit sur l'estimation de la PEEP par la méthode des moindres carrés. PEEPnc: PEEP estimée avant correction du débit; PEEPc: PEEP estimée après correction du débit; PEEPmes: valeur de la pression dans le soufflet à la fin de l'expiration.

2.3.2. Nouveau-nés

Pour tous les cycles retenus (les 11 présentant un plateau assez long pour que le débit se stabilise en fin d'inspiration) le débit corrigé est nul en fin d'inspiration, comme illustré sur la figure 2.8. Les résultats de la comparaison entre *Rf,calc* et *Rf,mes* chez les nouveau-nés sont présentés sur les figures 2.9 et 2.10.

La différence moyenne entre *Rf,calc* et *Rf,mes* n'est pas différente de 0 (87 ± 99 $cmH_2O.l^{-1}.s$). La méthode de calcul de *Rf* est en accord avec la mesure directe comme le montre la relative étroitesse de la zone de confiance à 95% par rapport aux valeurs moyennes de *Rf*. En effet, l'intervalle de confiance à 95% pour le biais va de 20.4 à 153.5 $cmH_2O.l^{-1}.s$, pour la limite inférieure d'accord de –226.5 à 4.1 $cmH_2O.l^{-1}.s$ et pour la limite supérieure d'accord de 169.8 à 400.3 $cmH_2O.l^{-1}.s$. Ces intervalles sont relativement petits par rapport à la valeur moyenne de *Rf* (2828.1 $cmH_2O.l^{-1}.s$), illustrant donc un lien étroit entre les deux méthodes.

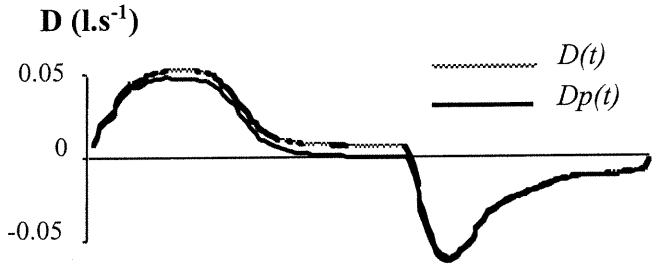

Figure 2.8: Exemple de débit corrigé après calcul de *Rf*. L'efficacité de la correction de la fuite peut être mise en évidence par la valeur nulle du débit corrigé (*Dp(t)*) pendant le plateau de pression de fin d'inspiration.

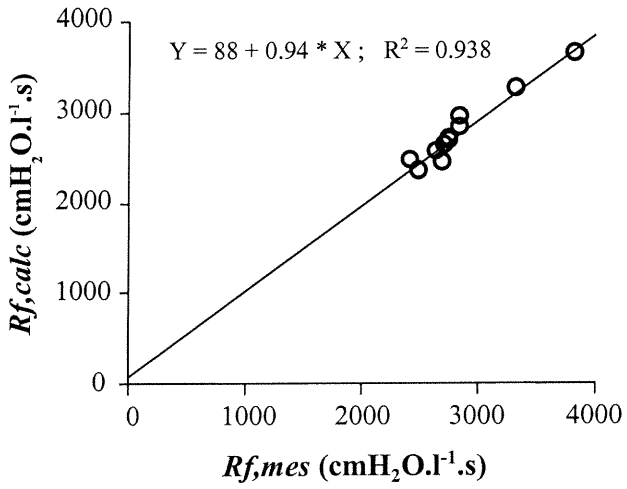

Figure 2.9: Comparaison de *Rf* estimée (*Rf,calc*) avec *Rf* mesurée directement (*Rf,mes*) chez les nouveau-nés. La ligne continue représente la droite de régression. La pente n'est pas statistiquement différente de 1 et l'ordonnée à l'origine n'est pas statistiquement différente de 0 ($p<0.05$ dans les 2 cas).

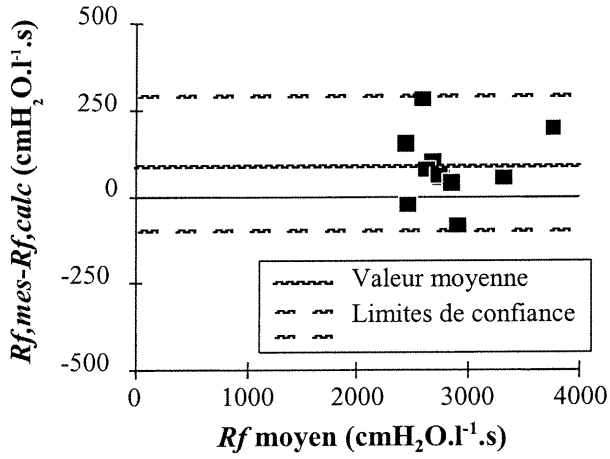

Figure 2.10: Niveau de concordance entre *Rf,calc* et *Rf,mes* chez les nouveau-nés. L'amplitude de la zone de confiance à 95% est inférieure à 20% de la valeur moyenne de *Rf*.

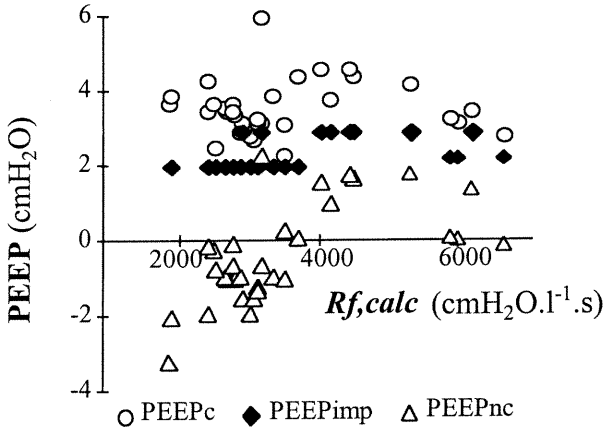

Figure 2.11: Effet de la correction du débit sur l'estimation de la PEEP par l méthode des moindres carrés. PEEPnc: PEEP estimée avant correction du débit PEEPc: PEEP estimée après correction du débit; PEEPimp: PEEP imposée par l ventilateur.

La correction du débit améliore nettement l'estimation de la PEEP totale par la méthode des moindres carrés puisque la PEEP estimée passe en moyenne de -0.3 ± 3.6 cmH_2O, avant correction, à 1.3 ± 0.7 cmH_2O, après correction. Cependant cette valeur est significativement supérieure ($p<0.05$) à la PEEP imposée moyenne (2.2 ± 0.4 cmH_2O). Sur la figure 2.11, les valeurs de PEEP estimées ou imposées sont portées en fonction de la valeur calculée de *Rf*. L'erreur sur l'estimation de la PEEP avant correction augmente lorsque *Rf* diminue, c'est à dire lorsque le débit de fuite augmente.

2.4. DISCUSSION

Nous avons montré qu'il est possible de corriger le débit instantané par une estimation simple de la résistance de fuite *Rf*. L'intérêt de cette méthode repose essentiellement sur le fait que près du tiers des nouveau-nés présente une fuite (Seear, 1991). On peut espérer retirer un bénéfice clinique de l'application de cette nouvelle méthode à deux niveaux: le premier sera de guider le clinicien dans le choix de la sonde à utiliser, le second sera d'améliorer la surveillance de la mécanique ventilatoire: en effet, la mauvaise mesure du débit liée à l'existence d'une fuite entraîne une mauvaise estimation de la mécanique ventilatoire.

L'hypothèse que *Rf* ne dépend pas du débit de fuite est à la base de notre méthode. Les mesures exposées à la figure 2.4 ne permettent en aucun cas de valider ou d'infirmer cette hypothèse. Nous estimons cependant que les faibles débits de fuite habituellement rencontrés (sur la figure 2.8, on peut estimer ce débit à environ 10 $ml.s^{-1}$) permettent de supposer l'hypothèse vérifiée dans ces conditions.

Dans le cas d'enfants normaux, on peut considérer que les variations du diamètre de la trachée sur un cycle respiratoire sont suffisamment petites pour que l'on puisse admettre l'hypothèse que le rapport entre le diamètre de la trachée et le diamètre du tube endotrachéal est constant. Ceci n'est cependant pas vrai dans le cas d'une trachéomalacie, caractérisé par un ramollissement de la trachée causée par une dégénérescence des cartilages (Wittenborg, 1967).

Notre méthode repose aussi sur l'estimation de la pression à l'extrémité de la sonde à partir du signal de pression donné par le ventilateur et des caractéristiques résistives de la sonde. Ces dernières ne peuvent être connues parfaitement pour deux raisons: 1) les lois d'écoulement font que la résistance n'est pas la même à l'inspiration et à l'expiration (Chang, 1981) et 2) en situation clinique, on sait que la sonde va s'encombrer progressivement. Cet encombrement est levé périodiquement par des aspirations et il pourrait être estimé par des méthodes directes de mesure de la surface de section du conduit (Van Surell, 1994)

En ce qui concerne les simulations, nous n'avons pas essayé de simuler plusieurs valeurs des paramètres mécaniques car ce n'était pas le but du travail. L'important était de pouvoir estimer directement le débit de fuite pour différentes valeurs de Rf . Dans nos simulations, la résistance de fuite était dix fois plus faible que chez les nouveau-nés, ce qui aurait pu entraîner une plus forte non linéarité de la fuite. L'ensemble de nos mesures semble montrer qu'il n'en était rien.

Les résistances de fuite obtenues en simulation sont environ dix fois inférieures à celles obtenues en clinique. Ces valeurs sont cohérentes avec le fait que la sonde trachéale de diamètre 5.5 mm (en simulation) est dix fois moins résistive que celle utilisée avec les nouveau-nés.

En ce qui concerne les enregistrements sur les nouveau-nés, il a été relativement difficile de trouver des cycles présentant les caractéristiques requises, c'est à dire avec des patients complètement passifs, présentant une fuite et un plateau inspiratoire long. Nous avons

donc peu de valeurs de contrôle puisque nous avions choisi, pour de simples raisons d'éthique, de ne modifier en aucun cas les paramètres ventilatoires fixés par le médecin traitant. La mesure de la résistance de fuite n'a été réalisable que lorsque la pause durait suffisamment longtemps pour que le débit de fin d'inspiration atteigne une valeur stable. Le débit de fuite a alors pu être estimé par le rapport entre la pression maximale et la résistance de fuite, donnant des valeurs comprises entre 4 et 7.5 $ml.s^{-1}$ pour des débits de l'ordre de 100 $ml.s^{-1}$. Dans tous les autres cas, la résistance de fuite estimée par le rapport *Pression de fin d'inspiration/débit de fin d'inspiration* est très nettement inférieur à *Rf* calculée par notre méthode ce qui laisse penser que le débit mesuré n'est pas uniquement le débit de fuite mais que le poumon continue à se gonfler.

La méthode proposée de calcul des résistances de fuite présente l'avantage que *Rf* est estimée pour chaque cycle sur lequel elle est appliquée. Il est donc possible de corriger le débit chaque fois qu'il est mesuré et de mettre en œuvre les méthodes d'estimation des paramètres de mécaniques ventilatoires avec un débit corrigé même si la fuite change entre deux estimations. En pratique clinique, dans le cas de la présence de fuites trop importantes et d'une hypoventilation alvéolaire, l'action du clinicien sera de changer le diamètre du tube trachéal plutôt que de prendre le risque d'une surcompensation ou d'un barotraumatisme pulmonaire. Par ailleurs, il est évident que notre méthode ne pourra pas être utilisée avec des nouveau-nés très peu passifs.

L'application numérique et graphique de l'étude statistique de Bland et Altman (Bland, 1986) a mis en évidence un lien étroit entre les deux méthodes proposées. Il est vrai

cependant, que la répétition des mesures obtenues chez un même sujet (le sujet 2) diminue la variabilité inter-individus.

Nous n'avons utilisé la méthode des moindres carrés que pour évaluer l'apport de la correction du débit en cas de fuite. Nous avons choisi cette méthode car elle permet d'estimer la PEEP totale (imposée + intrinsèque), importante en clinique, à l'inverse de la FFT (Peslin, 1994) mais le modèle retenu aurait pu être nettement amélioré. Le fait que la résistance "des voies aériennes" est négligeable dans notre simulation n'allait pas dans le sens de la complexification du modèle à appliquer (Kano, 1994; Peslin, 1992).
Il semble normal que la PEEP estimée soit supérieure en moyenne à la PEEP imposée car dans certains cas (comme celui illustré sur la figure 2.11) il y a probablement de la PEEP intrinsèque qui est prise en compte par la méthode des moindres carrés.

En conclusion, nous pensons que cette méthode simple à mettre en œuvre dès que l'on connaît les caractéristiques du tube trachéal, devrait être appliquée avec succès à la surveillance des caractéristiques de mécanique ventilatoire des nouveau-nés et pourrait être utilisée avec profit chez les adultes de façon systématique puisque, en l'absence de fuite (Rf infinie), la correction du débit n'a pas lieu.

ANNEXE: CALCULS DÉTAILLÉS DE LA RÉSISTANCE DE FUITE

Ecoulement à l'extrémité de la sonde:

A tout instant, le débit dans la sonde trachéale est la somme du débit allant vers le poumon et de celui passant par la fuite:

$$D = Df + Dp \tag{1}$$

Ecoulement dans la fuite:

Si on suppose que la résistance de fuite (*Rf*) ne dépend pas du débit ou de la pression, on peut écrire l'équation qui caractérise cet écoulement:

$$Ptr = Df.Rf \tag{2}$$

Les intégrales sur une durée donnée de 2 quantités égales étant égales, on peut écrire:

$$\int Ptr \cdot dt = \int Rf \cdot Df \cdot dt = Rf \cdot \int Df \cdot dt \tag{3}$$

Or on peut raisonnablement supposer qu'en état stationnaire (pas de variation du volume courant pulmonaire ni du volume de fin d'expiration d'un cycle à l'autre) l'intégrale sur un cycle du débit des voies aériennes est nulle, qu'il y ait ou non hyperinflation dynamique.

$$\int_{cycle} Dp \cdot dt = 0 \tag{4}$$

Si l'on calcule l'intégrale sur un cycle du débit dans la sonde trachéale, on obtient, en utilisant successivement (1) et (4):

$$\int_{cycle} D \cdot dt = \int_{cycle} (Dp + Df) \cdot dt = \int_{cycle} Dp \cdot dt + \int_{cycle} Df \cdot dt = \int_{cycle} Df \cdot dt \tag{5}$$

A l'aide des équations (3) et (5) on démontre alors aisément que:

$$Rf = \frac{\int_{cycle} Ptr \cdot dt}{\int_{cycle} D \cdot dt} \tag{6}$$

Il est alors possible de calculer le débit pulmonaire à chaque instant:

$$Dp(t) = D - Df = D(t) - \frac{Ptr(t)}{Rf} \tag{7}$$

APPENDIX: COMPUTATION OF LEAK RESISTANCE

Flow at the extremity of the tube:

The flow through the endotracheal tube is the sum of the actual flow of air going to the lung (*Dp*) and the leak flow (*Df*):

$$D = Df + Dp \tag{1}$$

Flow through the leak:

Assuming a constant leak resistance (*Rf*) throughout the breath (independent of pressure or airflow), the flow through the leak will obey the following equation:

$$Ptr = Df.Rf \tag{2}$$

The integration of Eq.2 over a finite period of time gives:

$$\int Ptr \cdot dt = \int Rf \cdot Df \cdot dt = Rf \cdot \int Df \cdot dt \tag{3}$$

In steady conditions (no variation in tidal volume and end-expiratory lung volume from one breathing cycle to the next), the integral of airflow (area under the curve) over the breath should be equal to zero, even in the presence of dynamic hyperinflation:

$$\int_{cycle} Dp \cdot dt = 0 \tag{4}$$

The integral of the flow in the endotracheal tube can be obtained for each breathing cycle, by combining Eqs. 1 and 4:

$$\int_{cycle} D \cdot dt = \int_{cycle} (Dp + Df) \cdot dt = \int_{cycle} Dp \cdot dt + \int_{cycle} Df \cdot dt = \int_{cycle} Df \cdot dt \tag{5}$$

The leak resistance (*Rf*) is thus obtained by combining Eq. 3 and 5:

$$Rf = \frac{\int_{cycle} Ptr \cdot dt}{\int_{cycle} D \cdot dt} \tag{6}$$

Finally, the actual airflow going into the lung is estimated by the following relationship:

$$Dp(t) = D - Df = D(t) - \frac{Ptr(t)}{Rf} \tag{7}$$

CHAPTER 3

MECHANICAL OUTPUT IMPEDANCE OF THE LUNG DETERMINED FROM CARDIOGENIC OSCILLATIONS

Authors:

Bijaoui Eve, Baconnier Pierre F. and Bates Jason H.T.

Published in:

Journal of Applied Physiology (2001); 91(2): 859-865

LINK WITH CHAPTER 2

In Chapter 2, we have established, using a simple mathematical model, a noninvasive method for correcting the error introduced in respiratory mechanics estimates by the presence of a leak around the ETT and the trachea of mechanically ventilated subjects. The measurements were done continuously, without interfering with the ventilation and with no active contribution from the subject. We showed that, with accurate pressure and flow recordings, respiratory mechanics serve as an efficient tool for monitoring lung function in ventilator-dependent subjects and/or during sleep. The choice of the method for assessing respiratory mechanics depends on the desired information and the clinical context. In Chapter 2, these mechanical properties were estimated by fitting pressure and flow signals to a simple model of the respiratory system using a multiple linear regression method. Alternatively, by applying a known oscillatory flow signal to the respiratory system and measuring the resulting pressure signal, one can compute its mechanical properties in terms of a mechanical impedance. In Chapter 3, we use the cardiogenic oscillations as a natural perturbation to the respiratory system, from which an output impedance can be estimated. Cardiogenic oscillations are associated with the presence of central apneas during sleep and are often observed during expiration in mechanically ventilated subjects. We recorded pressure and flow signals originating from cardiogenic oscillations, measured the corresponding cardiogenic impedance and compared them to impedance obtained using the conventional FOT method.

ABSTRACT

The beating heart naturally oscillates the lung because of their close juxtaposition, producing cardiogenic oscillations (CO) in flow that can be measured at the mouth when the glottis is open. Correspondingly, if the mouth is occluded, the same phenomenon produces cardiogenic pressure oscillations that can be measured just distal to the site of occlusion. The Fourier-domain ratio of these oscillations in pressure and flow constitutes what we call the cardiogenic respiratory impedance (Z_C). We calculated Z_C between about 1.5 and 10 Hz in relaxed normal subjects at FRC with open glottis. Z_C was insensitive to heart rate changes induced by exercise and had an imaginary part close to zero at all frequencies investigated. Its real part was similar to or smaller than resistance determined by the forced oscillation technique. We speculate that Z_C measures the flow resistance of the central and upper airways of the lung. Z_C may be useful as a means of obtaining information about lung mechanics without the need for an external source of flow perturbations.

3.1. INTRODUCTION

The mechanical properties of the respiratory system are conveniently encapsulated in terms of its mechanical impedance (Z), a complex function of frequency (f) that accounts for both the conservative and dissipative properties of the system. Z is usually determined by the so-called forced oscillation technique in which an external generator, such as a loud-speaker or piston pump, generates a broad-band flow into the lungs via the mouth while pressure is measured at the mouth simultaneously. Input impedance (Z_{in}) is then obtained as the Fourier-domain ratio of pressure to flow (Peslin, 1986). Alternatively, a transfer impedance (Z_{tr}) of the respiratory system may be obtained from the Fourier-domain relationship between pressure oscillations applied to the body surface and flow measured at the mouth or vice versa (Peslin, 1998). It is also possible to obtain regional lung impedance if the applied pressures and flows can be confined to some local region of the lung, such as the alveolar input impedance (Z_A) provided by the alveolar capsule oscillator technique in dogs (Davey, 1993). Z_{in}, Z_{tr} and Z_A are not equivalent quantities, but rather give complementary information about respiratory mechanics, each with its own particular advantages.

Thus, in general terms, some Z relating to the mechanical properties of the respiratory system can be obtained from any oscillatory source capable of generating corresponding pairs of pressure and flow signals whose relationships are somehow affected by respiratory system mechanics. To date, virtually all endeavors of this nature have utilized external power sources to generate the necessary oscillations in pressure and flow. This

allows the spectral contents of the applied signals to be optimized for the application at hand, but also requires a certain amount of instrumentation that may, in some cases, be cumbersome and impractical.

In the present study, we utilize the fact that the beating heart naturally oscillates the lung because of their close juxtaposition. This results in so-called cardiogenic oscillations (CO) in flow that can be measured at the mouth when the glottis is open. Correspondingly, if the mouth is occluded, the same phenomenon leads to CO in pressure that can be measured just distal to the site of occlusion. The Fourier-domain relationship between these flow and pressure oscillations constitutes a cardiogenic output impedance (Z_C), according to the classic notion of a Thevinin equivalent circuit in which an idealized pressure source (due to the heart) acts upon a series source output impedance. Exactly what Z_C corresponds to physiologically is unknown, but it has the potential advantage of not requiring an external oscillator to produce perturbations in flow. In contrast, while Z_{in} does require an external oscillator, its physiological interpretation is well understood. Therefore, the purpose of the present study was to elucidate the physiological interpretation of Z_C by investigating how it relates to Z_{in} in normal human volunteers.

3.2. METHODS

We studied five healthy human volunteers (2 female, 3 male) with no history of lung disease. The study was approved by our Institutional Review Board, and written informed consent was obtained from each subject.

Resting measurements of Z_C and Z_{in} were made first (see below). The subjects then exercised on a cycle ergometer in three-minute stages and from 10 to 50 W (depending on the subject). At the end of each stage, the subject got off the bicycle and immediately sat down at the measurement apparatus and Z_C and Z_{in} recordings were again taken.

Measurement of Z_C: Subjects wore a nose clip and sat upright in a straight-backed chair while breathing through a mouth-piece (Fig. 3.1A). Measurements were made at functional residual capacity (FRC) over a period of up to 10 s during which subjects attempted to relax all respiratory muscles while supporting the cheeks with the hands and keeping the glottis open. During the first half of the measurement period, cardiogenic flow ($\dot{V}_C$) at the mouth was measured with a pneumotachograph (Fleisch #1) connected to the mouthpiece. A piezoresistive differential pressure transducer (SensorTechnics HCXPM002D6V) was connected by the shortest possible length of flexible tubing to the 2 ports of the pneumotachograph. During the final half of the measurement period, the outflow port of the pneumotachograph was occluded and cardiogenic pressure (P_C) was measured with a gauge differential pressure transducer (Fujikura, FPM-02PG) positioned just proximal to the mouthpiece. $\dot{V}_C$ and P_C were low-pass filtered at 50 Hz with 6-pole

Bessel anti-aliasing filters and sampled at 128 Hz with a 12-bit analog-digital converter (DT EZ-01, Data Translation, Marlborough, MA) before being stored on a PC computer using the LABDAT^{TM} data acquisition software (RHT-InfoDat, Montreal).

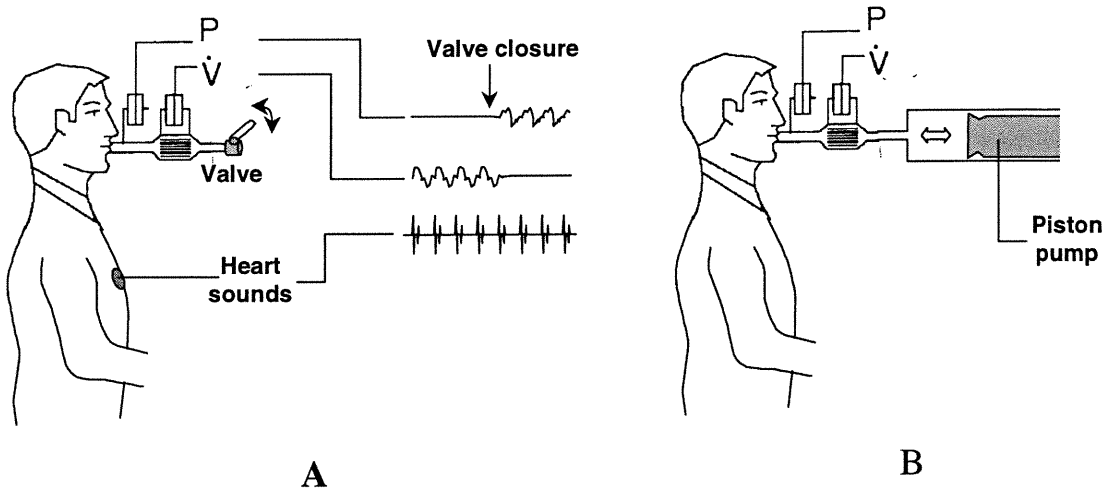

Figure 3.1: Experimental setup for (A) the cardiogenic oscillation recordings, and B) the forced oscillation technique. Pressure at the airway opening (P) was measured via a lateral tap near the mouth piece. Flow ($\dot{V}$) was measured with a pneumotachograph.

Figure 3.2 shows a representative example of the cardiogenic signals obtained in one of the subjects, and demonstrates that the oscillatory segments of P_C and $\dot{V}_C$ are not measured simultaneously because the oscillations in $\dot{V}_C$ arise before the airway opening is occluded while those in P_C occur afterward. However, in order to calculate Z_C, these signals need to be phase-matched which requires an independent reference signal related to the mechanical activity of the heart and which can be measured regardless of whether the airway is occluded or not. This reference was provided by the heart sound signal measured by placing a microphone over the chest (Fig. 3.1). The first heart sound, which

had the largest amplitude and identifies the onset of ventricular systole, was used as the phase reference for each cardiogenic oscillation in either P_C or $\dot{V}_C$.

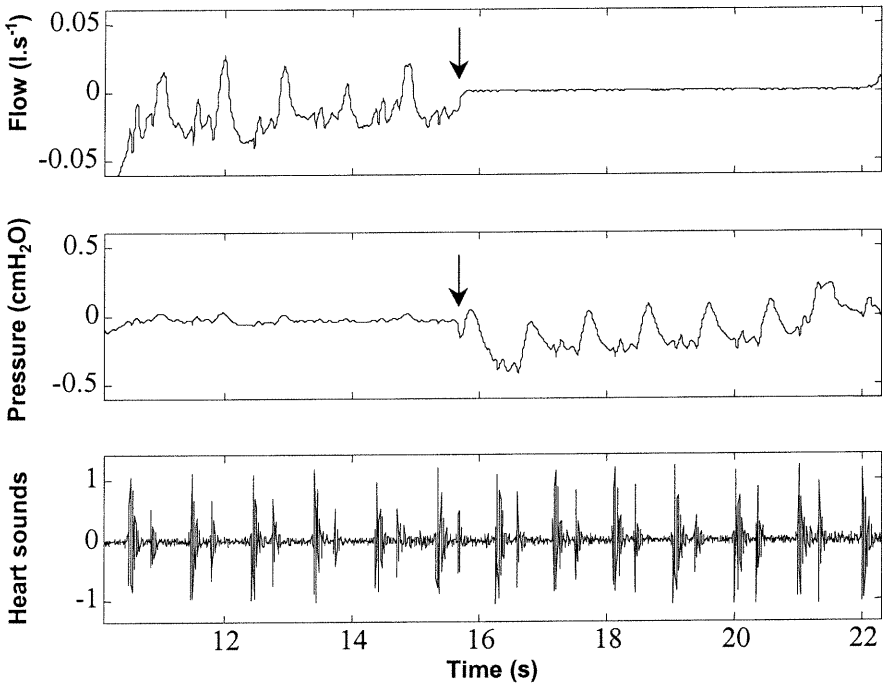

Figure 3.2: Representative examples of flow and pressure measured at the mouth of subject sitting quietly at FRC with open glottis, together with the heart sounds recorded over the chest. The arrows indicate the time of closure of the valve. The heart sounds units are arbitrary.

Measurement of conventional Z_{in}: Conventional forced oscillatory measurements were made using a 50-ml piston oscillator (Fig. 3.1B) which generated an 8 s broad-band volume perturbation consisting of the superposition of 7 discrete sinusoidal components having mutually prime f between 0.5 to 10.25 Hz. The amplitude (A) of each sinusoidal component was chosen according to the formula

$$A = a + \frac{b}{f}$$

where $a = 0.1$ and $b = 0.2$. This formula gives roughly equal power to each frequency in applied flow, with somewhat proportionately greater power at high frequencies, in an attempt to optimize the signal-to-noise ratio in the measurements. Piston position was recorded with a linear variable differential transducer (Trans-Tek, model 0244-0000) calibrated in units of volume displacement (ml). The peak-peak amplitude of the piston stroke was set to 10 ml so as to generate flows of comparable amplitude to $\dot{V}_C$. Subjects were connected to the oscillator through the same mouthpiece as used for the cardiogenic oscillation measurements (see above). During the application of the 8 s forced oscillations, the subject remained relaxed and apneic with open glottis at FRC.

The pressure signal required for calculation of Z_{in} was measured with the same transducer system as used for determining Z_C (see above). Data acqusition was again performed using LABDAT^{TM}. The piston oscillator was controlled by the computer via a digital-analog converter (DAC-02, Keithley Metrabyte, Cleveland, OH). Pressure (P) and flow ($\dot{V}$) signals were low-pass filtered at 50 Hz (6-pole Bessel filter), sampled at 128 Hz and stored for further analysis.

Data processing: Data analysis was carried out using the Matlab^{TM} 5.3 mathematical software (The Mathworks, Nattick, MA). To calculate Z_C, we first used the heart sound signal to divide $\dot{V}_C$ and P_C into individual heart cycles. Figure 3.2 shows typical recordings $\dot{V}_C$ and P_C, for a subject at rest, together with the heart sound signal that identifies each cycle. Next, $\dot{V}_C$ and P_C were divided into individual cycles, and each

cycle re-sampled using linear interpolation to have exactly an integer power of two data points (usually 128). The individual $\dot{V}_C$ and P_C cycles were then ensemble-averaged (Fig. 3.3).

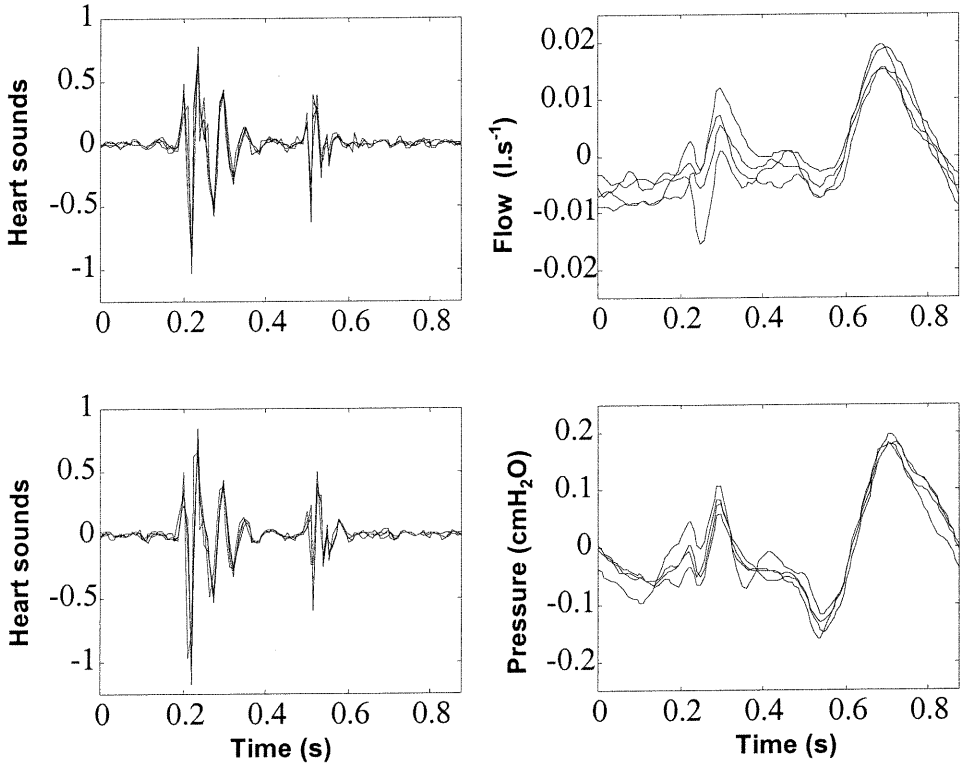

Figure 3.3: Representative recording of cardiogenic oscillations at rest. The top two panels show heart sounds (left-hand side) and mouth flow (right-hand side) prior to valve closure, each overlayed cycle-by-cycle. The bottom two panels show cycle-by-cycle heart sounds (left-hand side) and mouth pressure (right-hand side) after valve closure.

Finally, Z_C was calculated by taking the ratio of the Fourier transform of the averaged P_C to the transform of the averaged $\dot{V}_C$ at those frequencies having power equal to 2% or more of the maximum. This assumes that the P_C and $\dot{V}_C$ signals were stationary, i.e. the only difference between successive cycles was random noise. To test the validity of this

assumption, we calculated Z_C for subject #1 using each possible pair of individual P_C and $\dot{V}_C$ cycles. Figure 3.4 shows the mean and a standard deviation of the individual real parts (R_C) and imaginary parts (X_C) of Z_C, and demonstrates that for most frequencies the variation in individual Z_C is small, which supports our assumption of stationarity for $\dot{V}_C$ and P_C.

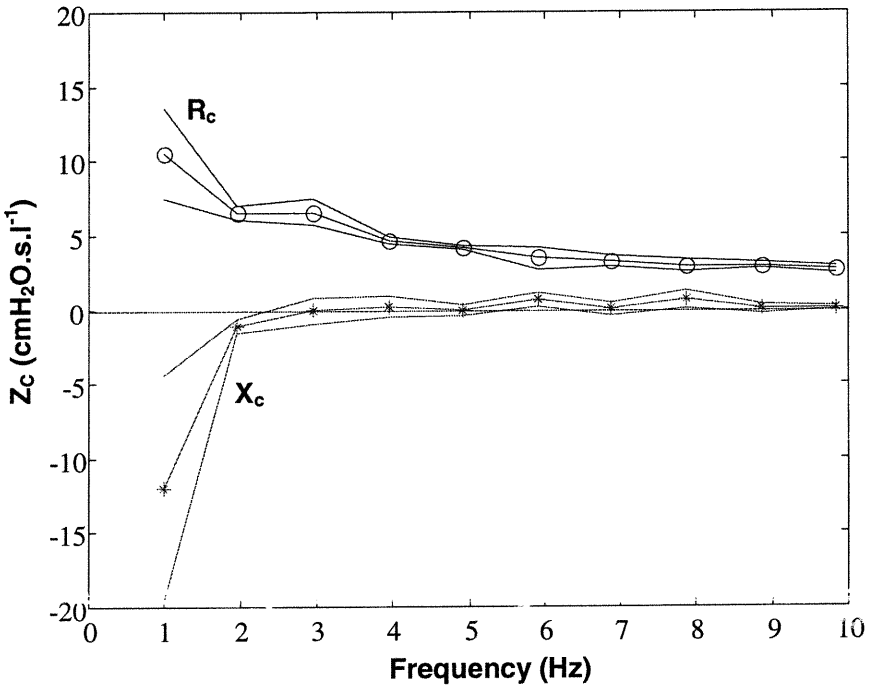

Figure 3.4: Mean (± SD) of the cardiogenic impedances (Z_C) determined using all combinations of heart cycles of $\dot{V}_C$ and P_C for subject #1 at rest. R_C is the real part of Z_C (resistance) and X_C is the imaginary part of Z_C (reactance).

Z_{in} was computed from the 8 s forced oscillation recordings as follows. First, $\dot{V}$ and P were divided in 4 s time windows overlapping by 50% and the first window in each signal was discarded. Next, the fast Fourier transform of each remaining window was

calculated and the average auto- and cross-power spectrum between $\dot{V}$ and P calculated ($G_{\dot{V}\dot{V}}$ and $G_{P\dot{V}}$, respectively). Finally, impedance was calculated as

$$Z_{in} = \frac{G_{P\dot{V}}}{G_{\dot{V}\dot{V}}}$$

The coherence was computed as

$$\gamma^2 = \frac{\left|G_{P\dot{V}}\right|^2}{G_{PP}G_{\dot{V}\dot{V}}}$$

where G_{PP} denotes the auto-power spectrum for P. Only values of Z_{in} with $\gamma^2 \geq 0.90$ were accepted.

3.3. RESULTS

Figure 3.5 shows Z_C and Z_{in} for all subjects studied at rest. In two of the subjects (nos. 3 and 5) R_c and R_{in} agree well over most of the frequency range, while in the three remaining subjects R_c is markedly lower than R_{in}. The reactances are quite different in 4 of the subjects, with X_{in} being considerably lower than X_C at all frequencies. Only in subject 5 are X_{in} and X_C similar. The most striking finding, however, is that X_C is essentially zero at all frequencies in all subjects.

Figure 3.6 shows the effects of exercise, and hence of increased heart rate (which reached levels 20-40% greater than baseline) on R_C. Values of R_C at rest and two exercise levels are shown for all subjects, normalized to the value at rest at 2 Hz. None of the values at any frequency or exercise level are significantly different (ANOVA, $p<0.05$). The mean values of X_C at the same frequencies, for all exercise levels, are given in Table 3.1. None was significantly different from zero (one sample t-distribution, $p<0.05$). These results show that increasing heart rate had no effect on the estimated Z_C.

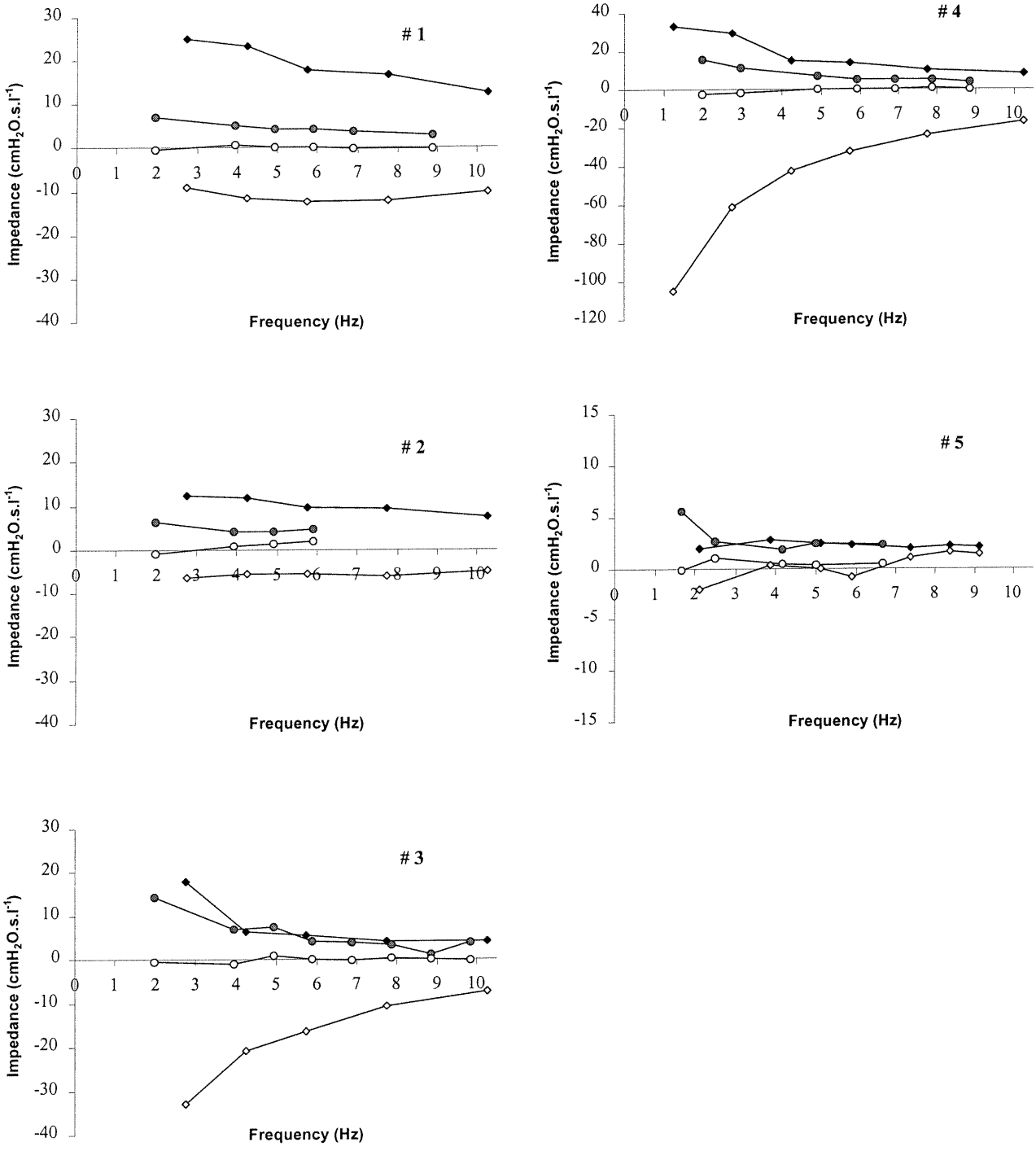

Figure 3.5: Z_C (circles) and Z_{in} (diamonds) for all the subjects studied at rest. Closed symbols are resistance, open symbols are reactance.

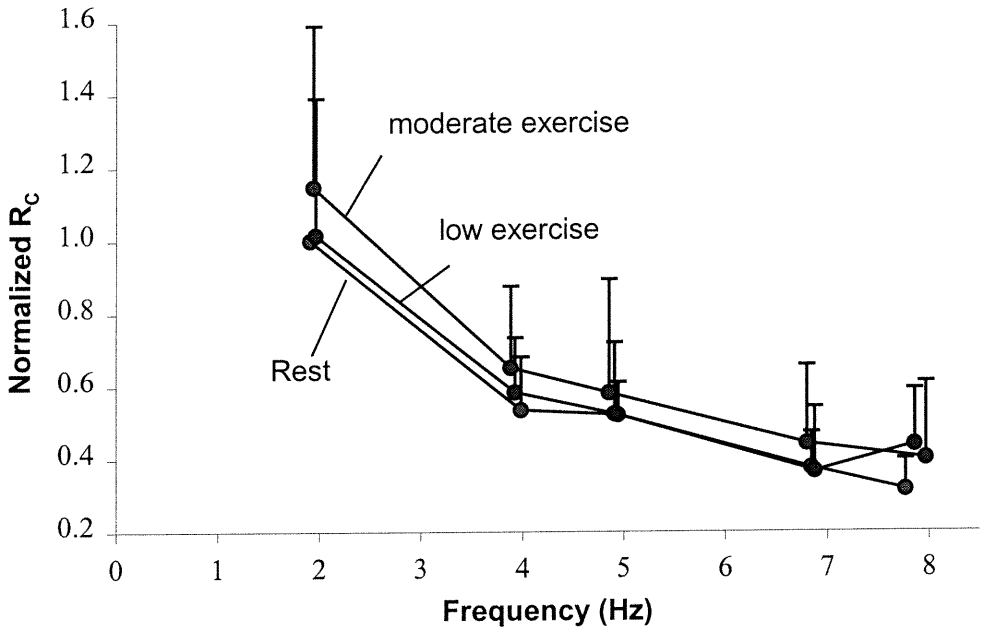

Figure 3.6: R_C at rest and at low and moderate levels of exercise (mean and SD for all subjects). Values are normalized to the resting values at 2 Hz.

Table 3.1: Imaginary part of Z_C.

Freq	#1	#2	#3	#4	#5
2 Hz	-0.675 ± 0.275	-1.124 ± 0.551	0.728 ± 1.291	-4.029 ± 2.848	-0.872 ± 0.771
5 Hz	-0.134 ± 0.295	1.173 ± 0.203	-0.005 ± 1.050	-0.124 ± 0.302	-0.533 ± 0.271
7 Hz	-0.252 ± 0.172	0.532 ± 1.285	-0.133 ± 0.199	0.497 ± 0.445	0.518 ± 0.393

Values (mean ± SD) are expressed in $cmH_2O.s.l^{-1}$

3.4. DISCUSSION

Each beat of the heart produces an asymmetric deformation of the lung which causes the fluctuations in airway flow (or pressure) known as CO. The amplitude of these oscillations increases with increases in cardiac output and filling pressure (Imanaka, 2000), both of which increase the mechanical deformation applied to the lung. Conversely, CO in flow are diminished or absent when airway resistance is increased (Engel, 1977). These observations lead to the notion that CO may harbor useful information about heart and/or lung function. Despite this, relatively little has been done to try and extract any such information. A few studies (Heckman, 1982; Johnson, 1981; Wessale, 1985; Wessale, 1988) have investigated CO as a means of tracking changes in stroke volume. CO have also been used as a qualitative index for differentiating between obstructive and central apneas during sleep (Ayappa, 1999; Idiong, 1998; Lemke, 1996). However, in most situations, CO are regarded as a nuisance and attempts are frequently made to eliminate them from recordings of airway opening pressure and flow and esophageal pressure (Schuessler, 1997; Schuessler, 1995). CO have also been associated with troublesome auto-triggering of mechanical ventilators (Imanaka, 2000).

Our goal was to investigate the use of CO in airway flow and pressure as means for determining a mechanical output impedance related to lung function. This involved first obtaining and processing P_C and $\dot{V}_C$ in an appropriate way, and then interpreting the resulting Z_C in physiological terms. The data acquisition and processing steps involved a number of assumptions. First, we assumed that the oscillations in $\dot{V}_C$ measured prior to

airway occlusion corresponded to the oscillations in P_C measured afterwards, and that each bore the same phase relationship to the heart sounds measured throughout the recording period. This assumption seems reasonable as we do not expect that occluding the airway of a relaxed apneic subject will have had any immediate affect on the activity of the heart. Another issue is that a period of apnea would be expected to cause a progressive change in cardiac activity, and possibly lung mechanics, as a result of neural effects and changes in blood gases. There was slight decrease in heart rate throughout the breath-hold maneuver, but it was small enough to be considered negligible and the individual cycles of P_C and $\dot{V}_C$ were highly reproducible (Figure 3.3). Furthermore, when Z_C was calculated with different combinations of the individual cycles in P_C and $\dot{V}_C$, the resulting Z_C showed good reproducibility (Figure 3.4).

CO have interested physiologists for a long time, particularly in terms of their manifestations in expired gas concentrations (Engel, 1986). CO in flow measured at the mouth are probably due to a direct action of the heart on the lung parenchyma (Engel, 1986), although exactly how is complicated and still somewhat obscure. The heart has an irregular shape and contracts with a twisting action producing localized transient inflations and deflations of the lung. This produces transient redistribution of gas throughout the lung (Engel, 1986), so there is no simple relationship between movement of the heart and the size of the CO in flow seen at the mouth. Also, the total heart volume varies very little throughout its beat (Hoffman, 1987), so the CO in flow presumably have little to do with stroke volume. It seems inevitable that CO in both pressure and flow should be modulated by anatomical or physiological factors (Engel, 1986; Johnson, 1981;

Wessale, 1985), such as exercise, lung volume and body posture. In the five subject we studied, the peak-peak swings in P_C at rest were 0.377 (SD 0.073) cmH_2O. During the two level of exercise these swings were 0.423 (SD 0.227) cmH_2O and 0.492 (SD 0,297) cmH_2O, respectively. The corresponding swings in $\dot{V}_C$ were 0.0350 (SD0.0278) $l.s^{-1}$ at rest and 0.0346 (SD 0.0376) $l.s^{-1}$ and 0.0314 (SD 0.0287) $l.s^{-1}$, respectively, at the two levels of exercise. The magnitudes of the CO in both pressure and flow were thus, perhaps surprisingly, essentially unaffected by the exercise even thought there was considerable variation between subjects. We also observed differences in the morphology of the oscillations in the same subject when repeated measurements were made on different days.

An important aspect of our study was thus to ascertain the extent to which Z_C is reproducible with variations in the nature of the heart beat. We investigated this issue by determining Z_C at rest and after low and moderate exercise (we did not attempt severe exercise because the subjects had to remain relaxed and apneic for 8 s immediately afterward for the measurements to be made). The subjects were all young and healthy so minimal exercise-induced bronchodilation and changes in respiratory mechanics were expected. We found that Z_C was highly reproducible regardless of the changes in heart rate and stroke volume produced by the exercise (Figure 3.4) which supports the notion that Z_C does indeed reflect a well-defined quantity.

In order to elucidate the physiological interpretation of Z_C, we compared it to Z_{in} measured using the forced oscillation technique. Obviously, we could not determine Z_{in} at

exactly the same frequency as the heart rate using the same amplitude of the flow as the CO because the very presence of the CO would have interfered with the determination of Z_{in}. Therefore, we identified Z_{in} over a range of frequencies bracketing the heart rate and its first few harmonics. We also used flow amplitudes that were similar to those of the CO in an attempt to make Z_C and Z_{in} comparable, as Z_{in} is known to depend to a certain extent on flow amplitude (Peslin, 1986). However, this resulted in a poorer γ^2 than would have been obtained with a larger amplitude flow perturbation. We attempted to achieve a compromise between requiring an adequate γ^2 and retaining sufficient data to make an effective comparison between Z_{in} and Z_C by setting our acceptance cutoff at $\gamma^2 \geq 0.90$.

The most striking aspect of the comparison between Z_{in} and Z_C (Fig. 3.5) is that X_C is essentially zero at all frequencies while X_{in} is mostly negative and increasing with frequency. Some of the subjects (nos. 3 and 4) exhibited quasi-hyperbolic X_{in} as described in numerous previous studies (Peslin, 1986) while the remaining subjects had X_{in} that varied less with frequency. These differences may be due to differences in the degree of relaxation among the subjects, as any respiratory muscle tone would be expected to have a large effect on respiratory tissue stiffness and hence on X_{in}. Nevertheless, the absence of any appreciable X_C indicates that Z_C was essentially purely resistive. This conclusion is further supported by the observation that X_C remained essentially zero despite increases in heart rate (Table 3.1).

The agreement between R_C and R_{in} was good in subjects 3 and 5 (Figure 3.5), while in the remaining three subjects R_{in} was uniformly higher than R_C. One possibility for such discrepancies is that the spectral content of the applied flow oscillations used to obtain Z_{in} was not the same as that producing Z_C. In particular, the harmonics of $\dot{V}_C$ fell off quickly with increasing frequency while the components of $\dot{V}$ used to produce Z_{in} did not. As respiratory impedance depends on many factors, including flow amplitude (Hantos, 1986; Oosteven, 1989; Wessale, 1988), it is possible that imperfect matching of measurement conditions could have accounted for the discrepancies between R_C and R_{in}. However, it is also possible that R_C and R_{in} reflect different quantities. R_{in} is a measure of the resistance of the total respiratory system and, even at high frequencies, contains components from both the airways and the chest wall tissues (Bates, 1989a). The fact that Z_C is purely real suggests that R_C is a measure of an airway flow resistance only, without any contribution from the respiratory tissues (which are viscoelastic and would give rise to a significant reactive component to Z_C). Therefore, we speculate that R_C is a measure of the resistance of the central and upper airways. In other words, when the mouth and glottis are open, the beating heart acts as a flow generator by compressing the lung tissue at the base of the airway tree. This produces $\dot{V}_C$ at the mouth. When the mouth is occluded, the pressure oscillations producing $\dot{V}_C$ are transmitted to the mouth to produce P_C. The ratio of P_C to $\dot{V}_C$ then yields a measure of the output impedance of the respiratory system, which in this case is the flow resistance of the conduit between the site of origin of the oscillations and the measurement point at the mouth.

It is perhaps somewhat curious that there is no appreciable imaginary part to Z_C. Given that the movement of the heart is known to produce local redistribution of flow in the lungs (Engel, 1986), one might expect there to be some effect of a local shunt compliance. In such a situation, the imaginary part of Z_C would reflect this compliance. It is possible that the shunt compliance was small and not discernable above the noise in our measurements. Interestingly, however, the real parts of Z_C tend to decrease with frequency (Figs. 3.4 and 3.5). The only way this can happen, barring nonlinear effects, is if there is a reactive component to the system. Some of the Z_C imaginary parts in Fig. 3.5 have a tendency to increase very slightly with frequency. Although these trends are not significant, they may hint at a small finite reactive component hidden in the noise.

As a further test of this interpretation of Z_C, we repeated its measurement in two of our subjects before and after the addition of an external resistance between the mouth and the pressure and flow transducers. The resistor had a value (1.5 $cmH_2O.s.l^{-1}$) comparable to that of normal human airway resistance. Four measurements were made under resting conditions in each configuration. In one subject, the real part of Z_C at 2 Hz with the added resistance had a mean value of 7.29 (SD 2.06) $cmH_2O.s.l^{-1}$, while without the added resistance the mean value was 5.32 (SD 1.13) $cmH_2O.s.l^{-1}$. In the other subject the mean value was 4.94 (SD 0.84) $cmH_2O.s.l^{-1}$ with the added resistance and 3.85 (SD 1.29) $cmH_2O.s.l^{-1}$ without the added resistance. The added resistance thus made a difference in the real part of Z_C for the two subjects of 1.97 and 1.09 $cmH_2O.s.l^{-1}$, respectively. These differences are not precisely equal to the added resistance of 1.5 cmH2O.s.l^{-1}, but this could easily be due to slight differences in measurement conditions (e.g. lung volume,

glottic aperture) between the measurements made with and without the added resistor. However, the values of resistance obtained with the added resistance bracket that of the added resistance itself, which supports the notion that Z_C gives a measure of the resistance due to flow of gas through airways.

In order to be able to measure CO in P_C and $\dot{V}_C$ reliably, it was necessary for our subjects to remain relaxed with an open glottis throughout the measurement period. This is not an easy thing to do and requires a considerable degree of subject cooperation. Untrained subjects tend to either close the glottis shortly after they suspend breathing or cannot discern whether their glottis is open or closed (Hantos, 1986; Morrell, 1995). This problem is almost certainly exacerbated with dyspnea following exercise. Our subjects became quite practiced at sitting relaxed with open glottis, and the measurements of Z_{in} and Z_C were made as close together in time as possible. We also observed that the signals measured during the first 4 s of the forced oscillation measurements were similar to those obtained during the second 4 s, which suggests that glottic aperture was consistent during these measurements. Nevertheless, it is still possible that our comparisons of Z_{in} and Z_C were affected by differences in glottic aperture.

In summary, we calculated Z_C between about 1.5 and 10 Hz using CO in airway pressure and flow measured in relaxed normal subjects at FRC with open glottis. Z_C was insensitive to heart rate changes induced by exercise and had an imaginary part close to zero at all frequencies investigated. R_C was similar to or smaller than R_{in} determined by the forced oscillation technique. We speculate that Z_C provides a measure of the flow

resistance of the central and upper airways of the lung. Z_C may thus be useful as a means of obtaining information about lung mechanics without the need for an external source of flow perturbations.

CHAPTER 4

ESTIMATING RESPIRATORY MECHANICS IN THE PRESENCE OF FLOW LIMITATION

Authors:

Bijaoui Eve, Tuck Stephanie A., Remmers John E. and Bates Jason H.T.

Published in:

Journal of Applied Physiology (1999); 86(1): 418-426

LINK WITH CHAPTER 3

The methods presented in previous chapters essentially apply to ventilator-dependent subjects, with or without an underlying respiratory pathology. The study of respiratory mechanics during spontaneous breathing helps in the diagnosis of respiratory diseases, in the follow up of a therapy and ultimately in understanding some of the causes and maybe preventing some of the consequences of a specific pathology. In the case of obstructive diseases, dynamic collapse of the airway and flow limitation are likely to complicate the assessment of respiratory mechanics and their interpretation. In Chapter 4, we study the effect of flow limitation during sleep on the airways and tissue mechanical properties embodied in respiratory mechanics. We compute the time-varying estimates of respiratory mechanical parameters by recursive implementation of multiple linear regression to a fit single compartment model to pressure and flow data. The results are expressed in terms of histograms where the contribution of a particular parameter value to its histogram is weighted by a corresponding estimate of the parameter variance. The use of the mean and standard deviation of the parameter histograms as indexes of flow limitation is studied in simulated data and in experimental data collected from obese sleeping pigs.

ABSTRACT

Dynamic collapse of the pulmonary airways, leading to flow limitation, is a significant event in a number of respiratory pathologies including obstructive sleep apnea syndrome and chronic obstructive pulmonary disease. Quantitative evaluation of the mechanical status of the respiratory system in these conditions provides useful insights into airway caliber and tissue stiffness which are hallmarks of such abnormalities. However, assessing respiratory mechanics in the presence of flow limitation is problematic because the single-compartment linear model upon which most assessment methods are based in not valid over the entire breath. Indeed, even deciding which parts of a breath are flow limited from measurement of mouth flow and pleural pressure often proves to be difficult. In this study, we investigated the use of two approaches to assessing the overall mechanical properties of the respiratory system in the presence of inspiratory flow limitation. The first method is an adaptation of the classic Mead-Whittenberger method, and the second method is based on information-weighted histograms obtained from recursively estimated signals of respiratory resistance and elastance. We tested the methods on data simulated using a computer model of the respiratory system and on data collected from obese sleeping pigs. We found that the information-weighted histograms provided the more robust overall estimates of respiratory mechanics.

4.1. INTRODUCTION

The modern approach to assessing respiratory mechanics in patients or animals is to match measurements of pressure, flow and volume made at the airway opening to the equation of a single-compartment linear model characterized by a resistance (R) and an elastance (E). This is done most efficiently on a computer using multiple linear regression. However, this model assumes that both R and E are constant over the data record being analyzed which, although satisfactory in many cases, breaks down completely in the presence of flow limitation because the effective flow resistance of the respiratory system changes markedly as flow limitation begins. Indeed while flow is limited one cannot even think of the system as having a resistance in the conventional sense because the flow is independent of the driving pressure. Consequently, the single-compartment linear model cannot be applied to an entire breath when flow limitation is present during some part of it. Nevertheless, clinical situations, such as ventilated patients with chronic obstructive pulmonary disease (D'Angelo, 1991; Guerin, 1993), frequently present the need to assess respiratory mechanics during flow limitation.

In this study, we investigate two approaches for assessing respiratory mechanics in the presence of flow limitation. The first is based on the so-called Mead-Whittenberger (Mead, 1953) technique in which E is estimated from the pressure change between the beginning and the end of inspiration. Substracting the product of E and volume from pressure then yields the resistive pressure throughout the breath. The resistive pressure may be a very nonlinear function of flow when flow limitation occurs at some point in

the breath. However, the Mead-Whittenberger method as traditionally implemented uses only two data points per breath to estimate E and so is particularly sensitive to noise. We have therefore developed a robust modification to the Mead-Whittenberger method that uses all the data within a breath to estimate E.

Our second approach to dealing with flow limitation is based on the recursive least squares (RLS) algorithm which allows one to track changes in R and E with a very short memory. We suspected this might allow us to estimate R and E adequately during those parts of the breath that are not flow limited, and possibly even detect the onset of flow limitation itself. The variations of the model parameter estimates over the breath can be represented by information-weighted histograms (Lauzon, 1991). The purpose of the present study was to evaluate both the modified Mead-Whittenberger and the RLS technique for assessing respiratory mechanics during flow limitation in both simulated and experimental data.

4.2. METHODS

4.2.1. Modeling the respiratory system

We modeled the lung, as shown in Figure 4.1, as a single compartment connected to a single airway. The flow-resistive pressure drop (P_{aw}) across the airway obeys Rohrer's equation

$$P_{aw} = K_1\dot{V} + K_2|\dot{V}|\dot{V} \qquad (1)$$

where $\dot{V}$ is ventilatory flow, K_1, K_2 are constants, and their values are listed in Table 4.1. The resistance (R_{aw}) of the airway is thus $K_1 + K_2|\dot{V}|$.

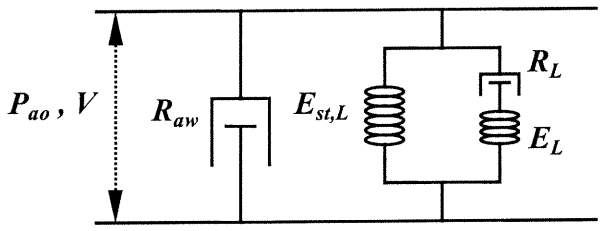

Figure 4.1: A five-parameter model of the lung. The model consists of a flow-dependent airway resistance R_{aw} (which contains two parameters through Eq. 1) together with a Kelvin body (characterized by the three parameters $E_{st,L}$, R_L and E_L), accounting for the viscoelasticity of the lung tissue according to D'Angelo *et al.* (1991).

The viscoelastic properties of the lung tissues are accounted for by a Kelvin body having parameters for static pulmonary elastance ($E_{st,L}$), overall lung resistance (R_L) and lung elastance E_L (Bates, 1989a; Fung, 1981; Guerin, 1993). These parameters were assigned values found in normal subjects by Guerin *et al.* (1993) and are listed in Table 4.1. The

Kelvin body is connected between the two moving components of the compartment, as shown in Figure 4.1.

Table 4.1: Model parameter values

	Parameter	Value
Lung	R_L ($cmH_2O.s.l^{-1}$)	3.44
	τ (s)	1.07
	E_L ($cmH_2O.l^{-1}$)	3.21
	$E_{st,L}$ ($cmH_2O.l^{-1}$)	8.2
Airways	K_1 ($cmH_2O.s.l^{-1}$)	1.85
	K_2 ($cmH_2O.s^2.l^{-2}$)	0.427

R_L: lung resistance; τ: time constant equal to R_L/lung elastance (E_L); $E_{st,L}$: static lung elastance; K_1 and K_2: Rohrer constants defining R_{aw} according to Eq. 1.

The pressure (P_{Kelvin}) across the Kelvin body obeys the equation (Fung, 1981):

$$P_{Kelvin}(t) + \frac{R_L}{E_L}\dot{P}_{Kelvin}(t) = E_{st,L}V(t) + R_L\left(1 + \frac{E_{st,L}}{E_L}\right)\dot{V}(t) \qquad (2)$$

where $\dot{P}_{Kelvin}$ is the time derivative of P_{Kelvin} and V is volume. The pressure (P_{ao}) at the airway opening (i.e. at the entrance to the airway) is then given by

$$P_{ao} = R_{aw}\dot{V} + P_{Kelvin} \qquad (3)$$

and therefore, the general motion equation of the model is:

$$E_L P_{ao}(t) + R_L \dot{P}_{ao}(t) = E_L E_{st,L} V(t) + \left[R_L(E_L + E_{st,L}) + E_L R_{aw}\right]\dot{V}(t) + R_L R_{aw}\ddot{V}(t) + R_L \dot{R}_{aw}\dot{V}(t) \qquad (4)$$

where $\dot{P}_{ao}$ is the time derivative of P_{ao}, $\ddot{V}$ is the time derivative of $\dot{V}$, and $\dot{R}_{aw}$ is the time derivative of R_{aw}. The model was driven by a $P_{ao}(t)$ waveform that increased linearly during inspiration and then returned within a few milliseconds to zero during expiration. The breathing frequency was 10 breaths/min and the inspiratory duty cycle was 0.33. Inspiratory flow limitation (IFL) was implemented in the model by never allowing $\dot{V}$ to exceed a specified threshold value, regardless of the driving pressure.

We simulated data using Matlab 4.2/Simulink 1.3 mathematical and simulation software. The model was solved using a fourth order Runge-Kutta integration method with a precision setting of six decimal places. Signals were sampled at the rate of 100Hz. We defined seven levels of IFL, going from "no flow limitation" to a threshold of 0.2 $l.s^{-1}$.

4.2.2. Experimental data

Three castrated male Vietnamese pot-bellied pigs were fed so that their body weight doubled in a few months (Tuck, 1997). The pigs were 21, 24 and 20 months of age and weighed 103, 104 and 118 kg, respectively. All protocols were approved by the Animal Care Committee at the University of Calgary. Sleep states were identified using EEG, EMG and nose twitch as an indicator of phasic rapid eye movement (REM) sleep. The pleural pressure (P_{pl}) was also measured by placing a balloon in the pleural space. The animals were anesthetized and mechanically ventilated during the surgical procedures required to implant these devices.

The pigs breathed spontaneously through a facemask-pneumotachograph system to record respiratory airflow $\dot{V}$. The facemask was constructed and adapted for each pig and then attached to a pneumotachograph (3700, Hans Rudolph) connected to a differential pressure transducer (MP-45-15, Validyne). The system had a total deadspace of 130 ml. The pleural balloon was inflated and connected to a differential pressure transducer (MP-45-32, Validyne) and referred to mask pressure. In *pig 1* a cylindrical balloon of 7 ml was used, while in *pigs 2* and *3* a square balloon of 1 ml was used. Sequences of data, lasting from 60 to 70 s, and containing 14 to 26 breaths, were recorded in non-rapid eye movement (NREM) sleep in each animal. Sections of the data containing between 4 and 14 consecutive breaths were selected for analysis. P_{pl} and $\dot{V}$ signals were sampled with a 16-bit analog-to-digital converter at 100Hz.

4.2.3. Data processing

Recursive least squares (RLS) and information-weighted histograms: We fit our data to the equation of motion of the single-compartment linear model of the respiratory system. This equation is expressed in matrix notation as

$$\mathbf{Y} = \mathbf{XA} \qquad (5)$$

where

$$\mathbf{Y} = \begin{pmatrix} P_1 \\ P_2 \\ . \\ . \\ . \\ P_N \end{pmatrix} \tag{6}$$

is the vector of dependent variables, where N is the number of data points

$$\mathbf{X} = \begin{pmatrix} \dot{V}_1 & V_1 & 1 \\ \dot{V}_2 & V_2 & 1 \\ . & . & . \\ . & . & . \\ . & . & . \\ \dot{V}_N & V_N & 1 \end{pmatrix} \tag{7}$$

is the matrix of independent variables, and

$$\mathbf{A} = \begin{pmatrix} R \\ E \\ K \end{pmatrix} \tag{8}$$

is the parameter vector. P_i, V_i and $\dot{V}_i$ are the ith measurements of tracheal pressure, volume and flow, respectively. V was obtained by a Simpson's rule integration of $\dot{V}_i$. The parameters R and E are referred as resistance and elastance (respectively) of the system, and K is the value of pressure in the model when both flow and volume are equal to zero.

The conventional least squares estimate of A (i.e. the estimate provided by fitting the model to all the data at once in the usual way) is given by

$$\hat{\mathbf{A}} = \left[\mathbf{X}^{\mathrm{T}}\mathbf{X}\right]^{-1}\mathbf{X}^{\mathrm{T}}\mathbf{Y} = \mathbf{Q}\mathbf{X}^{\mathrm{T}}\mathbf{Y} \tag{9}$$

where **Q** is the so-called "information matrix" of the system and **T** is the transpose operator. The leading diagonal elements of **Q** are proportional to the standard deviations (SDs) of the estimates of the parameters. Thus, if these diagonal elements are large, the confidence regions about the corresponding parameter estimates are also large.

In contrast to conventional least squares, the RLS algorithm begins by assuming that all parameters values are zero, and then proceeds to update the parameters each time a new data set arrives. In other words, the RLS algorithm performs conventional multiple linear regression on a finite data set, but it does so recursively so that a sequence of estimates is obtained for each parameter rather than just a single value for the entire data set. Thus, if $\hat{\mathbf{A}}_k$ is the estimated parameter vector obtained from the first k measurements, then the estimated parameter vector obtained from the first $k+1$ measurements is given by

$$\hat{\mathbf{A}}_{k+1} = \hat{\mathbf{A}}_k + \mathbf{Q}_{k+1}\mathbf{X}_{k+1}\left(y_{k+1} + \mathbf{X}_{k+1}^{\mathbf{T}}\hat{\mathbf{A}}_k\right)/\left(\rho + \mathbf{X}_{k+1}^{\mathbf{T}}\mathbf{Q}_k\mathbf{X}_{k+1}\right) \qquad (10)$$

where y_{k+1} is the most recent measurement of the dependent variable and

$$\mathbf{Q}_{k+1} = \frac{1}{\rho}\left[\mathbf{Q}_k - \mathbf{Q}_k\mathbf{X}_{k+1}\mathbf{Q}_k/\left(\rho + \mathbf{X}_{k+1}^{\mathbf{T}}\mathbf{Q}_k\mathbf{X}_{k+1}\right)\right] \qquad (11)$$

ρ is a constant ($0 < \rho \leq 1$) called the forgetting factor and is related to the time constant τ_{mem} of the memory by the relation $\tau_{mem} = -\delta t/\ln(\rho)$ where δt is the sampling interval. The RLS algorithm was initialized with $\hat{\mathbf{A}}_0 = 0$ and $\mathbf{Q_0} = 10^6\mathbf{I}$ (**I** is the identity matrix). For both simulated and experimental data, τ_{mem} was 0.4 s, similar to previous studies (Avanzolini, 1995; Bates, 1992).

Figure 4.2 shows an example of a complete breath of $\dot{V}$ and $\boldsymbol{P}$ simulated by the model, together with the recursively estimated R and E both without IFL (Fig. 4.2A) and when the IFL threshold was 0.3 $l.s^{-1}$ (Fig. 4.2B). Even without IFL, there is some variation in both R and E throughout the breath (Fig. 4.2A) because of the flow dependence of R_{aw} and the frequency dependence of the viscoelastic tissue mechanical properties. However, this variation is greatly accentuated in the presence of IFL (Fig. 4.2B). In particular, R begins to decrease and E begins to increase markedly as soon as IFL starts.

We calculated "information-weighted histograms", as defined by Bates and Lauzon (1992), from the recursively estimated R and E. This requires that the value of τ_{mem} be chosen appropriately. If τ_{mem} is too large then there will be systematic deviations between the measured $\boldsymbol{P}$ signal and that predicted by the model, because R and E will not be able to change their values fast enough to account for all the variation in the data. Conversely, if τ_{mem} is too small then the model will predict not only the deterministic parts of $\boldsymbol{P}$ but also any noise it contains. Choosing τ_{mem} appropriately in between the extremes allows the model to account for the deterministic variation in the data, but not the noise. This gives rise to R and E signals that generally exhibit considerable variations over a breath. These variations were represented in what we call information-weighted histograms. That is, rather than simply assigning each value in a parameter signal to its appropriate bin, as is usually done when constructing a histogram, we first scaled each point in the parameter signal by the inverse of its corresponding diagonal element in the information matrix ($\mathbf{Q}$). In other words, we calculated histograms from the products of each parameter with the inverse of its variance.

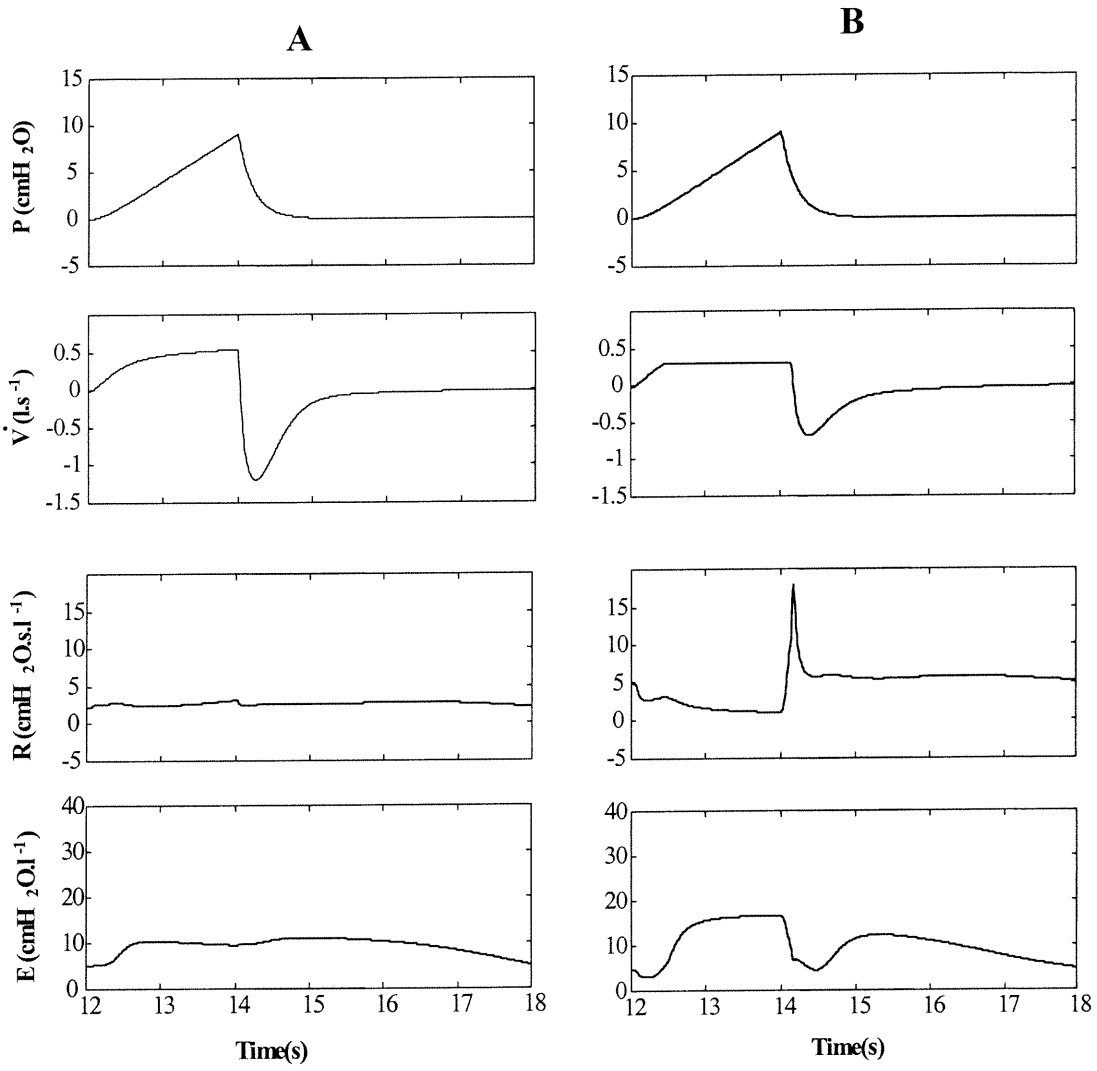

Figure 4.2: Time-course of resistance R and elastance E, obtained by recursive least squares, applied to simulated data (A) without flow limitation, and (B) with an IFL threshold of 0.3 l.s^{-1}. $\dot{V}$: ventilatory airflow; P: tracheal pressure.

Figure 4.3 gives the information-weighted histograms of *R* and *E* for a complete breath without IFL (Fig. 4.3A) and when the IFL threshold was 0.3 l.s^{-1} (Fig. 4.3B). The information-weighted histograms without IFL are reasonably narrow, reflecting the modest variability of *R* and *E* seen in Fig. 4.2A. By contrast, the histograms obtained

with IFL are wide and multimodal, reflecting the large degree of parameter variability seen in Fig. 4.2B.

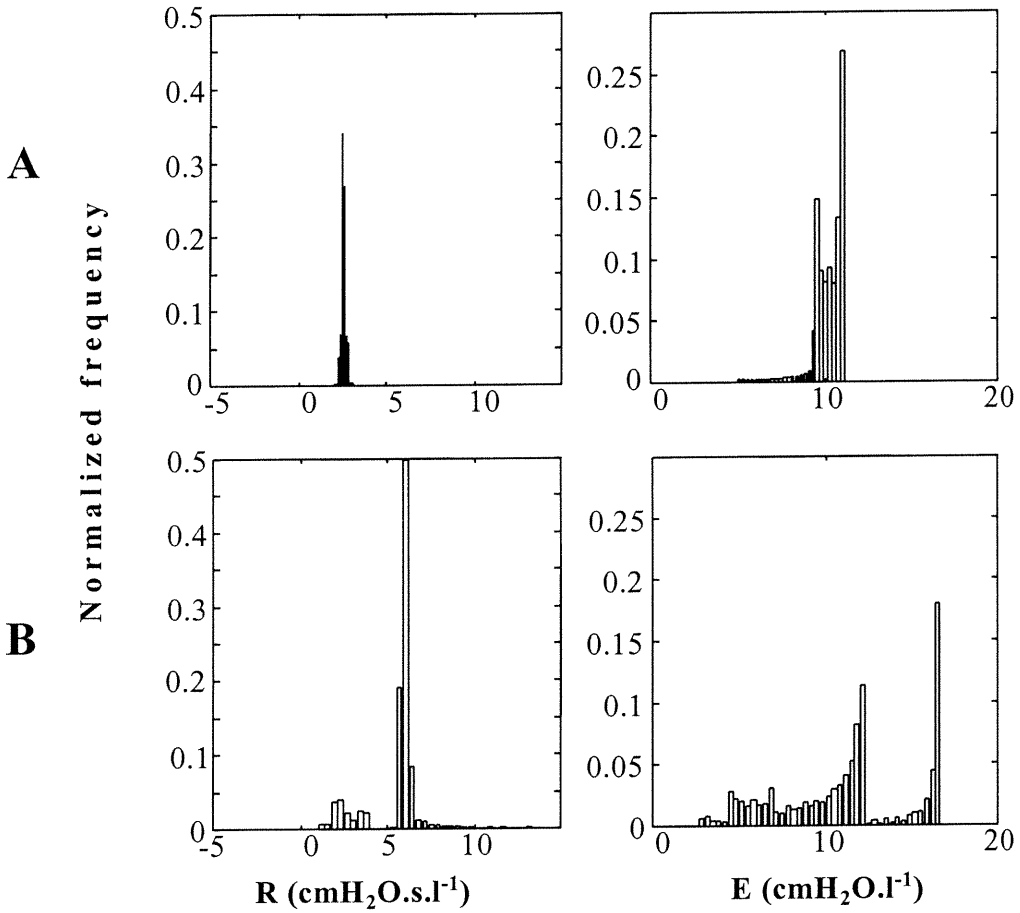

Figure 4.3: Information-weighted histograms for *R* and *E*, (A) without flow limitation, and (B) with an IFL threshold of 0.3 $l.s^{-1}$.

Modified Mead-Whittenberger method: The original Mead-Whittenberger method assumes a constant elastance between two points of zero flow to obtain elastic pressure. At each of these two points the term $\boldsymbol{R\dot{V}}$ in Eq. 4 becomes zero, so that $E = \Delta P/\Delta V$ where ΔP and ΔV are the differences in pressure and volume between the two points.

Consequently, E is determined by only two points in the entire breathing cycle and is therefore very susceptible to errors in the measurement of P or V at these points. In particular, P tends to change very rapidly at the end of inspiration so the accurate identification of the zero-flow point here can be problematic.

We thus decided to modify the Mead-Whittenberger method as follows. We assumed that the resistive pressure, $\boldsymbol{P}_{res}$, is a single-valued, although nonlinear, function of $\dot{\boldsymbol{V}}$. This means that $\boldsymbol{P}_{res}$ plotted against $\dot{\boldsymbol{V}}$ over the breath should define a single curve with no looping. That is,

$$\int_{cycle} \boldsymbol{P}_{res} \cdot d\dot{\boldsymbol{V}} = 0 \tag{12}$$

where

$$\boldsymbol{P}_{res} = \boldsymbol{P} - \boldsymbol{E}\boldsymbol{V} - \boldsymbol{K} = \boldsymbol{R}\dot{\boldsymbol{V}} \tag{13}$$

This leads to

$$\int_{cycle} \boldsymbol{P} \cdot d\dot{\boldsymbol{V}} - \int_{cycle} \boldsymbol{K} \cdot d\dot{\boldsymbol{V}} - \boldsymbol{E} \int_{cycle} \boldsymbol{V} \cdot d\dot{\boldsymbol{V}} = 0 \tag{14}$$

so that

$$\boldsymbol{E} = \frac{\int_{cycle} \boldsymbol{P} \cdot d\dot{\boldsymbol{V}} - \int_{cycle} \boldsymbol{K} \cdot d\dot{\boldsymbol{V}}}{\int_{cycle} \boldsymbol{V} \cdot d\dot{\boldsymbol{V}}} \tag{15}$$

The constant K was estimated from the plateau in $\boldsymbol{P}$ at the end of expiration and then used in Eq. 13 along with E from Eq. 15 to yield $\boldsymbol{P}_{res}$ over the cycle. Dividing $\boldsymbol{P}_{res}$ by $\dot{\boldsymbol{V}}$ then

gave R over the breathing cycle. A mean value for R was estimated as the slope obtained from a linear regression analysis between $\boldsymbol{P}_{res}$ and $\dot{V}$ for each breath.

Figure 4.4A shows $\boldsymbol{P}_{res}$ obtained using the modified Mead-Whittenberger method both with and without IFL. Even without IFL, $\boldsymbol{P}_{res}$ plotted against $\dot{V}$ describes a loop, because the model has two mechanical degrees of freedom. In the presence of IFL (solid line), the $\boldsymbol{P}_{res}$ - $\dot{V}$ curve becomes very nonlinear during inspiration due to inspiratory $\dot{V}$ being clipped above the IFL threshold. Figure 4.4B shows the time-course of R during inspiration (R_I) obtained using the modified Mead-Whittenberger method, without (dotted line) and with (solid line) IFL. Without IFL, R_I is reasonably stable throughout inspiration. However, with the onset of IFL (at around 0.4s), R_I starts to increase significantly due to the increase of $\boldsymbol{P}_{res}$ while $\dot{V}$ is constant.

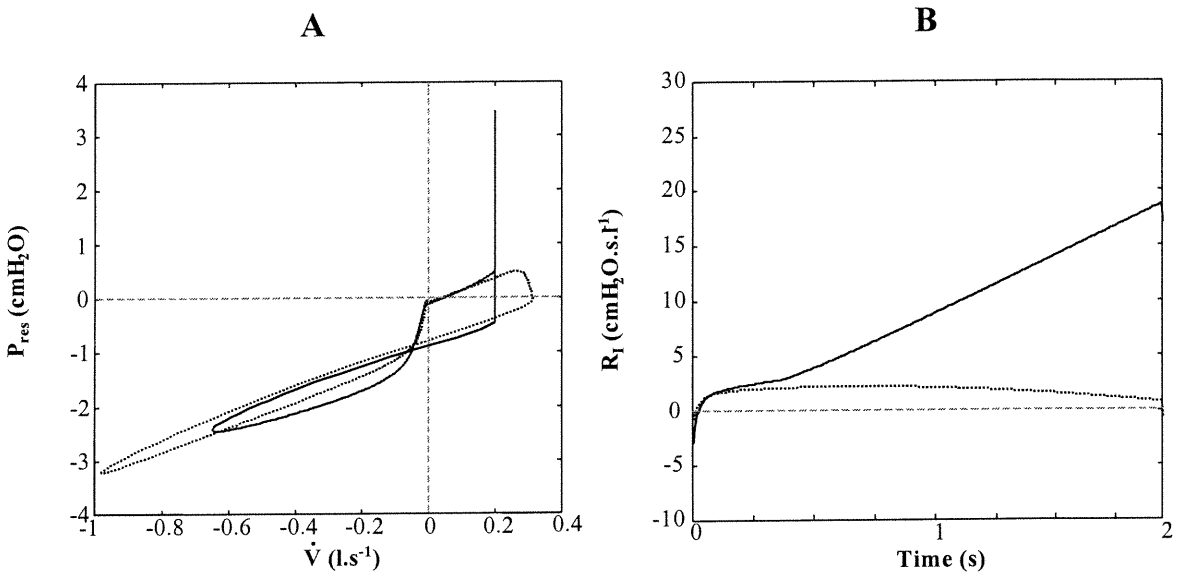

Figure 4.4: (A) Resistive pressure (P_{res}) vs. $\dot{V}$ curve without flow limitation (dotted line) and with an IFL threshold of 0.2 $l.s^{-1}$ (solid line). (B) Time variations of inspiratory resistance R_I without flow limitation (dotted line) and with an IFL threshold of 0.2 $l.s^{-1}$ (solid line).

4.3. RESULTS

We compared the estimates of R provided by the information-weighted histograms and the modified Mead-Whittenberger techniques as a function of the IFL threshold. Figure 4.5 shows the mean value ± SD of R provided by the information-weighted histograms and the mean value of R from modified Mead-Whittenberger method. Also shown in Figure 4.5 are the mean ± SD values of the actual RLS estimates themselves. For both RLS and modified Mead-Whittenberger methods, mean R increases rapidly with decreasing IFL threshold. The mean of the information-weighted histograms for R is the least sensitive to IFL, even though its standard deviation increases markedly.

Figure 4.6 gives an example of the $\boldsymbol{P}_{pl}$ and $\dot{V}$ signals over a single breathing cycle obtained from one of the pigs studied, both awake without IFL (Fig. 4.6A) and asleep with IFL (Fig. 4.6B). IFL was defined as being present if $\dot{V}$ reached a plateau for more than the latter half of the breath. The experimental data with IFL differ in some important ways from the simulated data shown above (Fig. 4.2B), particularly with regard to $\dot{V}$. Specifically, expiratory $\dot{V}$ can be divided into three parts, indicated as *i*, *ii* and *iii* in Fig. 4.6B. In part *i*, $\dot{V}$ is only slightly negative and relatively stable. This changes suddenly to a steep increase in slope in part *ii*. Finally, $\dot{V}$ levels off again in part *iii*. The corresponding $\boldsymbol{P}_{pl}$ signal shown in Fig. 4.6B is essentially flat throughout expiration, indicating that the various features seen in $\dot{V}$ are not due to respiratory muscle activity, and therefore presumably reflect time variations in expiratory flow resistance.

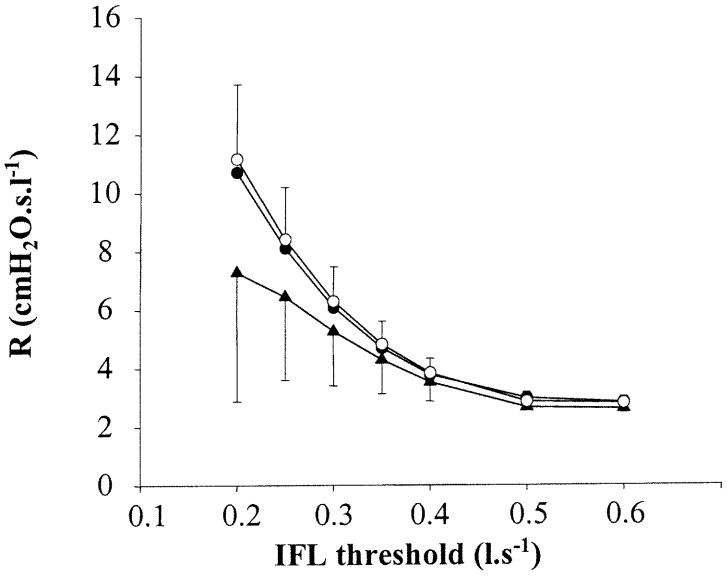

Figure 4.5: Resistance estimates (means ± SD) using recursive least squares (●), information-weighted histograms (▲) and modified Mead-Whittenberger (○) methods. The top error bars correspond to the least squares data (●).

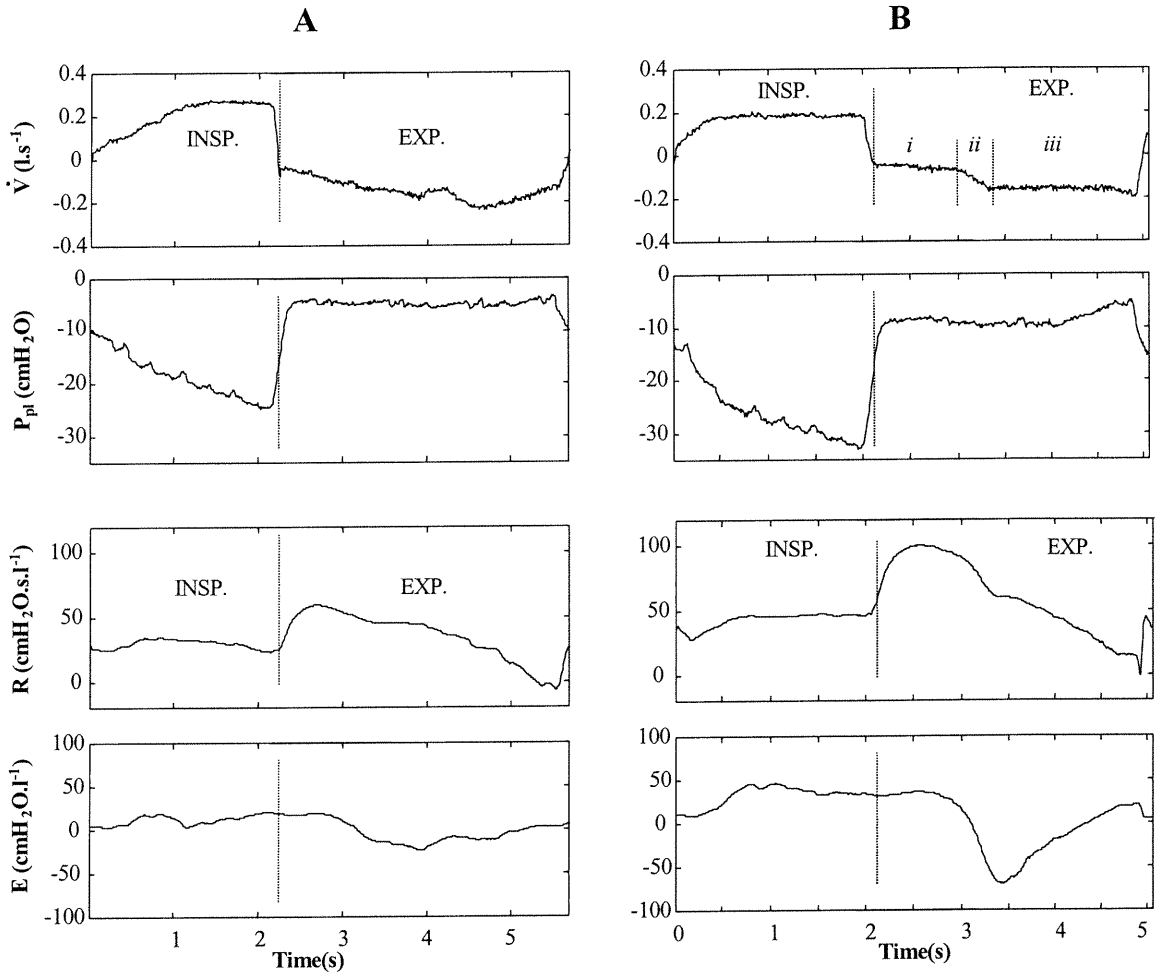

Figure 4.6: $\dot{V}$, pleural pressure (P_{pl}) signals, and time course or R and E obtained by recursive least squares from non flow-limited awake (A) and flow-limited NREM (B) data from *pig 1*. INSP.: inspiration; EXP.: expiration; *i*, *ii*, *iii*: 3 parts of expiratory $\dot{V}$ (see text)

Figure 4.7 shows examples of information-weighted histograms for R and E obtained from the three pigs studied. Figure 4.7A shows histograms without IFL while Figs. 4.7B-D show histograms with IFL. A number of consecutive breaths were analyzed under each condition, and the means and standard deviations of the histogram means and standard deviations are given in Table 4.2. All histograms were wide and multimodal, although the widths of the histograms (SD in Table 4.2) were greater for most of the IFL cases.

Figure 4.8 shows a plot of $\boldsymbol{P_{res}}$ versus $\dot{V}$ for the same data as Fig. 4.7. Each curve describes a "figure-of-eight" loop, similar to the data in Fig. 4.4. Mean values of R and E and their standard deviations obtained from multiple breaths analyzed in all pigs with the modified Mead-Whittenberger method are given in Table 4.2.

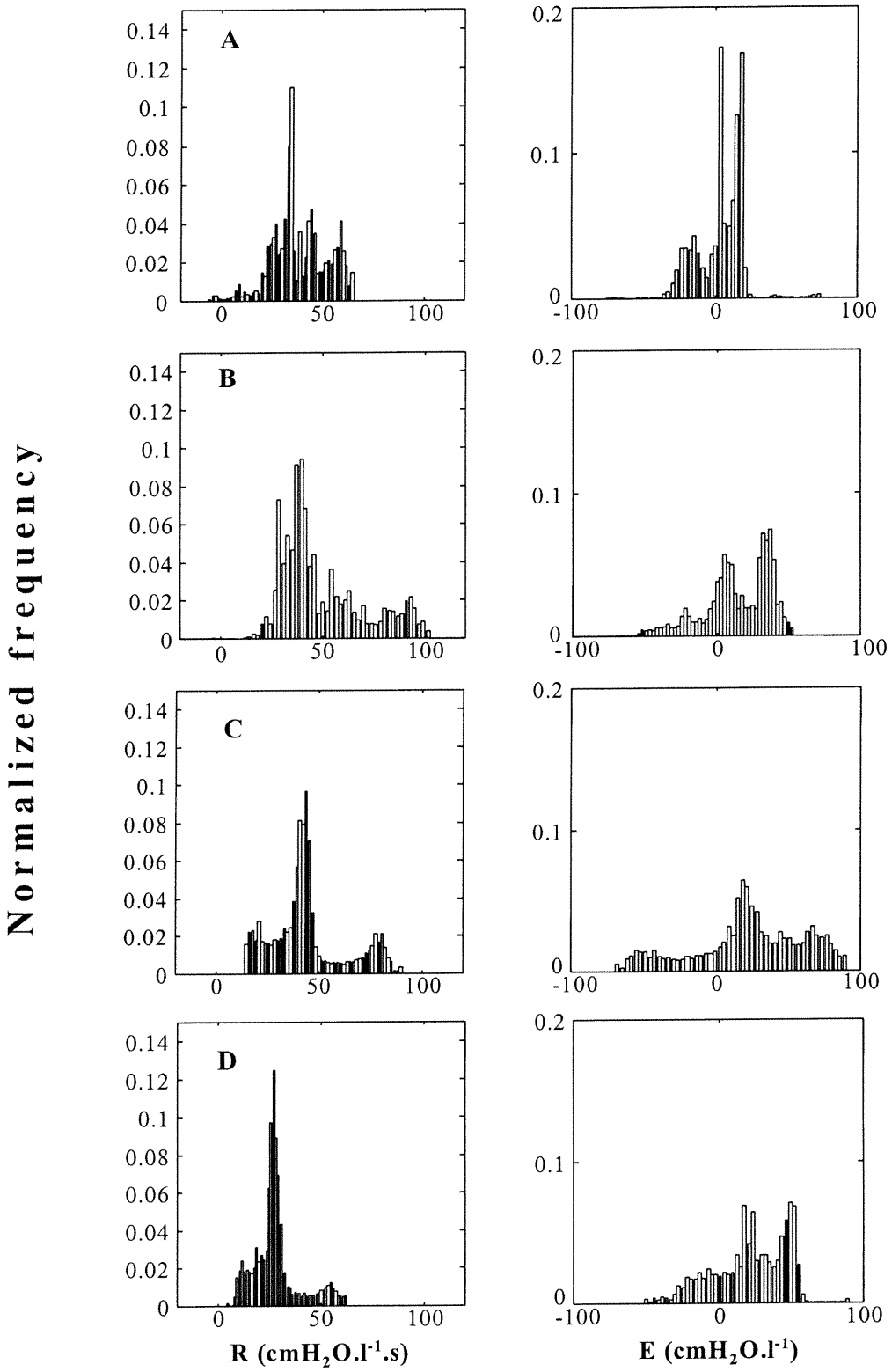

Figure 4.7: Information-weighted histograms for *R* and *E* from awake *pig 1* (A) and from NREM sleeping *pigs 1-3* (B-D). Data in A were non-flow limited, whereas data in B-D were flow-limited.

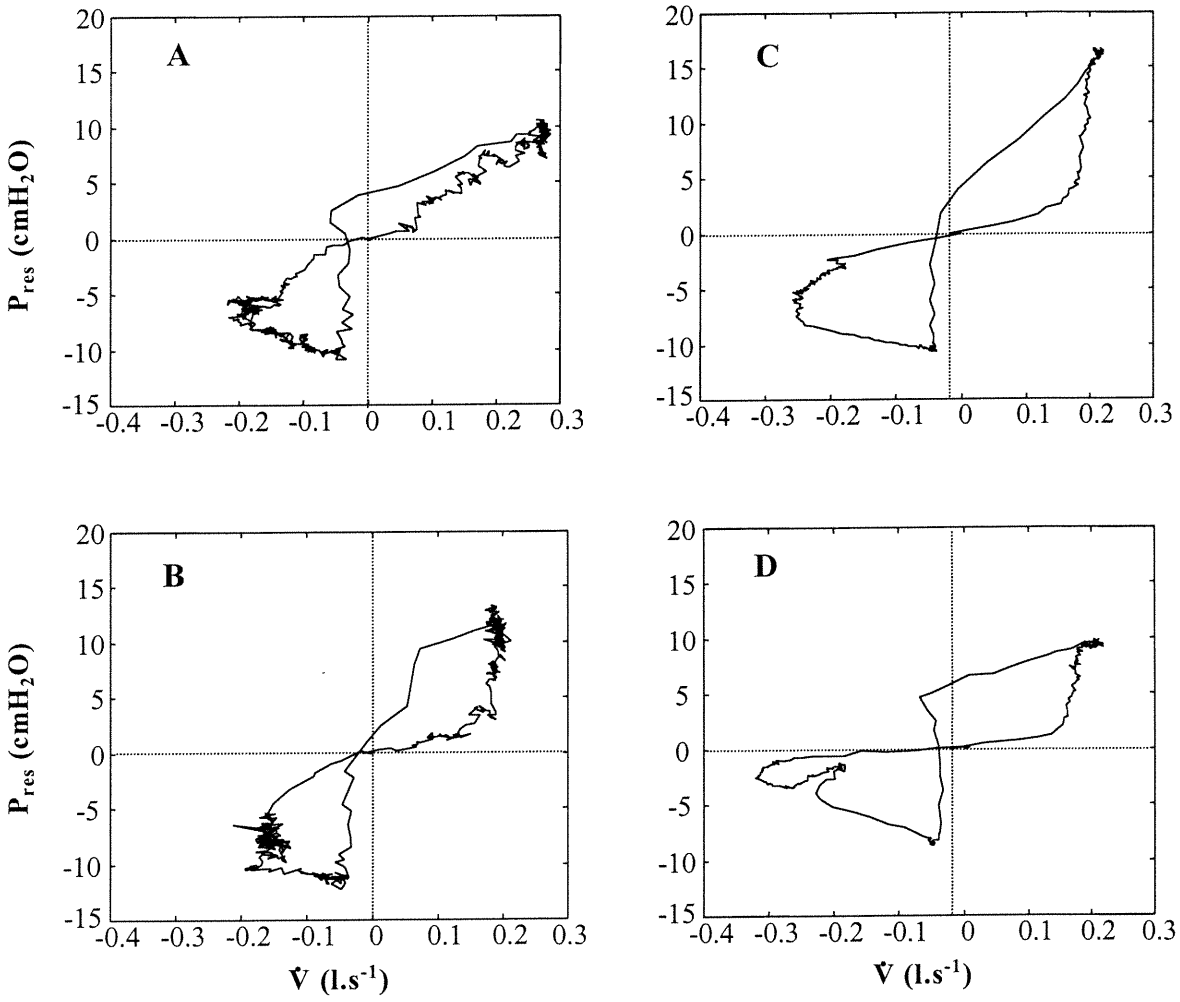

Figure 4.8: P_{res} vs. $\dot{V}$ curves for the awake *pig 1* (A) and from NREM sleeping *pigs 1-3* (B-D). Data in A were non-flow limited, whereas data in B-D were flow-limited.

Table 4.2: Results of analysis of *n* consecutive breaths in one non-flow limited pig (*pig 1* awake) and 3 flow limited pigs (*pigs 1-3*, NREM).

	***E* (MMW)** ($cmH_2O.l^{-1}$)	***R* (MMW)** ($cmH_2O.s.l^{-1}$)	**Mean *E* (IWH)** ($cmH_2O.l^{-1}$)	**SD *E* (IWH)** ($cmH_2O.l^{-1}$)	**Mean *R* (IWH)** ($cmH_2O.s.l^{-1}$)	**SD *R* (IWH)** ($cmH_2O.s.l^{-1}$)	***n***
Pig 1 awake	11.85 (5.61)	38.29 (4.26)	4.07 (1.02)	16.10 (5.61)	38.34 (1.37)	13.74 (1.32)	4
Pig 1 NREM	18.84 (1.15)	50.83 (6.56)	14.69 (2.18)	23.55 (3.73)	50.26 (6.53)	19.45 (4.72)	14
Pig 2 NREM	39.86 (0.56)	44.87 (2.27)	22.73 (3.76)	37.55 (3.07)	44.02 (1.45)	17.71 (1.49)	13
Pig 3 NREM	38.10 (1.43)	27.75 (1.69)	22.44 (5.64)	24.52 (2.05)	27.89 (1.98)	11.09 (1.20)	14

n: No. of breaths; NREM: non rapid eye movement; E: elastance; R: resistance; MMW: modified Mead-Whittenberger; IWH: information-weighted histograms; SD: standard deviation. Mean IWH parameter values are means of the histogram means. SD IWH values are SDs of the histogram means. SDs of all quantities are in parentheses.

4.4. DISCUSSION

Flow limitation is an important feature of chronic airway obstruction (Guerin, 1993). In subjects with obstructive sleep apnea syndrome, IFL often anticipates the appearance of an apnea or a respiratory-event-related arousal (Hudgel, 1984; Series, 1995; Skatrud, 1985). Flow limitation exists, by definition, when flow and respiratory efforts are dissociated, which implies that the respiratory system ceases to have a resistance in the conventional sense. Consequently, if flow limitation occurs at some point within a breath, then the usual mechanical parameters R and E can no longer be assessed in a meaningful way for that breath in its entirety. Of course, those parts of the breath that do not involve flow limitation may be used to estimate values for R and E in the usual way, although the challenge then becomes to determine where in the breath flow limitation occurs, or at least to analyze the data in such as way that the flow-limited portions do not exert undue influence on the results. We chose to examine the case where flow limitation occurs at some point during inspiration, because this was thought to be an important respiratory event occurring in our obese pigs with sleep-disordered breathing (Tuck, 1997).

We investigated two approaches to the problem of assessing respiratory mechanics in the presence of flow limitation. One of these approaches was based on the classic method suggested Mead and Whittenberger (Mead, 1953), which is generally invoked under the assumption that the respiratory system can be adequately represented as a single uniformly ventilated compartment with a resistance and elastance that remain constant

throughout the breathing cycle (i.e. Eq. 13). As a general tool for assessing respiratory resistance and elastance, the Mead-Whittenberger method has been superceded in recent years by the use of multiple linear regression for reasons of speed and robustness. However, whereas the assumption of constant resistance and elastance is binding for the multiple linear regression approach when applied to an entire breath, the Mead-Whittenberger method is only strictly limited by an assumption of constant elastance. The $\boldsymbol{P}_{res}$ curve that it returns, after subtraction of the product of E and V from $\boldsymbol{P}$, may take on any nonlinear shape as a function of $\dot{V}$, so that $\boldsymbol{P}_{res}$ divided by $\dot{V}$ may be similarly nonlinear. This means that the Mead-Whittenberger method should be applicable to the flow-limited situation, provided that E remains constant throughout the breath and can be accurately estimated.

The problem with the Mead and Whittenberger method, from a practical point of view, is that is uses only two data points - those at the beginning and end of inspiration when $\dot{V}$ is zero - to estimate E. This means that E is very sensitive to noise in the data. Even more problematic, it may be difficult to accurately determine pressure at points of zero $\dot{V}$ because pressure may be changing rapidly at these points (particularly in the transition from inspiration to expiration). Errors in the determination of E then lead to errors in $\boldsymbol{P}_{res}$ and R. We therefore modified the method in a manner that uses all the $\boldsymbol{P}$ and $\dot{V}$ data over the breath to determine E. The modification is based on the assumptions that E remains constant throughout the breath, and that $\boldsymbol{P}_{res}$ be a single-valued function of $\dot{V}$. Neither of these assumptions is particularly good. For example, E is expected to vary throughout the breath due to the nonlinear and multicompartmental nature of respiratory

system mechanics. Also, P_{res} is expected to depend on both lung volume and lung volume history, and indeed the effects of this are clearly visible in the looping of both the simulated data (Fig. 4.4) and the data from the pigs (Fig. 4.8). The potential utility of the modified Mead-Whittenberger method is demonstrated in Fig. 4.4, which shows the vertical segment of P_{res} versus $\dot{V}$ where IFL occurred in the simulated data. Although no such clear vertical spike is seen in the real data (Fig. 4.8), all three pigs show a nearly vertical segment of P_{res} at the end of inspiration, which presumably reflects IFL.

The pig data also showed some features not present in the simulated data. Specifically, in Fig. 4.6 the representative breath shown has been divided into three phases in expiration. In *phase i*, expiratory flow is small and relatively constant. One possibility for this observation is that these pigs were flow limited early in expiration as well as inspiration, as correlation between IFL and expiratory flow limitation has been previously reported (Stanescu, 1996). However, we think it most likely that the changes in expiratory resistance reflect actively regulated expiratory braking, probably by the larynx, whereby the obese animal regulates lung volume during expiration (Bartlett, 1973). The rapidly increasing expiratory flow in *phase ii* then presumably results from the sudden reopening of the upper airway. Finally, at the end of expiration flow again becomes limited and so levels off in *phase iii*. Furthermore, although we have not identified phases of expiration for the non-IFL pig (Fig. 4.6A), it seems that glottic braking is also occurring here, as $\dot{V}$ at the start of expiration is much less than later on. These factors all contribute to the substantial degree of looping seen in the P_{res} - $\dot{V}$ curves for all animals seen in Fig. 4.8.

The second method we investigated was based on the RLS method of fitting the single-compartment linear model to respiratory data. Although this approach is, in principle, bound by the same assumptions as conventional multiple linear regression, its recursive nature means that the model is effectively being fit to only a small segment of data at any one time (the data length being determined by the memory time-constant of the RLS algorithm). Our initial hope was that this might allow us to identify the point at which IFL began, as a sudden change in the natures of the recursively estimated values of R and E. Unfortunately, the issue is not completely clear in practice. Although it is certainly true that IFL did produce significant changes in R and E (Fig. 4.2B), R and E still varied somewhat without any IFL (Fig. 4.2A). This occurred because of the fact that the single-compartment linear model does not describe a nonlinear, multi-compartment respiratory system perfectly, so that variations in the best-fit values of R and E throughout a breath are expected even in the normal lung. Thus, the detection of flow limitation from changes in recursively estimated R and E values becomes a question of degree, and it is not clear how to decide *a priori* how much variation should be taken as an indication of flow limitation.

However, even though it may be difficult to identify the onset of flow limitation, the RLS method does enable us to deal with the situation where the single-compartment linear model gives a poor fit to the data from an entire breath. Specifically, by allowing R and E to vary over the breath, rather than requiring they achieve a single representative value, we can gain some measure of the departure of the mechanical behavior of the respiratory system from that of a single compartment. The obvious way to represent the variation of

a signal such as R or E in Fig. 4.2 is to construct a histogram of the values, thereby representing the relative frequencies of appearance of each value over the data record. Unfortunately, this does not always produce physiological sensible results, as the recursively estimated parameter values may be negative at some points during the breathing cycle. Bates and Lauzon (1992) found, however, that those portions of the data that produced such meaningless values invariably contained very little information, as reflected in the corresponding diagonal values of the information matrix (these diagonal values are proportional to the estimated variances of the estimated parameters). This led to the notion of the information-weighted histogram proposed by Bates and Lauzon (1992) and used subsequently by Avanzolini *et al.* (1995). Here, the variations in R and E are represented in a histogram, but the contribution of each value to the histogram is weighted by the inverse of the corresponding diagonal element of the information matrix. The result is a histogram largely dominated by only those parameter values that are strongly determined by the data, and hence the physiologically meaningless values tend to be almost completely suppressed.

The modest widths of the information-weighted histograms from the simulated data without IFL (Fig. 4.3A) are due to the modest degree of parameter variation over the breathing cycle (Fig. 4.2A). In contrast, the histograms from the IFL simulated data (Fig. 4.3B) are much wider, in keeping with the greater degree of variation in R and E (Fig. 4.2B). The histograms from the pig data (Fig. 4.7) are wider still, and significant portions of the E histograms are negative, even in the non-flow-limited example, despite the information weighting. The greater proportion of negative values in the histograms for E

as opposed to those for R (Fig. 4.7) could reflect an influence of inertance, as some parts of the $\dot{V}$ signals recorded from the pigs changed rapidly (Fig. 4.6).

In order to summarize the large amount of detail in the histograms, we characterized them in terms of their means and standard deviations. These are plotted for R estimated from the simulated data as a function of IFL threshold in Fig. 4.5, and show that as the fraction of inspiration that is flow limited increases (i.e. as the IFL threshold decreases), the standard deviations of the histograms also increase. This is to be expected because IFL produces an increased variation in R throughout the breath. The mean value of R also increases with the severity of IFL, in agreement with the findings of Hudgel *et al.* (1984) and Condos *et al.* (1994) who also found that mean R increased with the level of IFL. However, the increase we found in mean R from the information-weighted histogram is not as much as the increases in mean R calculated by either the modified Mead-Whittenberger method or the mean of the recursively estimated R signal (Fig. 4.5). This suggests that the information-weighted histograms may be the more robust means for arriving at an estimate of respiratory resistance in the presence of IFL. The information-weighted histograms were also quite reproducible from one breath to the next. Table 4.2 shows that both the means and standard deviations of the histograms obtained from each animal studied had relatively small standard deviations. Indeed, the standard deviations of the histogram means were of similar magnitudes to the standard deviations of the corresponding parameter values obtained by the modified Mead-Whittenberger method (Table 4.2).

To summarize, we have investigated the use of two methods for assessing respiratory mechanics in the presence of IFL; the modified Mead-Whittenberger method, and the RLS method with information-weighted histograms. Both methods clearly show that the effective R of the respiratory system varies significantly over the breathing cycle in the presence of IFL, and this variation increases as the IFL threshold decreases (i.e. as the fraction of inspiration in which flow is limited increases). Our results from simulated data suggest that the information-weighted histograms may be the more robust means for obtaining an effective overall value for R in the presence of IFL, even though the concept of resistance during IFL is somewhat dubious. The widths of the information-weighted histograms may also serve as an index of mechanical pathology. That is, a certain variability in R and E is expected throughout the breath, even from a normal lung, but when the respiratory system becomes abnormal and exhibits flow limitation during tidal ventilation, this variability is greatly increased.

CHAPTER 5

MECHANICAL PROPERTIES OF THE LUNG AND UPPER AIRWAYS IN PATIENTS WITH SLEEP-DISORDERED BREATHING

Authors:

Bijaoui Eve L., Champagne Victoria, Baconnier Pierre F., R. John Kimoff and Bates Jason H.T.

Submitted to:

American Journal of Respiratory and Critical Care Medicine (July 2001)

LINK WITH CHAPTER 4

Obstructive sleep apnea/hypopnea syndrome (OSAHS) is characterized by varying degrees of upper airway collapse and inspiratory flow limitation (IFL). Changes in lung mechanics are expected during OSAHS due not only to upper airway collapse and decrease in ventilation but also to changes in lung volume. In Chapter 5, we study the impact of OSAHS in humans on the upper airways and lower lung mechanical properties. We apply the two numerical methods developed in Chapter 4 to pressure and flow signals recorded in humans throughout the various stages of sleep.

ABSTRACT

We studied the changes in lung and upper airway mechanics in adult human subjects with obstructive sleep apnea/hypopnea syndrome (OSAHS) during wakefulness, sleep and at arousal from sleep. We used two numerical methods that we have previously developed specifically for dealing with inspiratory flow limitation during sleep, the modified Mead-Whittenberger method and information-weighted histograms obtained using recursive least squares *(JAP 1999; 86:418)*. Full polysomnography including esophageal pressure and airflow measurements was performed in 7 males with OSAHS (respiratory disturbance index: 55.8±23.2 events/h). Pharyngeal pressure was recorded in 4 of the subjects to partition lung mechanics into its upper airway and lower lung components. Both techniques showed that total lung resistance and elastance increased significantly ($p<0.05$) during obstructed breathing and that this increase was reversed at the end of the obstruction. The partitioning of mechanics showed that upper airway collapse was primarily responsible for the increase in lung resistance. Our results suggest that OSAHS may lead to transient abnormalities in the recruitment of lung units and the gas exchanging capacity of the lungs.

5.1. INTRODUCTION

Obstructive Sleep Apnea/Hypopnea Syndrome (OSAHS) is a disorder characterized by episodes of partial or complete upper airway obstruction during sleep. This manifests as a reduction (hypopnea) in or complete cessation (apnea) of airflow despite ongoing inspiratory efforts, and is terminated by a transient arousal from sleep and restoration of upper airway patency. OSAHS consequently lead to disturbances in blood gases and sleep structure and has been associated with a variety of neuro-behavioral and cardiovascular complications (Guilleminault, 1996; Narkiewicz, 1998; Sajkov, 1997; Stradling, 2000).

Because physical obstruction plays an important role in these patients, it is expected that the cycle of apnea and arousal will be accompanied by large changes in the mechanical properties of the respiratory system. In particular, it seems obvious that the resistance to airflow between the mouth/nose and the alveoli will be markedly increased as the obstruction manifests. Consequently, most previous studies of the mechanics of breathing during sleep have focused on changes in resistance (Clark, 1998; Hudgel, 1988; Navajas, 1998; Tamisier, 2000). However, there is reason to suspect that obstruction during sleep should influence other mechanical aspects of the respiratory system. If, for example, obstructive apneas were to be accompanied by changes in lung volume (Series, 1989; Zerah-Lancner, 1997), then lung elastic properties would likely be affected. We hypothesized, therefore, that sleep-disordered breathing caused by upper airway

obstruction produces adverse changes in both upper airway and lower lung mechanical properties.

The primary goal of the present study was thus to investigate how upper airway and lower lung mechanics change in adult human subjects with OSAHS as they progress through the various stages of sleep and at arousal. However, measuring lung mechanics in this context is particularly challenging from a technical standpoint because when flow is dynamically limited it becomes independent of driving pressure and the usual concept of resistance no longer applies. Indeed, Officer et al. (1998) showed that the presence of expiratory flow limitation can lead to an overestimation of dynamic elastance when using conventional multiple linear regression to estimate mechanical parameters from transpulmonary pressure and flow. Our approach was therefore to use numerical methods that we have developed previously specifically for dealing with inspiratory flow limitation (IFL) during sleep (Bijaoui, 1999). We have shown, both in simulated data and in data collected from obese sleeping pigs, that these techniques are capable of providing reasonable estimates of lung mechanics in the presence of IFL. However, they have not yet been applied to sleeping humans, so establishing their usefulness in this regard was a secondary goal of our study.

5.2. METHODS

We studied seven adult men with untreated obstructive sleep apnea diagnosed in the Sleep Laboratory of The Royal Victoria Hospital in Montreal. Subject characteristics are shown in Table 5.1. The subjects were aged 39.3 ± 10.7 yr with body mass index (BMI) 29.3 ± 7.0 kg/m^2 (mean ± SD).

Table 5.1: Individual characteristics

Subject	Age (yr)	Height (m)	Weight (kg)	BMI (kg/m^2)
1	43	1.83	101.7	30.4
2	56	1.83	90.8	27.1
3	31	1.89	99.9	28.0
4	40	1.83	147.6	44.1
5	44	1.80	79.0	24.3
6	22	1.80	74.9	23.0
7	39	1.66	77.2	28.1
Mean ± SD	**39.3 ± 10.7**	**1.8 ± 0.07**	**95.9 ± 25.3**	**29.3 ± 7.0**

The experimental protocol was approved by the Research Ethics Board of the Royal Victoria Hospital and informed consent was obtained from each subject.

5.2.1. Polysomnography

The subjects underwent full polysomnography, which included the monitoring of EEG activity (C_4/A_1, C_3/A_2), eye movement (EOG), submental EMG activity, oxygen saturation by pulse oxymetry, thoracoabdominal movements by inductive

plethysmography (RIP), body position by direct observation, and snoring by microphone. All signals were recorded on a computerized system (Sandman; Mallinckrodt/Nellcor Puritan Bennett, Ottawa, ON, Canada). Sleep staging was performed by a qualified sleep technologist based on standard criteria (Rectschaffen, 1968). For all subjects, the total sleep time (TST), sleep efficiency (SE = TST/time spent in bed), and time spent in the various sleep stages were determined. Six of the subjects were studied at night and one underwent a daytime sleep study due to a regular nightshift work schedule (Rudkowski, 2001; Series, 1991). One subject was excluded from our study because of inadequate sleep.

Respiratory events during sleep were scored according to standard criteria (Report, 1999) and classified into apneas (central, mixed and obstructive), hypopneas (central and obstructive) and increased upper airway resistance episodes. For purposes of our analysis, we wished to avoid complete cessation of airflow. Therefore, we asked the subjects who displayed obstructive apneas mostly in the supine position to switch to a lateral position, in order to favor only a partial collapse of the airway.

5.2.2. Respiratory monitoring

Airflow ($\dot{V}$) was measured with a pneumotachograph (Fleisch #2) connected to a differential pressure transducer (SensorTechnics, Model HCXPM002D6V). The pneumotachograph was attached to the opening of a tightly fitting full-face mask. The total dead space of the mask and pneumotachograph was less than 100 ml. Before each

study, the pneumotachograph was calibrated against a rotameter. A gauge pressure transducer (Fujikura, FPM-02PG) was connected to a side port of the mask to measure mask pressure (P_m). Respiratory effort was assessed in terms of the magnitude of swings in esophageal pressure (P_{eso}) measured with a small balloon-tipped catheter placed in the esophagus via the nasopharynx. Insertion of the catheter was aided by the application of a small amount (2-4ml) of 4% viscous Xylocaine to the nasopharynx. P_{eso} was recorded with a pressure transducer connected to the proximal end of the catheter and referenced to atmosphere. Transpulmonary pressure P_L (equal to P_{eso} - P_m) was used for the computation of lung mechanical properties. Figure 5.1 shows a typical recording of flow and esophageal pressure signals during wakefulness, during an episode of hypopnea during Stage 2 NREM with varying resistance and airflow, and during snoring in slow-wave sleep (SWS). These signals demonstrate the increase in amplitude of respiratory effort that occurs with the onset of airway obstruction.

Pharyngeal pressure P_{phar} was also measured in four of our subjects (nos. 4-7) using a silicone catheter with a pressure transducer at its tip (Gaeltec, 2 mm ID, Isle of Skye, Scotland). This catheter was passed through the same nostril as the esophageal catheter, under topical anesthesia, and advanced until its tip resided in the hypopharynx just below the base of the tongue. The catheter tip position was confirmed by visual inspection through the mouth (Hudgel, 1988). P_{phar} allowed us to partition the respiratory system into its upper airway component ($P_{UA} = P_{phar} - P_m$) and its lung ($P_{LL} = P_{eso} - P_{phar}$) component. Both esophageal and pharyngeal pressure transducers were calibrated using a conventional water manometer.

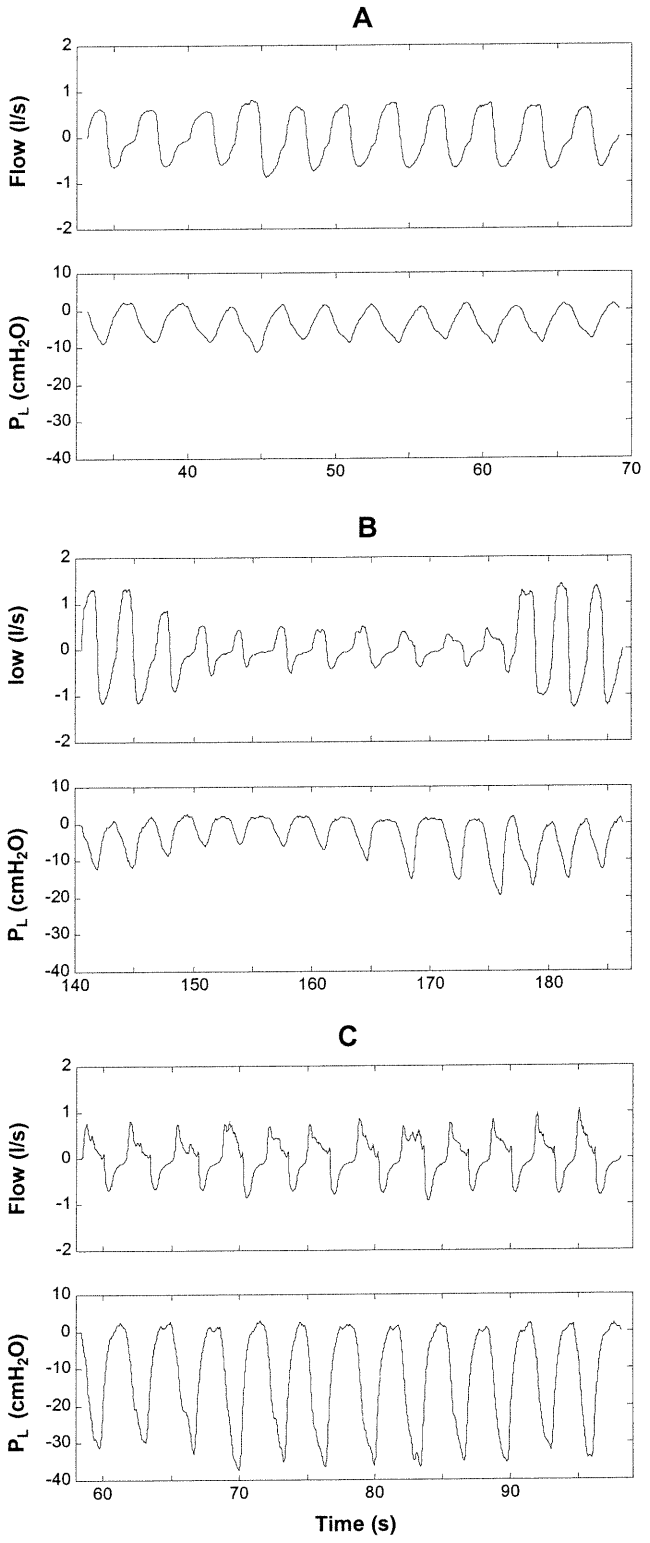

Figure 5.1: Example (subject no. 1) of changes in the shape of transpulmonary pressure (P_L) and flow signals across sleep-wake state. (A) Wakefulness, (B) during an episode of hypopnea with varying airway resistance in Stage 2 NREM sleep and (C) stable flow limitation during snoring in slow-wave sleep (SWS).

Table 5.2 gives the sleep characteristics of the subjects we studied, together with a summary of their obstructed events during sleep. All subjects had moderate to severe obstructive sleep-disordered breathing, but only three of them (nos. 1,2 and 7) managed to enter SWS.

Table 5.2: Sleep architecture and classification of sleep-related respiratory events

Subject	TST (min)	SE (%)	Stage 2 (% TST)	SWS (% TST)	RDI (/hr sleep)	AI (/hr sleep)	Nadir SaO_2 (%)
1	216.1	68.9	54.6	13.2	39.7	0	80.8
2	145.0	39.2	58.3	16.9	25.2	0	90.9
3	337.5	80.5	63.0	0	73.1	59.7	81.4
4	281.0	65.0	71.0	0	94.6	49.7	79.6
5	248.5	57.3	67.4	0	59.4	3.4	84.4
6	448.6	95.3	77.9	1.6	41.7	20.9	82.7
7	188.7	86.7	59.1	23.8	56.9	9.9	89
Mean	**266.5**	**70.4**	**64.5**	**13.9**	**55.8**	**28.7**	**84.1**
± SD	**± 101.7**	**± 19.0**	**± 8.2**	**± 9.3**	**± 23.2**	**± 24.8**	**± 4.3**

TST: total sleep time; *SE*: sleep efficiency (TST/total sleep period); *RDI*: respiratory disturbance index (apneas + hypopneas + respiratory event related arousals, number of events per hour of TST); *AI*: apnea index (number of events per hour of TST)

As well as being captured with the polysomnographic recording system, $\dot{V}$, P_{eso}, and P_{phar} were recorded at a sampling rate of 64Hz using LABDAT™ data acquisition software (RHT-InfoDat, Montreal, Quebec) on a personal computer mounted on a trolley at the bedside. The computer and all its associated electrical components were powered through a medical-grade isolation transformer connected to the hospital electrical mains. Data analysis was performed using the Matlab™ 5.3 mathematical software (The Mathworks, Nattick, MA).

5.2.3. Data processing

We restricted our analysis to NREM sleep because during REM sleep the data were very variable breath to breath and there was only a small amount of data available. We randomly selected segments of data in different stages of NREM sleep and wakefulness. Breathing was unobstructed during wakefulness. During Stage 2 NREM sleep we selected segments containing obstructive hypopneas and episodes of increased upper airway resistance. Within these segments we analyzed the breaths from the second obstructed breath until arousal, and from the second arousal breath until obstruction. We also chose obstructed segments during Stage 3&4 (SWS) NREM sleep in those subjects who reached this sleep stage, which was characterized mainly by stable snoring. We analyzed a total of 3028 breaths, averaging 79.3 (SD 63.7) breaths during wakefulness, 221.7 (SD 137.3) hypopneas and episodes of IFL in Stage 2 sleep, 51.3 (SD 29.0) breaths for arousal in Stage 2 sleep, and 187.3 (SD 133.4) breaths for SWS, in each patient.

We used two numerical methods to assess respiratory mechanics – information-weighted histograms (IWH) and a modified Mead and Whittenberger (MMW) method. We have previously described these techniques and demonstrated their application in data from sleeping obese pigs (Bijaoui, 1999). They are summarized briefly below.

Information-weighted histograms: IWH are calculated by first using recursive multiple linear regression (Lauzon, 1991) to fit the single-compartment linear model

$$P_L = R\dot{V}(t) + EV(t) + P_0 \qquad (1)$$

to measurements of P_L, $\dot{V}$ and V, where t is time, R is resistance, E is elastance, and P_0 is an estimate of positive-end-expiratory pressure. This yields signals of R, E and P_0 as functions of t. A memory time-constant τ was incorporated in the recursive estimation so that data in the past have an exponentially decreasing influence on current values R, E and P_0. The choice of τ constitutes a trade-off between insensitivity to noise and parameter tracking ability. The value of τ for a particular patient was chosen so that the residuals between data and model fit during wakefulness consisted only of noise including cardiogenic oscillations (assessed visually). The same value of τ was then used for analysis of all other data in that patient. The values of τ chosen ranged from 0.15 to 0.4 s.

The signals of $R(t)$ and $E(t)$ so obtained were then used to compute the IWH. These are histograms in which the contribution of each value in a parameter signal is weighted by the degree of confidence in that value, as determined by the current values in the information matrix (Bates, 1992). IWH were calculated for each complete breath and for the inspiratory and expiratory portions of each breath. Figure 5.2 shows the IWH obtained for R and E from typical normal and obstructed breaths. As expected, the mean values of these IWH are much larger for the obstructed breath compared to the normal breath. However, the width of the IWH is also much larger for the obstructed breath, indicating a substantially increased degree of variability in R and E as they are tracked over the breath. This increased variability arises from the presence of IFL, so the morphology of the IWH can be used as a marker for flow limitation.

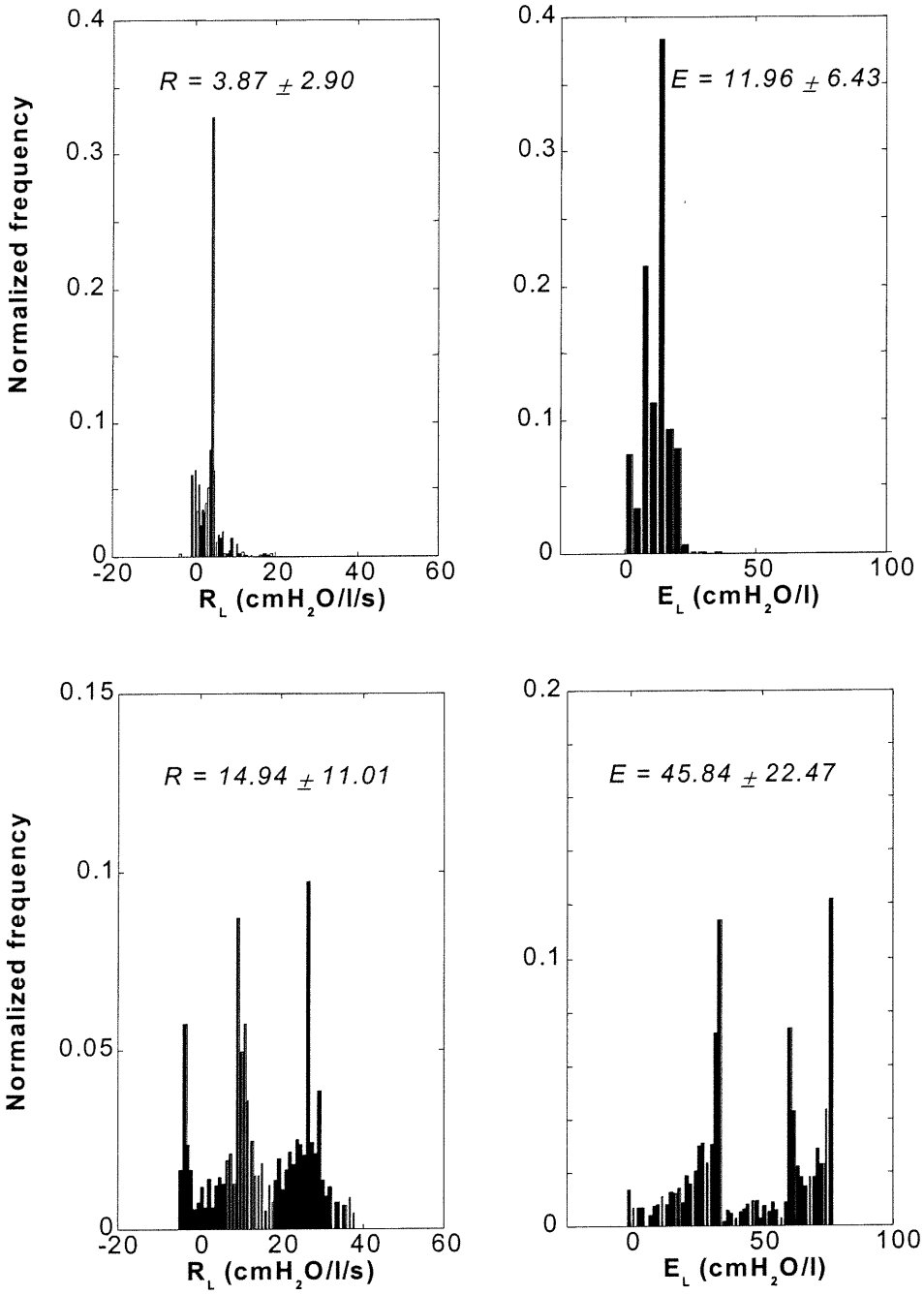

Figure 5.2: Example (subject no. 1) of information-weighted histograms (IWH) for lung resistance R_L and elastance E_L during (top) normal and (bottom) obstructive breathing. The means ± SD of each histogram are indicated on the figures.

Modified Mead-Whittenberger method: The MMW method is based on the classical Mead-Whittenberger method (Mead, 1953), in which Eq. 1 is fit to an entire data segment to yield single values for R and E. A limitation of the original method is that it uses only those data points at the extremes of lung volume to estimate E, and so is particularly vulnerable to noise in the data. We modified the original method to use all the data points over the breath to determine E, while retaining the basic assumptions that E does not vary throughout the breath. We then calculate the resistive pressure (P_{res}) as

$$P_{res}(t) = P_L(t) - EV(t) \qquad (2)$$

Figure 5.3 shows P_{res} versus $\dot{V}$ for the same normal and obstructed breaths used in Fig. 5.2. Although the model (Eq. 1) assumes these to be single valued relationships, in reality they describe loops. Typically, these loops are wide during obstruction when flow becomes limited and there is no unique relationship between $\dot{V}$ and driving pressure.

Both the IWH and the MMW methods were applied to P_L, P_{LL} and P_{UA} to provide, respectively, the mechanics of the whole lung, the lower lung and the upper airway.

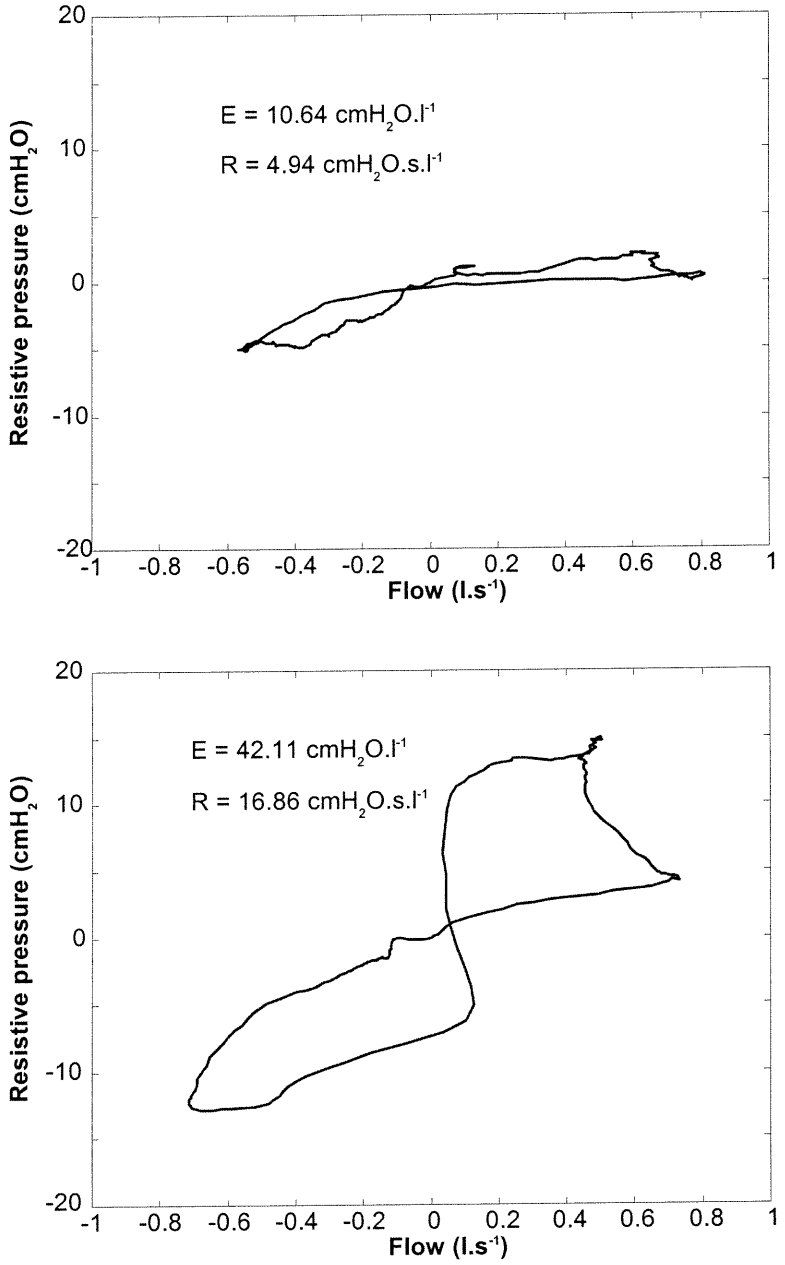

Figure 5.3: Example of lung resistive pressure P_{res} vs. flow $\dot{V}$ curve for normal (top) and obstructed (bottom) breaths (subject no. 1). E was obtained using the modified Mead-Whittenberger method. R was the obtained by regressing P_{res} against $\dot{V}$.

5.3. RESULTS

Figure 5.4 gives an example from a subject (no. 1) representative of the entire group of parameter estimates obtained with the IWH and the MMW methods for the whole breathing cycle and for each sleep state. The two methods yielded similar findings, showing that both lung resistance (R_L) and elastance (E_L) increase significantly with the presence of sleep-disordered breathing, from wakefulness to SWS.

Figures 5.5 and 5.6 show the partitioning of lung mechanics over the respiratory cycle for all subjects, using both IWH and MMW respectively. Using the IWH, mean values for R_L and E_L were calculated for the entire breathing cycle and for inspiration and expiration separately, during wakefulness, IFL and arousal in Stage 2 NREM sleep as well as for SWS when present. The MMW method (Figure 5.6) gives a single value for E_L throughout the breath and therefore the partitioning into inspiratory and expiratory components only applies to R_L. As expected, during wakefulness, there was no significant difference (t-test, $p<0.05$) between inspiratory and expiratory parameters, regardless of the method of estimation. As sleep progressed, however, both methods showed a significant increase (t-test, $p<0.05$) in parameters during both inspiration and expiration, compared to the values during wakefulness. With the onset of sleep (Stage 1 & 2 NREM), the upper airway became occluded, resulting in cessation or reduction of airflow. This persisted despite continuing respiratory efforts until there was a brief arousal from sleep, restoration of upper airway patency and resumption of airflow.

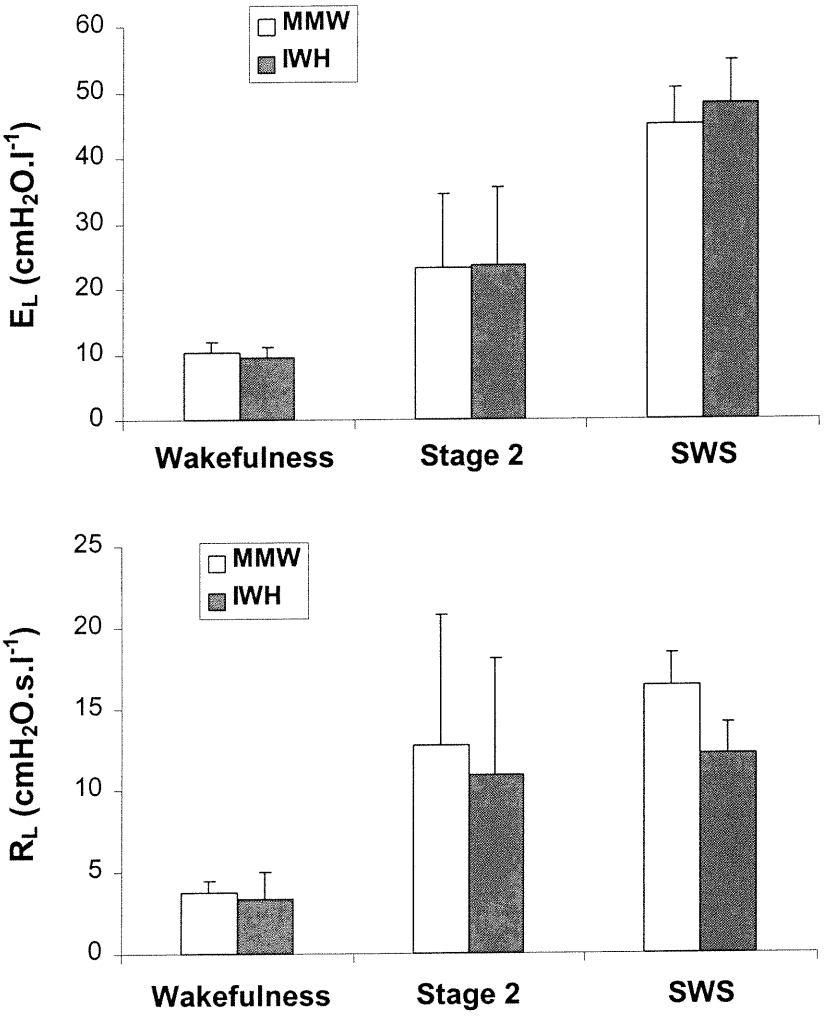

Figure 5.4: Example (subject no. 1) of the influence of sleep state on lung resistance R_L and elastance E_L estimated with modified Mead-Whittenberger (MMW, white bars) method and information weighted histograms (IWH, grey bars). Number of cycles: n = 90 for Wakefulness, n = 354 for Stage 2 NREM and n = 333 for SWS. Error bars are SDs.

The IWH and MMW techniques both showed a marked reduction in mechanical parameter values following arousal, returning to levels similar to those during wakefulness. However, the techniques differed somewhat in terms of inspiration versus expiration. R_L estimated with MMW during inspiration was greater than during expiration, whereas for the IWH the situation was reversed. We also performed a non-parametric analysis (Wilcoxon, $p<0.05$) of the inspiratory and expiratory parameters obtained during SWS, but due to the small amount of data available we were not able to show any statistically significant differences.

Figure 5.7 gives a typical example of the P_{res}-$\dot{V}$ curves obtained with the MMW method for the whole lung together with its lower lung and upper airway components. Curves are shown for a normal breath during wakefulness and for an IFL breath with snoring. These curves show that the increase in R_L occurring during sleep and snoring was caused almost entirely by an increase in R_{UA}. The same was true of all subjects as determined by both analysis methods (Fig. 5.8, bottom).

A novel finding in this study, as indicated in Figures 5.5 and 5.6, was that the onset of IFL correlated in all subjects with a significant increase in E_L. In those subjects in whom we measured P_{phar}, we were able to calculate the lower lung component of E_L. We found that the increase in E_L during IFL was largely accounted for by an increase in E_{LL} (Figure 5.8, top), that was reversed at the end of the obstructed period.

The widths of the IWH were quantitated in terms of their variances about the mean. These variances for the various sleep stages during inspiration and expiration are given in Table 5.3. We found statistically significant differences (F-test, $p<0.05$) for all the subjects between sleep and arousal. Also, during episodes of IFL, the variances during inspiration were significantly larger than during expiration for both R_L and E_L. Finally, although the mean values of R_L during wakefulness and arousal were not significantly different (Figure 5.4), their variabilities were (Table 5.3).

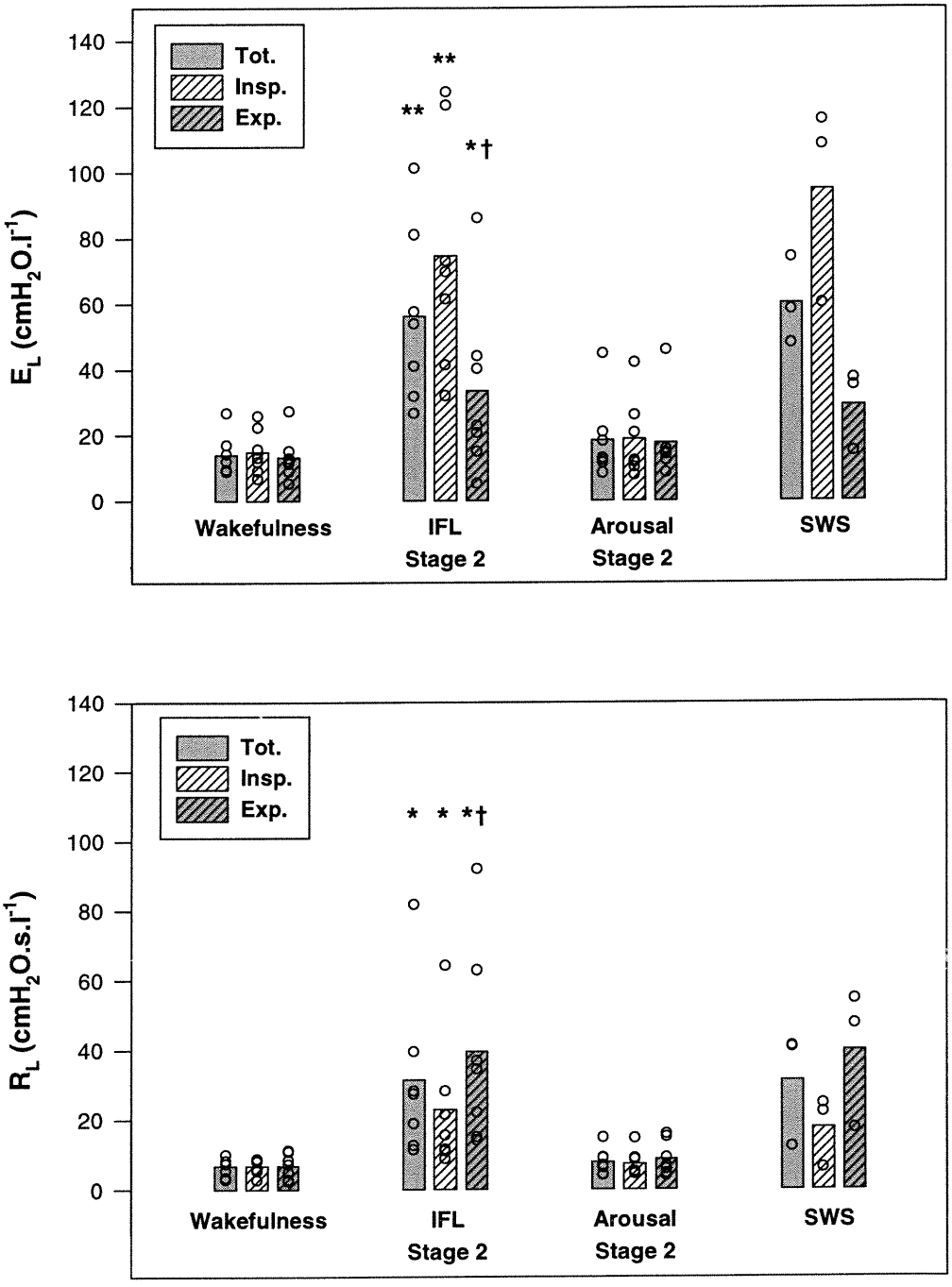

Figure 5.5: Partitioning of lung parameters (solid bars) into their inspiratory (white striped bars) and expiratory (grey striped bars) components for all subjects. Data points are means estimated from the information-weighted histograms for each patient. * represents $p<0.05$ and ** $p<0.005$ for comparison between sleep stages; † represents $p<0.05$ for comparison between inspiration and expiration;

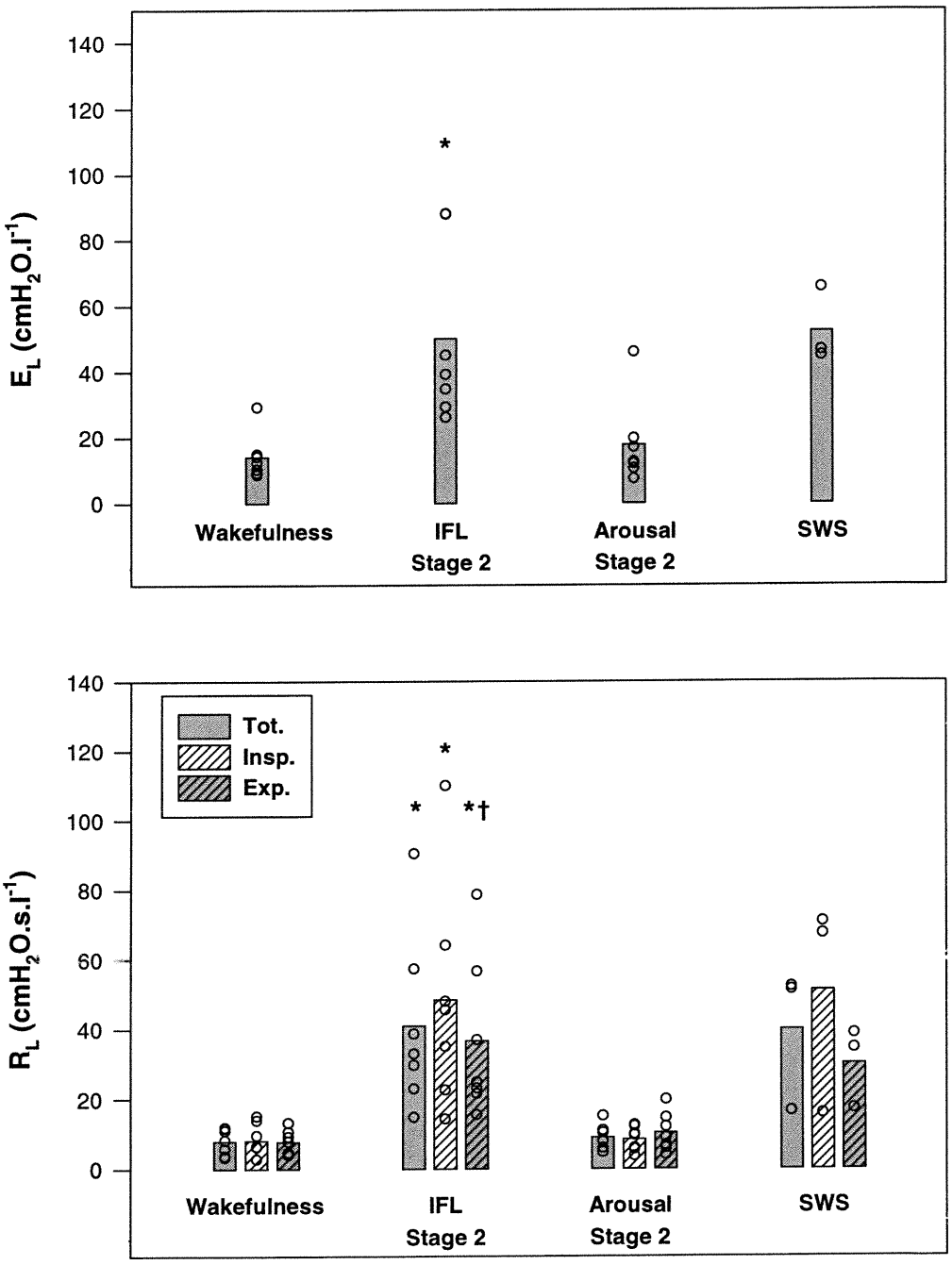

Figure 5.6: Partitioning of lung parameters (solid bars) into their inspiratory (white striped bars) and expiratory (grey striped bars) components for all subjects, estimated with the modified Mead-Whittenberger (MMW). * represents $p<0.05$ for comparison between sleep stages; † represents $p<0.05$ for comparison between inspiration and expiration;

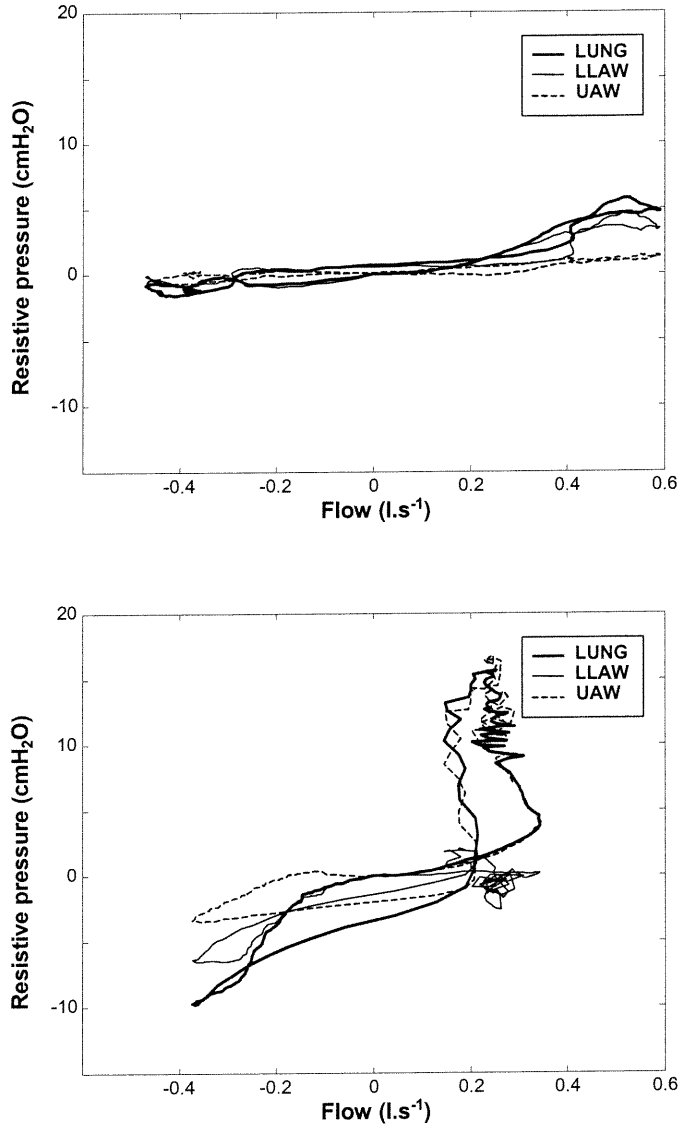

Figure 5.7: P_{res}-$\dot{V}$ curves during wakefulness (top) and during IFL in Stage 2 NREM sleep (bottom) in a representative subject (no. 4). Lung resistive pressure - solid thick line; Lower lung resistive pressure - solid thin line; Upper airway resistive pressure - dashed line.

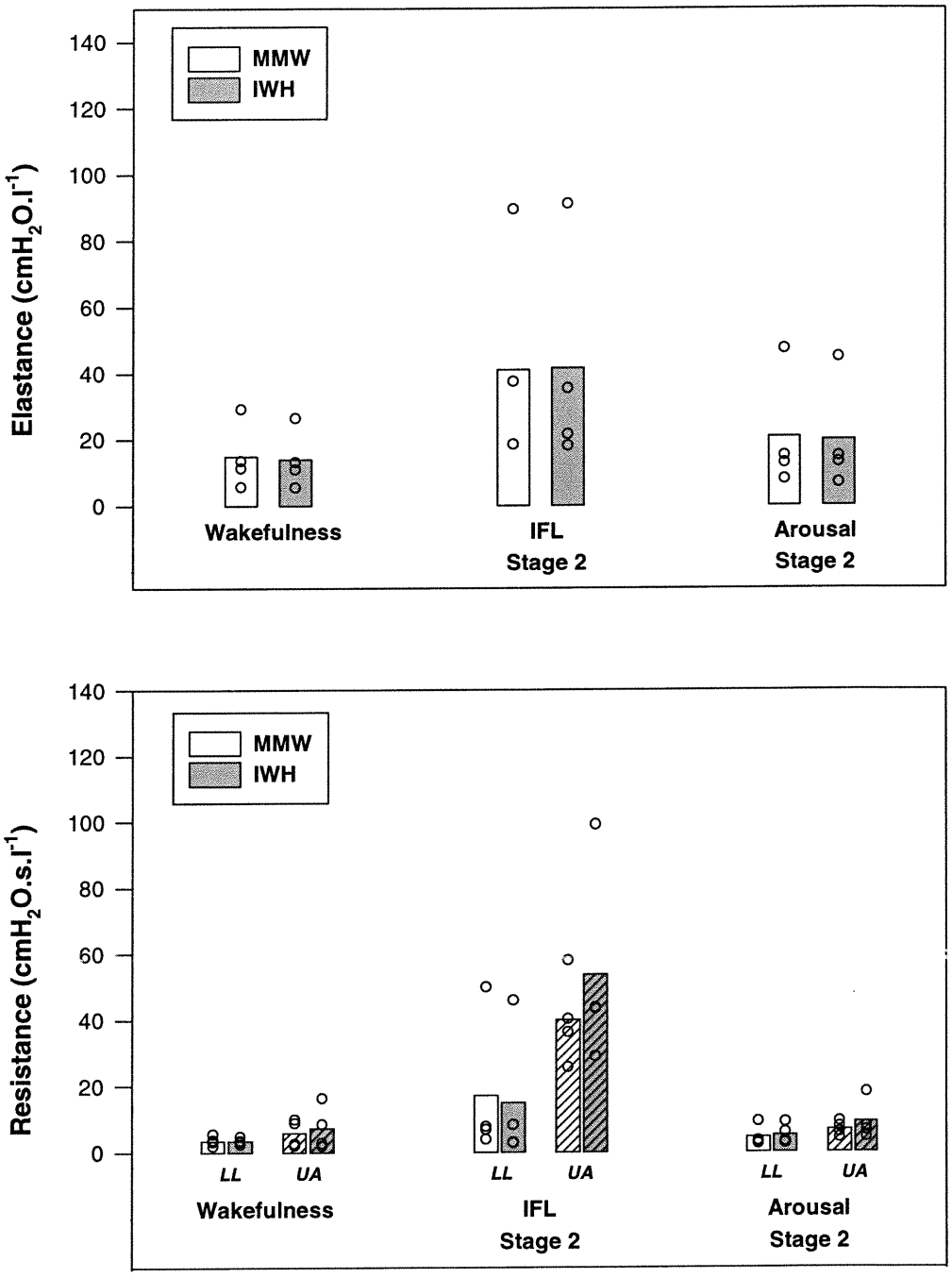

Figure 5.8: Top: Lower lung elastance estimated with the IWH (grey: mean values of histograms) and the MMW method (white) during wakefulness, stage 2 sleep and at arousal. Bottom: Corresponding estimates of resistance for both the lower lung (LL) and the upper airways (UA).

Table 5.3: Variability of lung parameters (for total cycle, inspiration and expiration) due to sleep-related disordered breathing

		Wake	IFL Stage 2	Arousal	SWS
$\mathbf{R_L}$	*Total*	6.7 ± 3.1	31.4 ± 16.3	7.8 ± 3.7	31.3 ± 22.2
($cmH_2O.s.l^{-1}$)	*Inspiration*	6.7 ± 3.6	23.0 ± 15.4	7.3 ± 3.7	17.7 ± 25.6
	Expiration	6.8 ± 2.1	39.6 ± 9.7	8.7 ± 2.1	39.8 ± 13.8
$\mathbf{E_L}$	*Total*	14.0 ± 6.3	56.1 ± 46.4	18.4 ± 8.5	60.2 ± 47.5
($cmH_2O.l^{-1}$)	*Inspiration*	15.0 ± 6.6	74.6 ± 42.2	18.7 ± 9.3	94.8 ± 35.5
	Expiration	13.3 ± 4.3	33.5 ± 31.1	17.7 ± 5.7	29.1 ± 29.1

Values are expressed as the mean for all the subjects of the IWH means ± IWH widths. IFL Stage 2: events of inspiratory flow limitation in Stage 2 NREM sleep; SWS: slow-wave sleep

5.4. DISCUSSION

Our study provides an evaluation of the mechanics of the whole lung, from mouth to pleural space, as well as its upper airway and lower lung components, in OSAHS patients through the various stages of sleep. A major finding in our study is that the onset of IFL is accompanied by a substantial increase in E_L. The partitioning of the mechanics of the whole lung into its lower lung and upper airway components confirms that this change in E_L occurs in the lower lung. We also found, as expected, that our patients had a normal R_L while awake, but a markedly increased R_L when IFL was present in the various stages of sleep. This increase was due almost entirely to an increase in upper airway resistance (Figure 5.7, bottom), resulting from collapse of the upper airway. Lower lung resistance changed very little (Figure 5.8, bottom).

One possible explanation for our finding of an increased E_L during sleep is that sleep induces a loss in the mechanical coupling between airways and lung parenchyma. This, in turn, would reduce the outward tethering forces exerted by the parenchyma, thereby allowing the airways to narrow more easily (Irvin, 2000). Alternatively, lung volume may have become reduced during sleep due to relaxation of the chest wall. This would affect both the lower (Zerah-Lancner, 1997) and upper (Van de Graaff, 1988) mechanical components of the lung. For example, a decrease in lung volume would not only decrease the parenchymal attachments but also increase the forces arising from surface tension, which would lead to an increase in elastance. Appelberg et al. (Appelberg, 2000) recently reported that expiratory reserve volume (ERV) is significantly lower in subjects with

sleep-related breathing disorders compared to non-snoring subjects. They also found a significant independent association between ERV and nocturnal obstructive apnea and oxygen desaturation frequency. Another study (Series, 1989) showed that the severity of apnea-induced desaturation was highly correlated with the supine ERV as well as with the difference between supine ERV and seated closing volume. This suggests that there is closure of some respiratory units during obstruction, which is reversed at the end of the obstruction. This explanation matches our findings since the increase in E_L observed during IFL in Stage 2 was reversed at the end of the obstructed period.

Another possibility is suggested by several studies that have reported changes in pulmonary hemodynamics following repetitive apneas. Fletcher et al. (Fletcher, 1999) proposed that a large number of obstructive apnea episodes might lead to the development of pulmonary edema, which in turn would lead to a worsening of gas exchange. These conclusions were drawn from measurements of oxygen saturations, blood pressures and ventilation-perfusion inequality, the latter also being significantly correlated with the degree of small airway closure (Sajkov, 1997). The extreme negative intrathoracic pressures generated during airway obstruction would also promote the development of edema, which might have contributed to the increased E_L that we observed. However, the rapidity with which the increase in E_L returned to baseline upon arousal suggests that edema did not play a significant role in our observations.

Large inspiratory efforts, or sighs, would also be expected to have a substantial effect in reducing E_L. Deep inspirations occur during wakefulness and Stage 2 NREM sleep

(arousal) and cause dilation of the airways and reinflation of atelectatic zones (Pelosi, 1999). This is exemplified in Figures 5.5 and 5.6, which show that E_L returns to near its wakefulness value after arousal. Although the arousal and wakefulness data are not significantly different, the variability of parameters is bigger for arousal than for wakefulness (Table 5.3), possibly due to variable degrees of airspaces recruitment in the former. Arousals and deep inspirations are absent in SWS and so presumably allow the atelectasis to accrue progressively. This is evidenced in Figures 5.5 and 5.6 which show a substantial increase in E_L during SWS compared to Stage 2 NREM and wakefulness.

Our estimates of R_L during various sleep stages behaved as expected and are in agreement with previous studies (Clark, 1998; Tamisier, 2000). Specifically, there was a significant increase in R_L (Figures 5.4, 5.5 and 5.6) as the patients went from a non-obstructed (Wakefulness, Arousal) to an obstructed (Stage 2, SWS) breathing pattern. The bigger error bars (Figure 5.4) during Stage 2 NREM can be explained by the marked changes in respiratory effort, upper airway caliber and tidal volume occurring over the cycle of hypopneas. In contrast, during SWS the breathing pattern was much more stable, explaining the small variation in R_L during SWS. The inter-subject variability was also smaller during normal compared to obstructed breathing (Figures 5.5 and 5.6), presumably due to differences in the degree of upper airway obstruction and inspiratory effort during the latter.

Resistance was also assessed over both inspiration and expiration, in accordance with the possibility of upper airway obstruction being both an inspiratory and an expiratory event,

as previously discussed (Sanders, 1983; Stanescu, 1996). We found an increase in the expiratory R_L during obstructed breathing in Stage 2 and SWS compared to wakefulness and arousal values, which supports the notion that both inspiratory and expiratory events are involved in the stability of the upper airway during wakefulness and sleep in patients with OSAHS.

The pharyngeal catheter allowed us to confirm that the increase in R_L during stage 2 NREM sleep was indeed due to an increase in upper airway resistance (Figure 5.8, bottom). The corresponding P_{res}-$\dot{V}$ curve for the upper airway (Figure 5.7) show some hysteresis, presumably due to the pharynx being narrower at end-inspiration compared to early-inspiration (Morrell, 1998; Schwab, 1993). This is believed to be influenced by the viscoelastic properties of the upper airway walls and the surface tension forces within the upper airway (Jokic, 1998). Such hysteresis was only observed during inspiratory flow limited breaths, which implies that a substantial narrowing of the upper airway is necessary for the hysteresis to occur.

Our study also provided an assessment of the IWH and MMW methods for monitoring flow limitation in humans. As both methods use all data points within the breathing cycle to compute their respective parameter estimates, they should be robust in the presence of noise. This is in contrast to the original Mead and Whittenberger method, which has been used recently for the assessment of R_L during sleep (Lofaso, 1998), and which uses only a small number of data points to estimate elastance. Both IWH and MMW methods gave similar results (Figure 5.4), despite the fact that the MMW method assumes a single value

of E_L for the entire breath, while the IWH lets E_L vary continuously throughout the breath. This supports the robustness of the two methods and their potential value as monitoring tools.

In summary, we have shown that E_L increased during IFL in sleeping subjects. This observation is most likely explained by a reduction in lung volume resulting in air space closure, as the increase in E_L was rapidly reversed after the end of the obstructed period. We found that most of the increase in R_L during IFL was due to the collapse of the upper airway, which was also reversed at the end of obstruction. We have also demonstrated that the MMW method and IWH can both be used in the setting of OSA for continuous estimation of lung mechanical parameters, and particularly for the detection of flow limitation. Furthermore, the width of the IWH gives an indication of the degree of airway obstruction.

CHAPTER 6

CONCLUSIONS

6.1. SUMMARY AND CONCLUSIONS

The overall aim of the work reported in this thesis was to demonstrate the usefulness of respiratory mechanics assessment as a noninvasive tool for monitoring lung function during mechanical ventilation and in spontaneously breathing subjects.

Pulmonary mechanics represent the intrinsic properties of the respiratory system that determine the amount of pressure necessary to inflate the lungs. Preterm infants with respiratory distress syndrome have compromised pulmonary mechanics and need ventilatory assistance. Two special considerations arise in characterizing the mechanical properties of the infant respiratory system using P and $\dot{V}$ measurements at the tracheal or airway opening. First, air leaks around the endotracheal tube (ETT), which are significant in a majority of ventilated infants, must be monitored to prevent a deterioration of gas exchange and errors in the autotriggering of mechanical ventilators. We have developed a robust noninvasive method, easy to implement, based on a simple model of the respiratory circuit, which estimates the resistance due to the leak and corrects tracheal airflow. The usefulness of the method was established in mechanically ventilated neonates under a controlled mode of ventilation. Although this is not necessarily the preferred mode of ventilation, it is still widely used in neonatal intensive care units and in anesthetized patients, which makes the spectrum of clinical applications of this method fairly large. The second consideration is that the resistance of the ETT must be determined and subtracted from the total resistance of the respiratory system. We did this in our study, although we measured the resistance of the ETT in vitro, which presumably

underestimates the value of the tube resistance when positioned in the trachea. Our leak correction method can also be applied in adults, since leaks around the ETT can occur when uncuffed tubes are used (e.g. in patients with neuromuscular disorders) or when there are changes in head or neck position. Leaks also occur in adults when uncuffed ETTs are used to minimize damage to the trachea after a prolonged period of intubation.

By applying an oscillatory flow to the respiratory system, the lung or one of its regions, one is able to obtain a mechanical input impedance. We developed a novel approach that exploits the mechanical interaction between the heart and the lungs as a natural dynamic perturbation to the system. This required isolating the so-called cardiogenic oscillations (CO) in tracheal pressure and flow signals, and phase-matching them using the heart sounds as a reference. The corresponding cardiogenic impedance (Z_C) was computed and expressed in terms of its real and imaginary parts. We showed that Z_C is essentially a purely real function of frequency, which we believe to provide an estimate of central airway resistance. The requirement for an open glottic recording of pressure and flow represents the main practical limitation of the method. The method may thus be best suited to intubated patients.

Most methods used to estimate respiratory or lung mechanics provide values of resistance and elastance on a breath-by-breath basis or over a series of breaths. They do not give any information pertaining to the time-course of mechanical alterations within the breathing cycle that would occur, for example, in the presence of inspiratory flow limitation (IFL) during sleep. We implemented two methods - the modified Mead-

Whittenberger (MMW) method and the information-weighted histograms (IWH) - specifically for dealing with IFL. Using simulated data and data from obese sleeping pigs, both methods showed that the occurrence of IFL at some point within the breath leads to an increase in the mean values of R and E for that breath. In addition, the standard deviation of the IWH is a quantitative index showing the relative increase in parameter variability with the occurrence of IFL. This is also assessed visually by the degree of looping of the P_{res}-$\dot{V}$ curves obtained with the MMW method.

It was shown in human subjects that the episodes of upper airway collapse during sleep were associated not only with an increase in upper airway resistance but also with an increase in lung elastance. These novel findings can be explained by a reduction in lung volume due to the obstruction, which would result in transient abnormalities in the recruitment of lung units and in a decrease of upper airway patency.

6.2. FUTURE DIRECTIONS

There are a number of ways in which the work reported in this thesis could be extended and some examples are listed below.

- Measurement of Z_C could be made at different lung volumes. This could be achieved, for example, in mechanically ventilated animals or in humans by applying a negative extrathoracic pressure with a thoracic cuirass. This would establish a relationship between the real part of Z_C and lung volume. An inverse curvilinear relationship, similar to the one existing between airway resistance and lung volume would validate our interpretation and demonstrate the utility of the method.

- The measurement of Z_C as an estimate of airway resistance would apply to situations in which the maintenance of an open glottis is not a limitation such as in anesthetized and paralyzed patients during surgery. For example, Z_C could be obtained in a ventilated patient by briefly occluding the airway at the end of a normal expiration and could serve as a useful marker of changes in airway resistance such as would be produced by an obstruction at the level of the ETT. General anesthesia also affects airway resistance in different categories of patients and surgical conditions, either by its effect on lung volume or by the development of airway complications such as edema. Alternatively, the method could be applied in intensive care units to patients with respiratory disease (e.g. chronic obstructive pulmonary disease, emphysema or

even an extrathoracic obstruction) artificially ventilated for respiratory complications (e.g. respiratory distress syndrome)

- We found that the elastance of the lower lung compartment is increased in the presence of obstructed breathing, and we explained it as a result of a fall in lung volume during these episodes. Direct measurement of lung volume during sleep would confirm this theory. So far, most of the attention given to respiratory mechanics during sleep focuses on the changes in upper airway mechanics. More systematic attention should be given to the mechanics of the lower airways and lung tissue, as this could help in understanding and maybe preventing some of the respiratory consequences of sleep-disordered breathing.

- The width of the information-weighted histogram increases along with its mean in the presence of an obstruction, which suggests that this width could be used on its own as an index of the severity of the obstructive event. The performance of the information-weighted histograms could be compared to input impedance, which has recently been used in sleep studies to assess the degree of obstruction and adjust the CPAP level.

6.3. STATEMENT OF ORIGINAL CONTRIBUTIONS TO THE FIELD

The following results constitute original contributions to the field of research.

- Our method for airflow correction in the presence of a leak around the endotracheal tube (ETT), based on non invasive recordings of airway opening pressure and flow signals and computation of leak resistance, was the first approach of its kind to be tested on human subjects.

- The influence of the leak was evaluated using PEEP values before and after correction of airflow. An accurate measurement of PEEP is essential for assessing the presence of intrinsic PEEP, which reflects dynamic hyperinflation and usually requires readjustments in the ventilator settings. This study thus showed that the absence of a correction for a leak between the ETT and the trachea can ultimately impede ventilatory management.

- We developed a method for assessing respiratory mechanics using cardiogenic oscillations (CO) in pressure and flow measured at the mouth of an apneic subject.

- To our knowledge, the use of CO as a natural mechanical perturbation to the respiratory system constitutes the first study in which CO are not regarded as a nuisance to the processing and interpretation of pressure and flow signals.

- We implemented a viscoelastic linear model of the respiratory system using Matlab/Simulink mathematical and simulation software. This provides a mean of generating pressure, flow and volume signals with and without flow limitation.

- Our assessment of mechanics in the presence of flow limitation is the first study using information-weighted histograms (IWH) to measure lung mechanics in spontaneously breathing subjects.

- We showed that P_{res}-$\dot{V}$ data from pigs can be used with a modified Mead-Whittenberger method and IWH to assess the presence and extent of flow limitation.

- We showed that the relative increase in the width of the IWH can serve as an index of the severity of obstruction

- We studied changes in lung resistance and elastance induced by the presence of an obstruction during sleep. To our knowledge, this is the first report on the effect of an obstruction during sleep on the elastance of the lung. We showed that this elastance is increased in sleep, probably due to a reduction in lung volume leading to airway closure.

- We showed that although mean parameter values from the IWH return at arousal to values similar to those during wakefulness, the widths of the histograms are bigger at arousal, which suggest that lung function is not entirely restored during these periods.

REFERENCES

AITTOKALLIO, T., SAARESRANTA, T., POLO-KANTOLA, P., NEVALAINEN, O. and POLO, O. (2001). Analysis of inspiratory flow shapes in patients with partial upper-airway obstruction during sleep. Chest 119(1): 37-44.

ALDRICH, M. S. (1999). Breathing during wakefulness and sleep. Sleep Medicine. PRESS, O. U.: 39-55.

APPELBERG, J., NORDAHL, G. and JANSON, C. (2000). Lung volume and its correlation to nocturnal apnoea and desaturation. Respir Med **94**(3): 233-239.

ARONSON, R. M., CARLEY, D. W., ONAL, E., WILBORN, J. and LOPATA, M. (1991). Upper airway muscle activity and the thoracic volume dependence of upper airway resistance. J Appl Physiol 70(1): 430-438.

AVANZOLINI, G. and BARBINI, P. (1985). A comparative evaluation of three on-line identification methods for a respiratory mechanical model. IEEE Trans Biomed Eng 32(11): 957-963.

AVANZOLINI, G., BARBINI, P. and CAPPELLO, A. (1992). Comparison of algorithms for tracking short-term changes in arterial circulation parameters. IEEE Trans Biomed Eng 39(8): 861-867.

AVANZOLINI, G., BARBINI, P., CAPPELLO, A. and CEVENINI, G. (1995). Influence of flow pattern on the parameter estimates of a simple breathing mechanics model. IEEE Trans Biomed Eng **42**(4): 394-402.

AVANZOLINI, G., BARBINI, P., CAPPELLO, A., CEVENINI, G. and CHIARI, L. (1997). A new approach for tracking respiratory mechanical parameters in real- time. Ann Biomed Eng 25(1): 154-163.

AYAPPA, I., NORMAN, R. G. and RAPOPORT, D. M. (1999). Cardiogenic oscillations on the airflow signal during positive airway pressure as a marker of central apnea. Chest **116**: 660-666.

BACONNIER, P. F., CARRY, P. Y., EBERHARD, A., PERDRIX, J. P. and FARGNOLI, J. M. (1995). A computer program for automatic measurement of respiratory mechanics in artificially ventilated patients. Comput Methods Programs Biomed **47**(3): 205-220.

BADEER, H. S. and HICKS, J. W. (1992). Hemodynamics of vascular 'waterfall': is the analogy justified? Respir Physiol 87(2): 205-217.

BADIA, J. R., FARRE, R., MONTSERRAT, J. M., BALLESTER, E., HERNANDEZ, L., ROTGER, M., RODRIGUEZ-ROISIN, R. and NAVAJAS, D. (1998). Forced oscillation technique for the evaluation of severe sleep apnoea/hypopnoea syndrome: a pilot study. Eur Respir J 11(5): 1128-1134.

BADIA, J. R., FARRE, R. O., JOHN KIMOFF, R., BALLESTER, E., HERNANDEZ, L., ROTGER, M., NAVAJAS, D. and MONTSERRAT, J. M. (1999). Clinical application of the forced oscillation technique for CPAP titration in the sleep apnea/hypopnea syndrome. Am J Respir Crit Care Med 160(5 Pt 1): 1550-1554.

BARBINI, P., CAPPELLO, A. and CEVENINI, G. (1988). Real-time tracking of breathing parameters in mechanically ventilated dogs. IEEE Engineering in Medicine and Biology Society, 10th Annual International Conference.

BARNAS, G. M., MILLS, P. J., MACKENZIE, C. F., ASHBY, M., SEXTON, W. L., IMLE, P. C. and WILSON, P. D. (1991). Dependencies of respiratory system resistance and elastance on amplitude and frequency in the normal range of breathing. Am Rev Respir Dis 143(2): 240-244.

BARTLETT, D., REMMERS, J. E. and GAUTIER, H. (1973). Laryngeal regulation of respiratory airflow. Respir Physiol **18**: 194-204.

BATES, J. H., BACONNIER, P. and MILIC-EMILI, J. (1988a). A theoretical analysis of interrupter technique for measuring respiratory mechanics. J Appl Physiol 64(5): 2204-2214.

BATES, J. H., BROWN, K. A. and KOCHI, T. (1989a). Respiratory mechanics in the normal dog determined by expiratory flow interruption. J Appl Physiol 67(6): 2276-2285.

BATES, J. H., DECRAMER, M., CHARTRAND, D., ZIN, W. A., BODDENER, A. and MILIC-EMILI, J. (1985a). Volume-time profile during relaxed expiration in the normal dog. J Appl Physiol 59(3): 732-737.

BATES, J. H., LUDWIG, M. S., SLY, P. D., BROWN, K., MARTIN, J. G. and FREDBERG, J. J. (1988b). Interrupter resistance elucidated by alveolar pressure measurement in open-chest normal dogs. J Appl Physiol 65(1): 408-414.

BATES, J. H., ROSSI, A. and MILIC-EMILI, J. (1985b). Analysis of the behavior of the respiratory system with constant inspiratory flow. J Appl Physiol 58(6): 1840-1848.

BATES, J. H., SHARDONOFSKY, F. and STEWART, D. E. (1989b). The low-frequency dependence of respiratory system resistance and elastance in normal dogs. Respir Physiol 78(3): 369-382.

BATES, J. H. T. and GOLDBERG, P. (1999). Fitting nonlinear time-domain models of respiratory mechanics to pressure-flow data from an intubated patient. BMES/EMBS Conference. Proceedings of the First Joint.

BATES, J. H. T. and LAUZON, A. M. (1992). A nonstatistical approach to estimating confidence intervals about model parameters: application to respiratory mechanics. IEEE Trans Biomed Eng 39(1): 94-100.

BAYDUR, A., SASSOON, C. S. and CARLSON, M. (1996). Measurement of lung mechanics at different lung volumes and esophageal levels in normal subjects: effect of posture change. Lung 174(3): 139-151.

BIJAOUI, E., TUCK, S. A., REMMERS, J. E. and BATES, J. H. T. (1999). Estimating respiratory mechanics in the presence of flow limitation. J Appl Physiol **86**(1): 418-426.

BLAND, M. J. and ALTMAN, D. G. (1986). Statistical methods for assessing agreement between two methods of clinical measurement. Lancet **8**: 307-310.

BRADLEY, T. D., BROWN, I. G., GROSSMAN, R. F., ZAMEL, N., MARTINEZ, D., PHILLIPSON, E. A. and HOFFSTEIN, V. (1986). Pharyngeal size in snorers, nonsnorers, and patients with obstructive sleep apnea. N Engl J Med 315(21): 1327-1331.

BROOKS, L. J., CASTILE, R. G., GLASS, G. M., GRISCOM, N. T., WOHL, M. E. and FREDBERG, J. J. (1984). Reproducibility and accuracy of airway area by acoustic reflection. J Appl Physiol 57(3): 777-787.

CARRY, P., BACONNIER, P., EBERHARD, A., COTTE, P. and BENCHETRIT, G. (1997). Evaluation of respiratory inductive plethysmography: accuracy for analysis of respiratory waveforms. Chest 111(4): 910-915.

CARRY, P. Y., PERDRIX, J. P., EBERHARD, A., FARGNOLI, J. M., LOCTIN, H. and BACONNIER, P. (1998). Model of expiratory flow limitation: effects of PEEPe (Abstract). Anesthesiology 89.

CASSIDY, K. J., HALPERN, D., RESSLER, B. G. and GROTBERG, J. B. (1999). Surfactant effects in model airway closure experiments. J Appl Physiol 87(1): 415-427.

CAUBERGHS, M. and VAN DE WOESTIJNE, K. P. (1989). Effect of upper airway shunt and series properties on respiratory impedance measurements. J Appl Physiol 66(5): 2274-2279.

CHANG, H. K. and MORTOLA, J. P. (1981). Fluid dynamic factors in tracheal pressure measurement. J Appl Physiol: Respirat Environ Execise Physiol **51**: 218-225.

CHAOUAT, A., WEITZENBLUM, E., KRIEGER, J., OSWALD, M. and KESSLER, R. (1996). Pulmonary hemodynamics in the obstructive sleep apnea syndrome. Results in 220 consecutive patients. Chest 109(2): 380-386.

CHAPMAN, F. W. and NEWELL, J. C. (1989). Estimating lung mechanics of dogs with unilateral lung injury. IEEE Trans Biomed Eng 36(4): 405-413.

CHELUCCI, G. L., BRUNET, F., DALL'AVA-SANTUCCI, J., DHAINAUT, J. F., PACCALY, D., ARMAGANIDIS, A., MILIC-EMILI, J. and LOCKHART, A. (1991). A single-compartment model cannot describe passive expiration in intubated, paralysed humans. Eur Respir J 4(4): 458-464.

CLARK, S. A., WILSON, C. R., SATOH, M., PEGELOW, D. and DEMPSEY, J. A. (1998). Assessment of inspiratory flow limitation invasively and noninvasively during sleep. Am J Respir Crit Care Med **158**(3): 713-722.

CONDOS, R., NORMAN, R. G., KRISHNASAMY, I., PEDUZZI, N., GOLDRING, R. M. and RAPOPORT, D. M. (1994). Flow limitation as a non-invasive assessment of residual upper airway resistance during continuous positive airway pressure therapy of obstructive sleep apnea. Am J Respir Crit Care Med **150**(475-480).

D'ANGELO, E., ROBATTO, F. M., CALDERINI, E., TAVOLA, M., BONO, D., TORRI, G. and MILIC-EMILI, J. (1991). Pulmonary and chest wall mechanics in anesthetized paralyzed humans. J Appl Physiol **70**(6): 2602-2610.

D'ANGELO, E., TAVOLA, M. and MILIC-EMILI, J. (2000). Volume and time dependence of respiratory system mechanics in normal anaesthetized paralysed humans. Eur Respir J 16(4): 665-672.

DAROCZY, B. and HANTOS, Z. (1982). An improved forced oscillatory estimation of respiratory impedance. Int J Biomed Comput 13(3): 221-235.

DAVEY, B. L. K. and BATES, J. H. T. (1993). Regional lung impedance from forced oscillations through alveolar capsules. Respir Physiol **91**: 165-185.

DAWSON, S. V. and ELLIOT, E. A. (1977). Wave-speed limitation on expiratory flow - a unifying concept. J Appl Physiol: Respirat Environ Exercise Physiol 43: 498-515.

DUBOIS, A. B., BRODY, A. W., LEWIS, D. H. and B.F., B. (1956). Oscillation mechanics of lungs and chest in man. J Appl Physiol 8: 587-594.

EBINA, M., YAEGASHI, H., TAKAHASHI, T., MOTOMIYA, M. and TANEMURA, M. (1990). Distribution of smooth muscles along the bronchial tree. A morphometric study of ordinary autopsy lungs. Am Rev Respir Dis 141(5 Pt 1): 1322-1326.

ENGEL, L. A. (1986). Dynamic distribution of gas flow. Handbook of Physiology - The Respiratory system Vol III: 588-590.

ENGEL, L. A. and MACKLEM, P. T. (1977). Gas mixing and distribution in the lung. Respir Physiol **14**: 37-82.

EYLES, J. G. and PIMMEL, R. L. (1981). Estimating respiratory mechanical parameters in parallel compartment models. IEEE Trans Biomed Eng 28(4): 313-317.

EYLES, J. G., PIMMEL, R. L., FULLTON, J. M. and BROMBERG, P. A. (1982). Parameter estimates in a five-element respiratory mechanical model. IEEE Trans Biomed Eng 29(6): 460-463.

FARRE, R., PESLIN, R., ROTGER, M., BARBERA, J. A. and NAVAJAS, D. (1999). Forced oscillation total respiratory resistance and spontaneous breathing lung resistance in COPD patients. Eur Respir J 14(1): 172-178.

FARRE, R., PESLIN, R., ROTGER, M. and NAVAJAS, D. (1994). Human lung impedance from spontaneous breathing frequencies to 32 Hz. J Appl Physiol 76(3): 1176-1183.

FARRE, R., RIGAU, J., MONTSERRAT, J. M., BALLESTER, E. and NAVAJA, D. (2001a). Relevance of Linearizing Nasal Prongs for Assessing Hypopneas and Flow Limitation During Sleep. Am. J. Respir. Crit. Care Med. 163(2): 494-497.

FARRE, R., RIGAU, J., MONTSERRAT, J. M., BALLESTER, E. and NAVAJAS, D. (2001b). Evaluation of a simplified oscillation technique for assessing airway obstruction in sleep apnoea. Eur Respir J 17(3): 456-461.

FARRE, R., ROTGER, M., MONTSERRAT, J. M. and NAVAJAS, D. (1997a). Analog circuit for real-time computation of respiratory mechanical impedance in sleep studies. IEEE Trans Biomed Eng 44(11): 1156-1159.

FARRE, R., ROTGER, M., MONTSERRAT, J. M. and NAVAJAS, D. (1997b). A system to generate simultaneous forced oscillation and continuous positive airway pressure. Eur Respir J 10(6): 1349-1353.

FISLER, R., SIEGEL, S. D., KUBICKA, R., MERINO, D. N. and BECK, G. J. (1988). Respiratory resistance and compliance in COPD measured with forced oscillations. IEEE Engineering in Medicine and Biology Society, 10th Annual International Conference.

FLETCHER, E. C., PROCTOR, M., YU, J., ZHANG, J., GUARDIOLA, J. J., HORNUNG, C. and BAO, G. (1999). Pulmonary edema develops after recurrent obstructive apneas. Am J Respir Crit Care Med **160**(5 Pt 1): 1688-1696.

FODIL, R., RIBREAU, C., LOUIS, B., LOFASO, F. and ISABEY, D. (1997). Interaction between steady flow and individualised compliant segments: application to upper airways. Med Biol Eng Comput 35(6): 638-648.

FREDBERG, J. J., KEEFE, D. H., GLASS, G. M., CASTILE, R. G. and FRANTZ, I. D., 3RD (1984). Alveolar pressure nonhomogeneity during small-amplitude high-frequency oscillation. J Appl Physiol 57(3): 788-800.

FREDBERG, J. J., WOHL, M. E., GLASS, G. M. and DORKIN, H. L. (1980). Airway area by acoustic reflections measured at the mouth. J Appl Physiol 48(5): 749-758.

FRY, D. and HYATT, R. S. (1960). Pulmonary mechanics. A unified analysis of the relationship between pressure, volume and gasflow in the lungs of normal and diseased human subjects. Am. J. Med. 24 (1960), pp. 672¯689. Am J Med 24(672-689).

FUNG, Y. C. (1981). Biomechanics: Mechanical properties of living tissues. New York, Springer-Verlag: 41-43.

GALAL, M. W., HABIB, R. H., JAEGER, D. D. and LISTER, G. (1998). Effects of rate and amplitude of breathing on respiratory system elastance and resistance during growth of healthy children. Pediatr Pulmonol 25(4): 270-277.

GAVER, D. P., 3RD, SAMSEL, R. W. and SOLWAY, J. (1990). Effects of surface tension and viscosity on airway reopening. J Appl Physiol 69(1): 74-85.

GAVRIELY, N. and JENSEN, O. (1993). Theory and measurements of snores. J Appl Physiol 74(6): 2828-2837.

GHADIALI, S. N. and GAVER, D. P., 3RD (2000). An investigation of pulmonary surfactant physicochemical behavior under airway reopening conditions. J Appl Physiol 88(2): 493-506.

GOMES, R. F., SHARDONOFSKY, F., EIDELMAN, D. H. and BATES, J. H. (2001). Respiratory mechanics and lung development in the rat from early age to adulthood. J Appl Physiol 90(5): 1631-1638.

GUERIN, C., COUSSA, M. L., EISSA, N. T., CORBEIL, C., CHASSE, M., BRAIDY, J., MATAR, N. and MILIC-EMILI, J. (1993). Lung and chest wall mechanics in mechanically ventilated COPD patients. J Appl Physiol **74**(4): 1570-1580.

GUILLEMINAULT, C., STOOHS, R., SHIOMI, T., KUSHIDA, C. and SCHNITTGER, I. (1996). Upper airway resistance syndrome, nocturnal blood pressure monitoring, and borderline hypertension. Chest **109**(4): 901-908.

HAKALA, K., STENIUS-AARNIALA, B. and SOVIJARVI, A. (2000). Effects of weight loss on peak flow variability, airways obstruction, and lung volumes in obese patients with asthma. Chest 118(5): 1315-1321.

HALL, G. L., HANTOS, Z., PETAK, F., WILDHABER, J. H., TILLER, K., BURTON, P. R. and SLY, P. D. (2000). Airway and respiratory tissue mechanics in normal infants. Am J Respir Crit Care Med 162(4 Pt 1): 1397-1402.

HANTOS, Z., DAROCZY, B., SUKI, B., GALGOCZY, G. and CSENDES, T. (1986). Forced oscillatory impedance of the respiratory system at low frequencies. J Appl Physiol **60**(1): 123-132.

HANTOS, Z., ADAMICZA, A., GOVAERTS, E. and DAROCZY, B. (1992). Mechanical impedances of lungs and chest wall in the cat. J Appl Physiol 73(2): 427-433.

HANTOS, Z., PETAK, F., ADAMICZA, A., DAROCZY, B. and FREDBERG, J. J. (1995). Differential responses of global airway, terminal airway, and tissue impedances to histamine. J Appl Physiol 79(5): 1440-1448.

HARTFORD, C. G., TURNER, M. J., VAN SCHALKWYK, J. M. and ROGERS, G. G. (1997). Frequency responses of infant air-balloon versus liquid-filled catheters for intra-esophageal pressure measurement. Pediatr Pulmonol 24(5): 353-363.

HECKMAN, J. L., STEWART, G. H., TREMBLAY, G. and LYNCH P, R. (1982). Relationship between stroke volume and pneumocardiogram. J Appl Physiol **52**: 1672-1677.

HEIL, M. (1999). Airway closure: occluding liquid bridges in strongly buckled elastic tubes. J Biomech Eng 121(5): 487-493.

HENDRICKS, J. C., KLINE, L. R., KOVALSKI, R. J., O'BRIEN, J. A., MORRISON, A. R. and PACK, A. I. (1987). The English bulldog: a natural model of sleep-disordered breathing. J Appl Physiol 63(4): 1344-1350.

HOFFMAN, E. A. and RITMAN, E. L. (1987). Heart-lung interaction: effect on regional lung air content and total heart volume. Ann Biomed Eng **15**: 241-257.

HOFFSTEIN, V., WRIGHT, S. and ZAMEL, N. (1989). Flow-volume curves in snoring patients with and without obstructive sleep apnea. Am Rev Respir Dis 139(4): 957-960.

HUANG, J., ITAI, N., HOSHIBA, T., FUKUNAGA, T., YAMANOUCHI, K., TOGA, H., TAKAHASHI, K. and OHYA, N. (2000). A new nasal acoustic reflection technique to estimate pharyngeal cross- sectional area during sleep. J Appl Physiol 88(4): 1457-1466.

HUANG, L. and WILLIAMS, J. E. (1999). Neuromechanical interaction in human snoring and upper airway obstruction. J Appl Physiol 86(6): 1759-1763.

HUDGEL, D. W., HENDRICKS, C. and HAMILTON, H. B. (1988). Characteristics of the upper airway pressure-flow relationship during sleep. J Appl Physiol **64**(5): 1930-1935.

HUDGEL, D. W., MARTIN, R. J., JOHNSON, B. and HILL, P. (1984). Mechanics of the respiratory system and breathing pattern during sleep in normal humans. J Appl Physiol: Respirat Environ Exercise Physiol **56**: 133-137.

HUDGEL, D. W. and SURRATT, P. M. (1994). The human airway during sleep. Sleep and Breathing, 2nd Ed. DEKKER, M. New York: 191-208.

HYATT, R., RODARTE, J., MEAD, J. and WILSON, T. (1979). Changes in lung mechanics; flow-volume relations. The Lung in Transition from Health to Disease: Lung Biology in Health and Disease. MACKLEM, P. and PERMUTT, S. New York, Dekker. 12: 73-112.

IDIONG, N., LEMKE, R. P., LIN, Y. J., KWIATKOWSKI, K., CATES, D. B. and RIGATTO, H. (1998). Airway closure durin mixed apneas in preterm infants: is respiratory effort necessary? J Pediatr **133**: 509-512.

IMANAKA, H., NISHIMURA, M., TAKEUCHI, M., KIMBALL, W. R., YAHAGI, N. and KUMON, K. (2000). Autotrigggering caused by cardiogenic oscillation during flow-triggered mechanical ventilation. Crit Care Med **28**: 402-407.

IRVIN, C. G., PAK, J. and MARTIN, R. J. (2000). Airway-parenchyma uncoupling in nocturnal asthma. Am J Respir Crit Care Med **161**(1): 50-56.

ISONO, S., FEROAH, T. R., HAJDUK, E. A., BRANT, R., WHITELAW, W. A. and REMMERS, J. E. (1997). Interaction of cross-sectional area, driving pressure, and airflow of passive velopharynx. J Appl Physiol 83(3): 851-859.

JARREAU, P. H., LOUIS, B., DASSIEU, G., DESFRERE, L., BLANCHARD, P. W., MORIETTE, G., ISABEY, D. and HARF, A. (1999). Estimation of inspiratory pressure drop in neonatal and pediatric endotracheal tubes. J Appl Physiol 87(1): 36-46.

JARREAU, P. H., LOUIS, B., DESFRERE, L., BLANCHARD, P. W., ISABEY, D., HARF, A. and MORIETTE, G. (2000). Detection of positional airway obstruction in neonates by acoustic reflection. Am J Respir Crit Care Med 161(5): 1754-1756.

JOHNSON, W. K. (1981). The dynamic pneumocardiogram: an application of coherent signal processing to cardiovascular measurement. IEEE Trans Biomed Eng **28**: 471-475.

JOKIC, R., KLIMASZEWSKI, A., MINK, J. and FITZPATRICK, M. F. (1998). Surface tension forces in sleep apnea: the role of a soft tissue lubricant: a randomized double-blind, placebo-controlled trial. Am J Respir Crit Care Med **157**(5 Pt 1): 1522-1525.

JONES, J. G., FRASER, R. B. and NADEL, J. A. (1975). Prediction of maximum expiratory flow rate from area-transmural pressure curve of compressed airway. J Appl Physiol 38(6): 1002-1011.

JULIA-SERDA, G., MOLFINO, N. A., CALIFARETTI, N., HOFFSTEIN, V. and ZAMEL, N. (1996). Tracheobronchial constriction in asthmatics induced by isocapnic hyperventilation with dry cold air. Chest 110(2): 404-410.

KACZKA, D. W., INGENITO, E. P. and LUTCHEN, K. R. (1999). Technique to determine inspiratory impedance during mechanical ventilation: implications for flow limited patients. Ann Biomed Eng 27(3): 340-355.

KACZKA, D. W., INGENITO, E. P., SUKI, B. and LUTCHEN, K. R. (1997). Partitioning airway and lung tissue resistances in humans: effects of bronchoconstriction. J Appl Physiol 82(5): 1531-1541.

KANO, S., LANTERI, C. J., DUNCAN, A. W. and SLY, P. D. (1994). Influence of nonlinearities on estimates of respiratory mechanics using multilinear regression analysis. J Appl Physiol **77**(3): 1185-1197.

KAPLAN, V., ZHANG, J. N., RUSSI, E. W. and BLOCH, K. E. (2000). Detection of inspiratory flow limitation during sleep by computer assisted respiratory inductive plethysmography. Eur Respir J 15(3): 570-578.

KATZ, I., ZAMEL, N., SLUTSKY, A. S., REBUCK, A. S. and HOFFSTEIN, V. (1990). An evaluation of flow-volume curves as a screening test for obstructive sleep apnea. Chest 98(2): 337-340.

KHIRANI, S., BIOT, L., EBERHARD, A. and BACONNIER, P. (2001). Positive end expiratory pressure and expiratory flow limitation: a model study. Acta Biotheoretica.

KIMOFF, R. J., MAKINO, H., HORNER, R. L., KOZAR, L. F., LUE, F., SLUTSKY, A. S. and PHILLIPSON, E. A. (1994). Canine model of obstructive sleep apnea: model description and preliminary application. J Appl Physiol 76(4): 1810-1817.

KONDO, T., MATSUMOTO, I., LANTERI, C. J. and SLY, P. D. (1997). Respiratory mechanics during mechanical ventilation: a model study on the effects of leak around a tracheal tube. Pediatr Pulmonol 24(6): 423-428.

KRIEGER, J., PETIAU, C., SFORZA, E., WEISS, T., THIBAULT, A. and BAZIN, A. (1998). [Starling resister and stability of sleep ventilation]. Neurophysiol Clin 28(6): 493-506.

KUO, C. Y., GERHARDT, T., BOLIVAR, J., CLAURE, N. and BANCALARI, E. (1996). Effect of leak around the endotracheal tube on measurements of pulmonary

compliance and resistance during mechanical ventilation: a lung model study. Pediatr Pulmonol 22(1): 35-43.

LAI-FOOK, S. J. and HYATT, R. E. (2000). Effects of age on elastic moduli of human lungs. J Appl Physiol 89(1): 163-168.

LANTERI, C. J., KANO, S., NICOLAI, T. and SLY, P. D. (1995). Measurement of dynamic respiratory mechanics in neonatal and pediatric intensive care: the multiple linear regression technique. Pediatr Pulmonol 19(1): 29-45.

LANTERI, C. J. and SLY, P. D. (1993). Changes in respiratory mechanics with age. J Appl Physiol 74(1): 369-378.

LAUZON, A. M. and BATES, J. H. T. (1991). Estimation of time-varying respiratory mechanical parameters by recursive least squares. J Appl Physiol **71**(3): 1159-1165.

LAUZON, A. M., DECHMAN, G. and BATES, J. H. (1992). Time course of respiratory mechanics during histamine challenge in the dog. J Appl Physiol 73(6): 2643-2647.

LAUZON, A. M., DECHMAN, G. and BATES, J. H. (1995). On the use of the alveolar capsule technique to study bronchoconstriction. Respir Physiol 99(1): 139-146.

LEBECQUE, P. and STANESCU, D. (1997). Respiratory resistance by the forced oscillation technique in asthmatic children and cystic fibrosis patients. Eur Respir J 10(4): 891-895.

LEMKE, R. P., AL-SAEDI, S. A., ALVARO, R. E., WISEMAN, N. E., CATES, D. B., KWIATKOWSKI, K. and RIGATTO, H. (1996). Use of a magnified cardiac airflow oscillation to classify neonatal apnea. Am J Respir Crit Care Med **154**: 1537-1542.

LOFASO, F., LORINO, A. M., FODIL, R., D'ORTHO, M. P., ISABEY, D., LORINO, H., GOLDENBERG, F. and HARF, A. (1998). Heavy snoring with upper airway resistance syndrome may induce intrinsic positive end-expiratory pressure. J Appl Physiol **85**(3): 860-866.

LONERGAN, R. P., 3RD, WARE, J. C., ATKINSON, R. L., WINTER, W. C. and SURATT, P. M. (1998). Sleep apnea in obese miniature pigs. J Appl Physiol 84(2): 531-536.

LORINO, A. M., BENHAMOU, D., LORINO, H. and HARF, A. (1986). A computerized method for measuring respiratory mechanics during mechanical ventilation. Bull Eur Physiopathol Respir 22(1): 81-84.

LORINO, A. M., LOFASO, F., DUIZABO, D., ZERAH, F., GOLDENBERG, F., D'ORTHO, M. P., HARF, A. and LORINO, H. (1998). Respiratory resistive impedance as an index of airway obstruction during nasal continuous positive airway pressure titration. Am J Respir Crit Care Med 158(5 Pt 1): 1465-1470.

LUDWIG, M. S. (1997). Role of lung parenchyma. Asthma. BARNES, P. J., GRUNSTEIN, M. M., LEFF, A. and WOOLCOCK, A. S. Philadelphia, Lipincott-Raven Press: 1319-1334.

LUDWIG, M. S., ROMERO, P. V. and BATES, J. H. (1989). A comparison of the dose-response behavior of canine airways and parenchyma. J Appl Physiol 67(3): 1220-1225.

LUTCHEN, K. R., EVERETT, J. R. and JACKSON, A. C. (1993a). Impact of frequency range and input impedance on airway-tissue separation implied from transfer impedance. J Appl Physiol 74(3): 1089-1099.

LUTCHEN, K. R., GIURDANELLA, C. A. and JACKSON, A. C. (1990). Inability to separate airway from tissue properties by use of human respiratory input impedance. J Appl Physiol 68(6): 2403-2412.

LUTCHEN, K. R., GREENSTEIN, J. L. and SUKI, B. (1996a). How inhomogeneities and airway walls affect frequency dependence and separation of airway and tissue properties. J Appl Physiol 80(5): 1696-1707.

LUTCHEN, K. R., HANTOS, Z., PETAK, F., ADAMICZA, A. and SUKI, B. (1996b). Airway inhomogeneities contribute to apparent lung tissue mechanics during constriction. J Appl Physiol 80(5): 1841-1849.

LUTCHEN, K. R. and JACKSON, A. C. (1992). Confidence bounds on respiratory mechanical properties estimated from transfer versus input impedance in humans versus dogs. IEEE Trans Biomed Eng 39(6): 644-651.

LUTCHEN, K. R. and SUKI, B. (1996c). Understanding pulmonary mechanics using the forced oscillation technique. Bioengineering approaches to pulmonary physiology and medicine. KHOO, M. C. New York, Plenum Press: 227-253.

LUTCHEN, K. R., SUKI, B., ZHANG, Q., PETAK, F., DAROCZY, B. and HANTOS, Z. (1994). Airway and tissue mechanics during physiological breathing and bronchoconstriction in dogs. J Appl Physiol 77(1): 373-385.

LUTCHEN, K. R., SULLIVAN, A., ARBOGAST, F. T., CELLI, B. R. and JACKSON, A. C. (1998). Use of transfer impedance measurements for clinical assessment of lung mechanics. Am J Respir Crit Care Med 157(2): 435-446.

LUTCHEN, K. R., YANG, K., KACZKA, D. W. and SUKI, B. (1993b). Optimal ventilation waveforms for estimating low-frequency respiratory impedance. J Appl Physiol 75(1): 478-488.

MANCZUR, T., GREENOUGH, A., NICHOLSON, G. P. and RAFFERTY, G. F. (2000). Resistance of pediatric and neonatal endotracheal tubes: influence of flow rate, size, and shape. Crit Care Med 28(5): 1595-1598.

MARSHALL, I., ROGERS, M. and DRUMMOND, G. (1991). Acoustic reflectometry for airway measurement. Principles, limitations and previous work. Clin Phys Physiol Meas 12(2): 131-141.

MARTIN, S. E., MARSHALL, I. and DOUGLAS, N. J. (1995). The effect of posture on airway caliber with the sleep-apnea/hypopnea syndrome. Am J Respir Crit Care Med 152(2): 721-724.

MEAD, J. and WHITTENBERGER, J. L. (1953). Physical properties of human lungs measured during spontaneous respiration. J Appl Physiol **5**: 779-786.

MEAD, J. (1969). Contribution of compliance of airways to frequency-dependent behavior of lungs. J Appl Physiol 26(5): 670-673.

MEAD, J., TURNER, M. J., MACKLEM, P. T. and LITTLE, J. B. (1967). Significance of the relationship between lung recoil and maximum expiratory flow. J Appl Physiol 22: 95-108.

MICHAELSON, E. D., GRASSMAN, E. D. and PETERS, W. R. (1975). Pulmonary mechanics by spectral analysis of forced random noise. J Clin Invest 56(5): 1210-1230.

MONTSERRAT, J. M., FARRE, R., BALLESTER, E., FELEZ, M. A., PASTO, M. and NAVAJAS, D. (1997). Evaluation of nasal prongs for estimating nasal flow. Am J Respir Crit Care Med 155(1): 211-215.

MORRELL, M. J. and BADR, M. S. (1998). Effects of NREM sleep on dynamic within-breath changes in upper airway patency in humans. J Appl Physiol **84**(1): 190-199.

MORRELL, M. J., BADR, M. S., HARMS, C. A. and DEMPSEY, J. A. (1995). The assessment of upper airway patency during apnea using cardiogenic oscillations in the airflow signal. Sleep **18**: 651-658.

NAGASE, T., FUKUCHI, Y., TERAMOTO, S., MATSUSE, T. and ORIMO, H. (1994). Mechanical interdependence in relation to age: effects of lung volume on airway resistance in rats. J Appl Physiol 77(3): 1172-1177.

NARKIEWICZ, K., MONTANO, N., COGLIATI, C., VAN DE BORNE, P. J. H., DYKEN, M. E. and SOMERS, V. K. (1998). Altered Cardiovascular Variability in Obstructive Sleep Apnea. Circulation **98**(11): 1071-1077.

NAVAJAS, D., FARRE, R., ROTGER, M., BADIA, R., PUIG-DE-MORALES, M. and MONTSERRAT, J. M. (1998). Assessment of airflow obstruction during CPAP by means of forced oscillation in patients with sleep apnea. Am J Respir Crit Care Med **157**(5 Pt 1): 1526-1530.

NAVAJAS, D., DUVIVIER, C., FARRE, R. and PESLIN, R. (2000). A simplified method for monitoring respiratory impedance during continuous positive airway pressure. Eur Respir J 15(1): 185-191.

NAVAJAS, D., FARRE, R., CANET, J., ROTGER, M. and SANCHIS, J. (1990). Respiratory input impedance in anesthetized paralyzed patients. J Appl Physiol 69(4): 1372-1379.

NORMAN, R. G., AHMED, M. M., WALSLEBEN, J. A. and RAPOPORT, D. M. (1997). Detection of respiratory events during NPSG: nasal cannula/pressure sensor versus thermistor. Sleep 20(12): 1175-1184.

NUCCI, G., MERGONI, M., BRICCHI, C., POLESE, G., COBELLI, C. and ROSSI, A. (2000). On-line monitoring of intrinsic PEEP in ventilator-dependent patients. J Appl Physiol 89(3): 985-995.

OFFICER, T. M., PELLEGRINO, R., BRUSASCO, V. and RODARTE, J. R. (1998). Measurement of pulmonary resistance and dynamic compliance with airway obstruction. J Appl Physiol **85**(5): 1982-1988.

OOSTEVEN, E., PESLIN, R., GALLINA, C. and ZWART, A. (1989). Flow and volume dependence of respiratory mechanical properties studied by forced oscillation. J Appl Physiol **67**(6): 2212-2218.

OTIS, A. B., MCKERROW, C. B., BARTLETT, R. A. and MEAD, J. (1956). Mechanical factors in the distibution of pulmonary ventilation. J Appl Physiol 8: 427-443.

PANCKERI, K. A., SCHOTLAND, H. M., PACK, A. I. and HENDRICKS, J. C. (1996). Modafinil decreases hypersomnolence in the English bulldog, a natural animal model of sleep-disordered breathing. Sleep 19(8): 626-631.

PANDIT, P. B., PYON, K. H., COURTNEY, S. E., ENGLAND, S. E. and HABIB, R. H. (2000). Lung resistance and elastance in spontaneously breathing preterm infants: effects of breathing pattern and demographics. J Appl Physiol 88(3): 997-1005.

PANKOW, W., PODSZUS, T., GUTHEIL, T., PENZEL, T., PETER, J. and VON WICHERT, P. (1998). Expiratory flow limitation and intrinsic positive end-expiratory pressure in obesity. J Appl Physiol 85(4): 1236-1243.

PEDLEY, T. J., SCHROTER, R. C. and SUDLOW, M. F. (1970a). Energy losses and pressure drop in models of human airways. Respir Physiol 9(3): 371-386.

PEDLEY, T. J., SCHROTER, R. C. and SUDLOW, M. F. (1970b). The prediction of pressure drop and variation of resistance within the human bronchial airways. Respir Physiol 9(3): 387-405.

PELOSI, P., CADRINGHER, P., BOTTINO, N., PANIGADA, M., CARRIERI, F., RIVA, E., LISSONI, A. and GATTINONI, L. (1999). Sigh in Acute Respiratory Distress Syndrome. Am. J. Respir. Crit. Care Med. **159**(3): 872-880.

PEREZ FONTAN, J. J., HELDT, G. P. and GREGORY, G. A. (1985). Resistance and inertia of endotracheal tubes used in infants during periodic flow. Crit Care Med **13**(12): 1052-1055.

PÉREZ-FONTAN, J. J., HELDT, G. P. and GREGORY, G. A. (1985). The effect of gas leak around endotracheal tube on the mean tracheal pressure during mechanical ventilation. Am Rev Respir Dis 132(339-342).

PERUN, M. L. and GAVER, D. P., 3RD (1995). Interaction between airway lining fluid forces and parenchymal tethering during pulmonary airway reopening. J Appl Physiol 79(5): 1717-1728.

PESLIN, R. (1986a). Methods for measuring total respiratory impedance by forced oscillations. Bull Eur Physiopathol Respir 22(6): 621-631.

PESLIN, R. and DUVIVIER, C. (1998). Partitioning of airway and respiratory tissue mechanical impedances by body plethysmography. J Appl Physiol **84**: 553-561.

PESLIN, R., DUVIVIER, C. and GALLINA, C. (1985). Total respiratory input and transfer impedances in humans. J Appl Physiol 59(2): 492-501.

PESLIN, R., FARRE, R., ROTGER, M. and NAVAJAS, D. (1996). Effect of expiratory flow limitation on respiratory mechanical impedance: a model study. J Appl Physiol 81(6): 2399-2406.

PESLIN, R., FELICIO DA SILVA, J., DUVIVIER, C. and CHABOT, F. (1993a). Respiratory mechanics studied by forced oscillations during artificial ventilation. Eur Respir J 6(6): 772-784.

PESLIN, R., FELICIO DA SILVA, J., CHABOT, F. and DUVIVIER, C. (1992). Respiratory mechanics studied by multiple linear regression in unsedated ventilated patients. Eur Respir J **5**: 871-878.

PESLIN, R. and FREDBERG, J. J. (1986). Oscillation mechanics of the respiratory system. Handbook of Physiology - The Respiratory system Vol III**:** 145-178.

PESLIN, R., GALLINA, C. and DUVIVIER, C. (1986b). Respiratory transfer impedances with pressure input at the mouth and chest. J Appl Physiol 61(1): 81-86.

PESLIN, R., GALLINA, C., SAUNIER, C. and DUVIVIER, C. (1994). Fourier analysis versus multiple linear regression to analyse pressure- flow data during artificial ventilation. Eur Respir J **7**(12): 2241-2245.

PESLIN, R., NAVAJAS, D., ROTGER, M. and FARRE, R. (1993b). Validity of the esophageal balloon technique at high frequencies. J Appl Physiol 74(3): 1039-1044.

POHLMAN, A., SEHATI, S. and YOUNG, D. (2001). Effect of changes in lung volume on acoustic transmission through the human respiratory system. Physiol Meas 22(1): 233-243.

RAUSCHER, H., POPP, W. and ZWICK, H. (1990). Flow-volume curves in obstructive sleep apnea and snoring. Lung 168(4): 209-214.

RECTSCHAFFEN, A. and KALES, A. (1968). A manual of standardized terminology, techniques, and scoring systems for sleep stages of human subjects. Washington, DC, U.S. Public Health Service.

REISCH, S., STELTNER, H., TIMMER, J., RENOTTE, C. and GUTTMANN, J. (1999). Early detection of upper airway obstructions by analysis of acoustical respiratory input impedance. Biol Cybern 81(1): 25-37.

REISCH, S., TIMMER, J., STELTNER, H., RUHLE, K. H., FICKER, J. H. and GUTTMANN, J. (2000). Detection of obstructive sleep apnea by analysis of phase angle using the forced oscillation signal. Respir Physiol 123(1-2): 87-99.

REPORT (1999). The Report of an American Academy of Sleep Medicine Task Force. Sleep-related breathing disorders in adults: recommendations for syndrome definition and measurement techniques in clinical research. Sleep **22**(5): 667-689.

ROTGER, M., PESLIN, R., OOSTVEEN, E. and GALLINA, C. (1991). Confidence intervals of respiratory mechanical properties derived from transfer impedance. J Appl Physiol 70(6): 2432-2438.

ROUSSELOT, J. M., PESLIN, R. and DUVIVIER, C. (1992). Evaluation of the multiple linear regression method to monitor respiratory mechanics in ventilated neonates and young children. Pediatr Pulmonol 13(3): 161-168.

RUDKOWSKI, J. C., VERSCHELDEN, P. and KIMOFF, R. J. (2001). Efficacy of daytime continuous positive airway pressure titration in severe obstructive sleep apnea. Eur Respir J **in press**.

SAJKOV, D. and MCEVOY, R. D. (1997). Pulmonary hemodynamics and hypoxemia in sleep apnea. Chest **111**(1): 256-257.

SANDERS, M. H. and MOORE, S. E. (1983). Inspiratory and expiratory partitioning of airway resistance during sleep in patients with sleep apnea. Am Rev Respir Dis **127**(5): 554-558.

SATO, J., SUKI, B., DAVEY, B. L. and BATES, J. H. (1993). Effect of methacholine on low-frequency mechanics of canine airways and lung tissue. J Appl Physiol 75(1): 55-62.

SCHUESSLER, T. F., GOTTFRIED, S. B. and BATES, J. H. T. (1997). A model of the spontaneously breathing patient: applications to intrinsic PEEP and work of breathing. J Appl Physiol **82**: 1694-1703.

SCHUESSLER, T. F., VOLTA, C. A., GOLDBERG, P., GOTTFRIED, S. B., KEARNEY, R. E. and BATES, J. H. T. (1995). An adaptative filter for the reduction of cardiogenic oscillations on esophageal pressure signals. 17th Ann Int Conf IEEE Eng Med Biol Soc.

SCHWAB, R. J. (1998). Upper airway imaging. Clin Chest Med 19(1): 33-54.

SCHWAB, R. J., GEFTER, W. B., HOFFMAN, E. A., GUPTA, K. B. and PACK, A. I. (1993). Dynamic upper airway imaging during awake respiration in normal subjects and patients with sleep disordered breathing. Am Rev Respir Dis **148**(5): 1385-1400.

SEEAR, M., WENSLEY, D. and WERNER, H. (1991). Comparison of three methods for measuring respiratory mechanics in ventilated children. Pediatr Pulmonol **10**(4): 291-295.

SERIES, F., CORMIER, Y. and LA FORGE, J. (1989). Role of lung volumes in sleep apnoea-related oxygen desaturation. Eur Respir J **2**(1): 26-30.

SERIES, F., CORMIER, Y. and LA FORGE, J. (1991). Validity of diurnal sleep recording in the diagnosis of sleep apnea syndrome. Am Rev Respir Dis **143**(5 Pt 1): 947-949.

SERIES, F. and MARC, I. (1995). Accuracy of breath-by-breath analysis of flow-volume loop in identifying sleep-induced flow-limited breathing cycles in sleep apnoea-hypopnoea syndrome. Clin Sci (Colch) **88**(6): 707-712.

SIMILOWSKI, T., LEVY, P., CORBEIL, C., ALBALA, M., PARIENTE, R., DERENNE, J. P., BATES, J. H., JONSON, B. and MILIC-EMILI, J. (1989). Viscoelastic behavior of lung and chest wall in dogs determined by flow interruption. J Appl Physiol **67**(6): 2219-2229.

SIMILOWSKI, T. and BATES, J. H. (1991). Two-compartment modelling of respiratory system mechanics at low frequencies: gas redistribution or tissue rheology? Eur Respir J **4**(3): 353-358.

SKATRUD, J. B. and DEMPSEY, J. A. (1985). Airway resistance and respiratory muscle function in snorers during NREM sleep. J Appl Physiol **59**: 328-335.

SLY, P. D., HAYDEN, M. J., PETAK, F. and HANTOS, Z. (1996). Measurement of low-frequency respiratory impedance in infants. Am J Respir Crit Care Med 154(1): 161-166.

STAMENOVIC, D., GLASS, G. M., BARNAS, G. M. and FREDBERG, J. J. (1990). Viscoplasticity of respiratory tissues. J Appl Physiol 69(3): 973-988.

STANESCU, D., KOSTIANEV, S., SANNA, A., LIISTRO, G. and VERITER, C. (1996). Expiratory flow limitation during sleep in heavy snorers and obstructive sleep apnoea patients. Eur Respir J **9**(10): 2116-2121.

STONE, K. C., MERCER, R. R., FREEMAN, B. A., CHANG, L. Y. and CRAPO, J. D. (1992). Distribution of lung cell numbers and volumes between alveolar and nonalveolar tissue. Am Rev Respir Dis 146(2): 454-456.

STRADLING, J. R., BARBOUR, C., GLENNON, J., LANGFORD, B. A. and CROSBY, J. H. (2000). Which aspects of breathing during sleep influence the overnight fall of blood pressure in a community population? Thorax **55**(5): 393-398.

SUKI, B. and LUTCHEN, K. R. (1992). Pseudorandom signals to estimate apparent transfer and coherence functions of nonlinear systems: applications to respiratory mechanics. IEEE Trans Biomed Eng 39(11): 1142-1151.

SUKI, B., YUAN, H., ZHANG, Q. and LUTCHEN, K. R. (1997). Partitioning of lung tissue response and inhomogeneous airway constriction at the airway opening. J Appl Physiol 82(4): 1349-1359.

SUKI, B., ZHANG, Q. and LUTCHEN, K. R. (1995). Relationship between frequency and amplitude dependence in the lung: a nonlinear block-structured modeling approach. J Appl Physiol 79(2): 660-671.

TAMISIER, R., PEPIN, J. L., WUYAM, B., SMITH, R., ARGOD, J. and LEVY, P. (2000). Characterization of pharyngeal resistance during sleep in a spectrum of sleep-disordered breathing. J Appl Physiol **89**(1): 120-130.

TUCK, S. A., DORT, J. C., OLSON, M. E. and REMMERS, J. E. (1999). Monitoring respiratory function and sleep in the obese Vietnamese pot- bellied pig. J Appl Physiol 87(1): 444-451.

TUCK, S. A. and REMMERS, J. E. (1997). Sleep-disordered breathing in obese pigs - a model of high upper airway resistance. Am J Respir Crit Care Med **155**: A416.

UHL, R. R. and LEWIS, F. J. (1974). Digital computer calculation of human pulmonary mechanics using a least mean square fit technique. Comput Biomed Res **7**: 489-495.

VAN DE GRAAFF, W. B. (1988). Thoracic influence on upper airway patency. J Appl Physiol **65**(5): 2124-2131.

VAN DER TOUW, T., CRAWFORD, A. B. and WHEATLEY, J. R. (1997). Effects of a synthetic lung surfactant on pharyngeal patency in awake human subjects. J Appl Physiol 82(1): 78-85.

VAN NOORD, J. A., CLEMENT, J., VAN DE WOESTIJNE, K. P. and DEMEDTS, M. (1991). Total respiratory resistance and reactance in patients with asthma, chronic bronchitis, and emphysema. Am Rev Respir Dis 143(5 Pt 1): 922-927.

VAN SURELL, C., LOUIS, B., LOFASO, F., BEYDON, L., BROCHARD, L., HARF, A., FREDBERG, J. and ISABEY, D. (1994). Acoustic method to estimate the longitudinal area profile of endotracheal tubes. Am J Respir Crit Care Med **149**(1): 28-33.

VASSILIOU, M. P., PETRI, L., AMYGDALOU, A., PATRANI, M., PSARAKIS, C., NIKOLAKI, D., GEORGIADIS, G. and BEHRAKIS, P. K. (2000). Linear and nonlinear analysis of pressure and flow during mechanical ventilation. Intensive Care Med 26(8): 1057-1064.

VEASEY, S. C., FENIK, P., PANCKERI, K., PACK, A. I. and HENDRICKS, J. C. (1999). The effects of trazodone with L-tryptophan on sleep-disordered breathing in the English bulldog. Am J Respir Crit Care Med 160(5 Pt 1): 1659-1667.

VEASEY, S. C., PANCKERI, K. A., HOFFMAN, E. A., PACK, A. I. and HENDRICKS, J. C. (1996). The effects of serotonin antagonists in an animal model of sleep- disordered breathing. Am J Respir Crit Care Med 153(2): 776-786.

VINCKEN, W. and COSIO, M. G. (1985). Flow oscillations on the flow-volume loop: a nonspecific indicator of upper airway dysfunction. Bull Eur Physiopathol Respir 21(6): 559-567.

WESSALE, J. L., BOURLAND, J. D., BABBS, C. F., MILEWSKI, R. C., ROCKENHAUSER, M. E. and GEDDES, L. A. (1985). Correlation of the cardiogenic

air flow in the respiratory airway (i.e. the pneumocardiogram) with left ventricular stroke volume in dogs. Jpn Heart J **26**: 777-785.

WESSALE, J. L., BOURLAND, J. D. and GEDDES, L. A. (1988). Relationship between tracheal air flow and induced changes in intrathoracic volume. A basis for calibration of pneumocardiogram. Jpn Heart J **29**: 99-106.

WITTENBORG, M. H., GYEPES, M. T. and CROCKER, D. (1967). Tracheal dynamics in infants with respiratory distress, stridor, and collapsing trachea. Radiology **88**(4): 653-662.

YANG, K. L. and WANG, C. (1996). An intrinsic positive end-expiratory pressure lung model, with and without flow limitation. Crit Care Med 24(7): 1261-1265.

YEN, F. C., BEHBEHANI, K., LUCAS, E. A., BURK, J. R. and AXE, J. R. (1997). A noninvasive technique for detecting obstructive and central sleep apnea. IEEE Trans Biomed Eng 44(12): 1262-1268.

ZERAH, F., HARF, A., PERLEMUTER, L., LORINO, H., LORINO, A. M. and ATLAN, G. (1993). Effects of obesity on respiratory resistance. Chest 103(5): 1470-1476

ZERAH-LANCNER, F., LOFASO, F., COSTE, A., RICOLFI, F., GOLDENBERG, F. and HARF, A. (1997). Pulmonary function in obese snorers with or without sleep apnea syndrome. Am J Respir Crit Care Med **156**(2 Pt 1): 522-527